論文 / 著書情報
Article / Book Information

題目(和文)	
Title(English)	Novel non-perturbative analyses of QCD spectral functions
著者(和文)	荒木賢志
Author(English)	Ken-Ji Araki
出典(和文)	学位:博士(理学), 学位授与機関:東京工業大学, 報告番号:甲第10393号, 授与年月日:2017年3月26日, 学位の種別:課程博士, 審査員:岡 眞,伊藤 克司,今村 洋介,肥山 詠美子,陣内 修
Citation(English)	Degree:Doctor (Science), Conferring organization: Tokyo Institute of Technology, Report number:甲第10393号, Conferred date:2017/3/26, Degree Type:Course doctor, Examiner:,,,,
学位種別(和文)	博士論文
Category(English)	Doctoral Thesis
種別(和文)	要約
Type(English)	Outline

Novel non-perturbative analyses of QCD spectral functions

Ken-Ji Araki

~ February 24, 2017 ~

Department of Physics,
Tokyo Institute of Technology
2-12-1 Ookayama, Meguro-ku, Tokyo, 152-8550, JAPAN

A dissertation submitted to Tokyo Institute of Technology
for the degree of Doctor of Philosophy

Abstract

Quantum Chromo-Dynamics (QCD) is widely accepted as the fundamental theory of elementary particles of quarks and gluons. This fact is supported by the good agreement between experimental observations and various theoretical predictions, lattice QCD, perturbative QCD, QCD sum rules and so on. Hadrons are composite particles consisting of quarks and gluons, so that their properties themselves are one of the main topics which should be clarified from QCD. Perturbative approaches in QCD are not applicable in the low energy region where most of the light hadrons live since the effective coupling constant becomes larger in the region. Furthermore, in addition to such a practical problem, some effects which in principle cannot be taken into account by the perturbation theory are believed to play important roles in the lower energy region. Thus, one states that a "non-perturbative" approach is necessary to resolve such practical and/or fundamental problems. Due to the above theoretical difficulty, related physics with hadron properties, confinement and spontaneous breaking of chiral symmetry, may not be satisfactorily understood from QCD even today. In association of recent development of computers, the lattice QCD simulation as a numerical approach has become a powerful non-perturbative method and clarifies hadron properties and the related physics. On the other hand, analytic approaches are also important to understand QCD more deeply. The QCD sum rule is one of the analytic non-perturbative approaches and is utilized to study hadrons from around the same time as the lattice QCD entered the stage. The QCD sum rule is a method to calculate a hadronic spectral function (SPF), which we would like to know from QCD in order to study hadron properties. This method consists of roughly two stages: construction of integral rules for SPF from QCD and determination of SPF from them.

The construction of integral rules is based on two important key words, *analyticity* and *factorization*. The analyticity of a correlation function leads to a dispersion relation, which gives the relation between the integral of SPF with a kernel and the correlation function in the virtual momentum region. Factorization enables us to obtain the correlation function in the special form: a sum of condensates multiplied by their Wilson coefficients. This is called operator product expansion (OPE). It is the condensate that reflects non-perturbative effects. Thus, we construct integral rules of SPF taking into account non-perturbative effects.

For the determination of SPF, traditionally one assumes its functional form to be simplified being "one pole + continuum". Although this scheme is successful to extract the information on the lowest (ground) state in the analyzed channel, one must ignore other (or excited) states. Recently, there appears an evolution to tackle this difficulty, that is, the application of the maximum entropy method (MEM) to QCD sum rules. In this method, by the help of the Bayesian probability, one can uniquely determine SPF from the integral rule without any strong assumption on its functional form as is done in the traditional method. It is, however, known

by some studies that only one peak is reproduced from the usual integral rule of Borel sum rules with MEM. From this point of view, we realize that there remain fundamental problems in the stage of construction of the integral rules.

In this thesis, two attempts are proposed to bring fundamental improvement of the QCD sum rule or go beyond the QCD sum rule. The first attempt is the generalization of the Borel sum rule to the complex variable sum rule. By carefully considering the analyticity in the stage of construction of integral rules, we show that the parameter of the integral rule, which is conventionally considered to be real values, can have also complex values. This simple discovery leads to the complex Borel sum rule (CBSR), where the Borel mass is generalized to have not only real values but also complex ones. It is shown that the analysis system using CBSR and MEM has the ability to reproduce the second peak. This approach is applied to charmonia (bound states of charm and anti charm quarks) at finite temperature. By temperature effects hadrons are expected to become free from the confinement to disappear (melt). Thus, the melting temperature is one of the important quantities to study the confinement. In this study, both the melting temperatures of the ground and excited states are estimated.

The second attempt is to take an infinite summation of partial series in the OPE. It is the OPE in the whole system of QCD sum rules that reflects the non-pertarbative future of QCD to hadronic SPF. Usually one truncates the expansion at a certain dimension of operators because the values of higher dimensional condensates are not well known and the calculation of their Wilson coefficients becomes more and more difficult. However, it is theoretically interesting to study what kind of roles such a truncated infinite series plays. It is shown that by using the Schwinger-Dyson equations one can systematically take an infinite summation of a partial series in the OPE. Actually, the infinite summation of the power series of $\langle\bar{q}q\rangle$ is analytically obtained by this approach, which results in the explicit pole shifts of correlation functions depending on $\langle\bar{q}q\rangle$. The result is theoretically interesting since the non-vanishing $\langle\bar{q}q\rangle$ is a signal of the spontaneous chiral symmetry breaking. Furthermore, it is discussed how the QCD sum rule analysis can be modified when such an infinite summation of non-perturbative effects is introduced.

Table of Contents

Chapter 1

Introduction

In this chapter, we briefly overview some essential concepts in hadron physics as a linking bridge with the present studies. The outline of the thesis is also given in the last section of this chapter.

1.1 Quark and hadron

The quarks are the elementary particles appearing in the standard model. Historically, the concept of quark has been first introduced in the quark model to systematically classify the newly discovered particles (hadrons) as composite particles of quarks [1–3]. Today the six kinds of quarks are discovered and distinguished by the quantum number called flavor: up, down, strange, charm, bottom and top. Their masses are shown in Table 1.1. The interaction between (among) quarks is induced by gluons. The dynamics of the quarks and the gluons is described by Quantum Chromo-Dynamics (QCD). QCD is established as a non-Abelian $SU(3)$ gauge field theory [4] whose internal degrees of freedom is called color. The quarks appear in QCD as the Dirac fermions which are the triplet states of the color. The gluons are the gauge fields in QCD which are the octet states of the color.

Flavor	Mass
up	$2.2^{+0.6}_{-0.4}$ MeV
down	$4.7^{+0.5}_{-0.4}$ MeV
strange	96^{+8}_{-4} MeV
charm	1.27 ± 0.03 GeV
bottom	$4.18^{+0.04}_{-0.03}$ GeV
top	160^{+5}_{-4} GeV

Table 1.1: Flavor of quarks and their masses [5]. The u, d, and s quark masses are the current quark masses in MS bar scheme at a scale of $\mu \sim 2$ GeV. The c and b quark masses are the running masses in the MS scheme. t quark mass is the MS bar mass from direct measurements.

Hadrons are the composite particles consisting of quarks. Mass spectra of hadrons and their properties are some of the main topics which should be clarified from QCD. In QCD, nevertheless, the perturbation theory, which is an analytic approach, is known not to be available in the low energy region where typical light hadrons live since the effective coupling constant becomes larger in the region. Furthermore, in addition to such a practical problem, some effects

which in principle cannot be taken into account by the perturbation theory are believed to play important roles in the lower energy region. Thus we conclude that "non-perturbative" approaches are necessary to resolve such practical and/or fundamental problems.

1.2 Basic properties of QCD

In this section, we will quickly overview the basic properties of QCD, especially, about the symmetries and the effective coupling constant. Let us first write down the QCD Lagrangian:

$$\mathcal{L}_{QCD} = \sum_f \bar{q}_f (i \not{D} - m_f) q_f - \frac{1}{8}\mathrm{Tr}[G_{\mu\nu}G^{\mu\nu}]. \tag{1.1}$$

q_f is a Dirac fermion field appearing in QCD, namely quark, and the subscript f represents its flavor. m_f is the current mass of each quark with flavor f. Further, let us note that the quark field has two implicit subscripts as q_i^α, where α and i represent its spinor and color indices, respectively. The gauge field A_μ^a appearing in the definition of the covariant derivative,

$$D_\mu = \partial_\mu - igA_\mu^a T^a, \tag{1.2}$$

is called gluon. T^a is the generator in the fundamental representation in color SU(3) acting on the color space of a quark. The field strength tensor $G_{\mu\nu}$ is defined as *

$$G_{\mu\nu} = \frac{i}{g}[D_\mu, D_\nu]. \tag{1.3}$$

From this simple lagrangian, we can, in principle, predict all the physics in QCD: the hadron spectroscopy, hadron scattering, QCD phase diagram and so on.

1.2.1 Gauge symmetry

Since QCD is constructed as the non-Abelian $SU(3)$ gauge theory [4], the Lagrangian is definitely invariant under the (local) gauge transformation. Here we will briefly check that. The transformation of the classical fields are defined as

$$q \rightarrow U(x)q, \tag{1.4}$$
$$D_\mu \rightarrow U(x)D_\mu U^\dagger(x), \tag{1.5}$$

where $U(x) = \exp(i\theta^a(x)T^a)$. From these definitions, it is almost obvious that the first term in the Lagrangian is invariant under the gauge transformation. The invariance of the second term is also understood in the following. By the definition of the field strength, it is transformed as

$$G_{\mu\nu} \rightarrow U(x)G_{\mu\nu}(x)U^\dagger(x) \tag{1.6}$$

according to Eq. (1.5). Thus, the invariance of the second term in the Lagrangian under the gauge transformation is evident by the trace invariance under cyclic permutation. Finally, we have checked the gauge invariance of the Lagrangian.

*Note that $G_{\mu\nu}^a$ is defined as $G_{\mu\nu}^a = T^a G_{\mu\nu}$.

1.2.2 Isospin symmetry

When we ignore the mass difference among different flavored quarks, the QCD Lagrangian becomes invariant under the flavor $SU(N_f)$ transformation. Here let us suppose $f = u, d$ considering the small mass difference between them. The transformation is defined as

$$q_f \to \exp(i\theta_V^a [I^a]_{ff'}) q_{f'}, \tag{1.7}$$

where $I^a = \frac{\sigma^a}{2}$, which is the generator of SU(2) acting on the flavor space. σ^a is the Puli matrices. The conserved current followed from Noether's theorem is

$$J_V^{a\,\mu} = \bar{q}_f \gamma^\mu [I^a]_{ff'} q_{f'}. \tag{1.8}$$

The conserved charge of its time-component is called isospin. It is used as the good quantum number to classify the hadrons.

1.2.3 Chiral symmetry

In the massless limit, the QCD Lagrangian has the chiral symmetry. Here let us consider such a limit for u and d quarks due to their quite small masses [†]. The Lagrangian becomes invariant under the transformation defined as

$$q_f^\alpha \to \exp(i\theta_A^a [\gamma^5]^{\alpha\beta} [I^a]_{ff'}) q_{f'}^\beta. \tag{1.9}$$

Note that this transformation also acts on the spinor space due to γ^5.

The conserved current followed from Noether's theorem is

$$J_A^{a\,\mu} = \bar{q}_f \gamma^\mu \gamma^5 [I^a]_{ff'} q_{f'}. \tag{1.10}$$

Let us briefly comment on the well-known physical meaning of the chiral symmetry. In the massless limit, QCD also holds the isospin symmetry and the relevant conserved current $J_V^{a\,\mu}$. Then we have the two kinds of conserved charge densities, J_A^{a0} and J_V^{a0}. By taking their linear combination of them, we can alternatively construct two kinds of charge densities as follows

$$c_R = \frac{1}{2}(J_V^{a\,0} + J_A^{a\,0}) \;=\; q_f^\dagger P_R [I^a]_{ff'} q_{f'}, \tag{1.11}$$

$$c_L = \frac{1}{2}(J_V^{a\,0} - J_A^{a\,0}) \;=\; q_f^\dagger P_L [I^a]_{ff'} q_{f'}, \tag{1.12}$$

where $P_R = \frac{1}{2}(1+\gamma^5)$ and $P_L = \frac{1}{2}(1-\gamma^5)$. Since P_R and P_L are projection operators to the right-handed and left-handed components in the spinor space, Eq. (1.11) and Eq. (1.12) mean that the isospin is independently conserved even in each right-handed and left-handed components.

[†]This approximation is meaningful when we focus on physics where only the light quarks participate. In QCD sum rules analyses, for example, spectra of the light hadrons can be well reproduced in the limit. And sometimes we also discuss this limit for the strange quark due to its relatively smaller mass than the masses of the charm, bottom and top quarks.

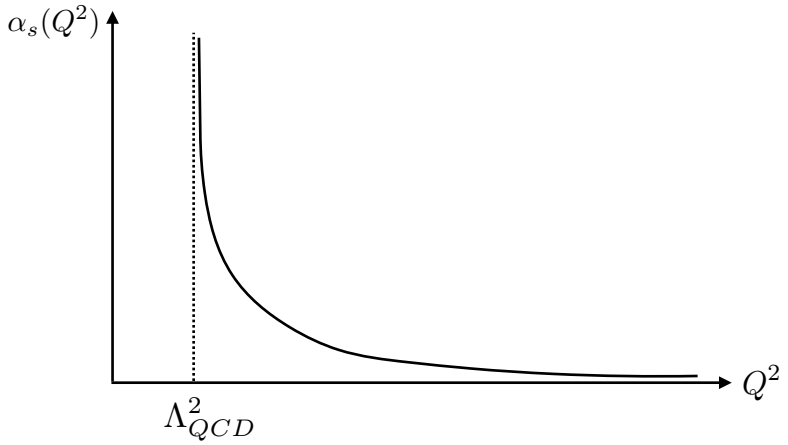

Figure 1.1: Schematic picture of QCD effective coupling constant.

1.2.4 Effective coupling constant in QCD

The effective coupling constant of QCD was calculated and investigated [6, 7] according to the analyses by the renormalization group [8–10]. At the leading order in the perturbation in the MS scheme, the effective coupling constant is given as

$$\alpha_s(Q^2) = \frac{4\pi}{(11 - \frac{2}{3}n_f)\ln\frac{Q^2}{\Lambda^2_{QCD}}} \quad (Q^2 = -q^2), \tag{1.13}$$

where Λ_{QCD} is called QCD scale defined as a momentum where the effective coupling constant reaches the unphysical pole in the low momentum region. Λ_{QCD} is regarded as the typical scale where the perturbation theory critically breaks down and it is considered that " non-perturbative effects" exist and play crucial roles in the low energy region. Though it is widely used in various contexts, the word of non-perturbative effects do not seem to be clearly defined. One possible definition may be as follows. Non-perturbative effects are any existing terms in Green functions which, in principle, cannot be introduced by the perturbation theory. In this thesis, we use the word of non-perturbative effects as this meaning.

On the other hand, the coupling constant logarithmically decreases at large momentum transfer. This property is usually called *asymptotic freedom*. By the asymptotic freedom, we have a chance of reliable calculations by perturbations for the hard process in QCD. When $n_f \leq 16$, the behavior of the effective coupling can be schematically shown in Fig. 1.1. It is believed that the unphysical pole survives even if we take all perturbative corrections of the beta function. It can be confirmed in the actual results up to three loops [11–15].

1.3 Spontaneous chiral symmetry breaking in QCD

The masses of u and d quarks are of the order of several MeV as shown in Table 1.1. Nevertheless, typical light hadrons have the masses of the order of 1 GeV. This mysterious mass gap is believed as a consequence of spontaneous chiral symmetry breaking in QCD, as is indicated by the NJL model [16]. In this section, first we will summarize the general definition of spontaneous symmetry breaking and Nambu-Goldstone (NG) theorem. Then we will discuss spontaneous chiral symmetry breaking in QCD.

1.3.1 Spontaneous symmetry breaking (SSB)

Let us consider a classical field theory described by the action which is invariant under a certain group transformation. In this situation, we can define the relevant conserved current J^μ, satisfying $\partial_\mu J^\mu = 0$, according to the Noether's theorem.

After the quantization, the conserved charge operator, $Q = \int J^0(x) d^3x$, satisfies Heisenberg equation

$$[Q, H] = 0, \tag{1.14}$$

where H is Hamiltonian. Q is identical with the generator which induces the relevant transformation on any state in the Hilbert space as follows:

$$|\text{state}\rangle' = \exp(i\theta Q)|\text{state}\rangle. \tag{1.15}$$

Definition of SSB

The statements so far are trivial to be concluded by the symmetry of the classical action. However, the vacuum $|0\rangle$ has the non-trivial nature: it can satisfy either of following two conditions

$$(a) \qquad Q|0\rangle = 0, \tag{1.16}$$

$$(b) \qquad Q|0\rangle \not\propto |0\rangle. \tag{1.17}$$

The condition (a) means that the vacuum is an eigenstate of Q and its eigenvalue is zero. On the other hand, the condition (b) means that the vacuum is not an eigenstate of Q. Spontaneous symmetry breaking is defined as the situation (b). When SSB is realized the vacuum does not have the symmetry by the definition, so that it is transformed into another state which has the same energy because of Eq. (1.14).

Order parameters

Although the SSB is the nature of the vacuum satisfying (b), we alternatively use the *order parameter* to judge whether the SSB actually occurs in the systems in our interests. The order parameter of SSB $\langle O \rangle$ is defined with an arbitrary local operator $A(x)$ as follows:

$$\langle O \rangle \equiv \langle 0|[Q, A(x)]|0\rangle. \tag{1.18}$$

The value of the order parameter is definitely zero when the vacuum satisfies the condition (a). On the other hand, it takes a non-zero value when the vacuum satisfies the condition (b), namely, the SSB is realized. So the non-zero value of the order parameter is the alternative definition of the SSB:

$$\langle O\rangle = \begin{cases} 0 & (a)\text{: non-SSB case} \\ \text{non-zero} & (b)\text{: SSB case.} \end{cases}$$

$\langle Q\rangle$ also seems to be a more naive order parameter. However, if it does not vanish it must diverge in proportion to the volume because of the space integration. On the other hand, the order parameter defined as Eq. (1.18) does not diverge in proportion to the volume because the effective region of the integration is limited to finite one by the commutation and causality [‡].

Nambu Goldstone theorem

We write down Nambu-Goldstone theorem:

When the SSB occurs, there exist zero-energy bosons (NG boson) $|NG\rangle$ and the matrix element $\langle 0|J^\mu|NG\rangle$ does not vanish.

The proof can be found in standard textbooks of the field theory (see, e.g. [17]).

1.3.2 Spontaneous chiral symmetry breaking in QCD and mass generation

Let us take the chiral limit to discuss spontaneous chiral breaking in QCD, so that it is characterized as follows:

- Conserved current : $\bar{q}\gamma^\mu\gamma^5 I^a q$,
- Conserved charge : $\int d^3x q^\dagger\gamma^5 I^a q$,
- Order parameter : $\langle\bar{q}q\rangle \equiv \langle\bar{q}_i^\alpha q_i^\alpha\rangle$ (i and α are the color and spinor indices, respectively),
- NG boson : Pion (π),

where we choose $\bar{q}\gamma^5 I^b q$ as $A(x)$ in Eq. (1.18) to derive the order parameter and $\langle\bar{q}q\rangle$ is called chiral condensate or quark condensate.

Let us understand the relation between the spontaneous chiral symmetry breaking and the quark (non-perturbative) effective mass. In the momentum space, the order parameter is written by using the quark propagator as follows:

$$\langle\bar{q}q\rangle = -\mathrm{Tr}\Big[\int\frac{d^4k}{(2\pi)^4}[G(k)]\Big], \tag{1.19}$$

where the trace acts in both the spinor and color space. The quark self-energy is generally decomposed into the two parts as follows:

$$\Sigma(k) = \hat{1}_c\big(\not{k}a(k^2) + \hat{1}_s b(k^2)\big), \tag{1.20}$$

where $\hat{1}_c$ and $\hat{1}_s$ are identity operators in the color and spinor spaces, respectively. By using this expression, the order parameter is rewritten as

$$\langle\bar{q}q\rangle = -3\,\mathrm{Tr}\Big[\int\frac{d^4k}{(2\pi)^4}\frac{i}{(1-a(k^2))^2}\frac{\not{k}(1-a(k^2)) + \hat{1}_s b(k^2)}{k^2 - \big(\frac{b(k^2)}{1-a(k^2)}\big)^2}\Big], \tag{1.21}$$

[‡] $[A(x), B(0)] = 0$ where x is space-like.

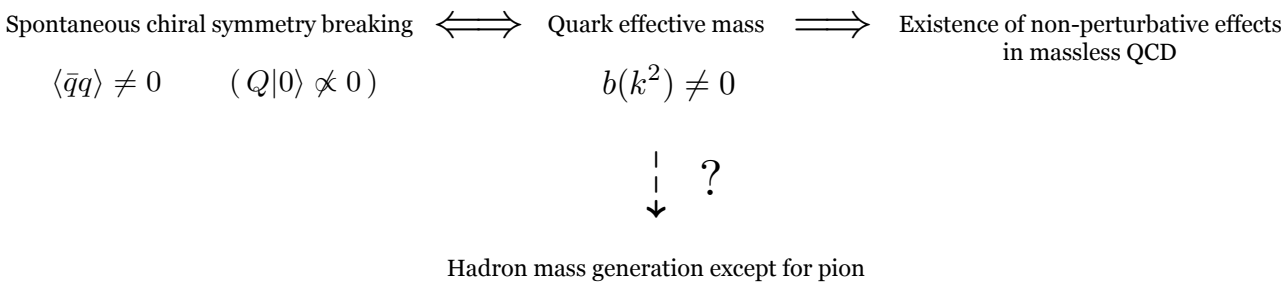

Figure 1.2: Logical correlation diagram about spontaneous chiral symmetry breaking in QCD. The relation between the quark effective mass and hadron mass is not logically evident at least by the discussion here.

where the factor of 3 comes from the trace in the color space. Since the traces of the gamma matrices are zeros, it finally leads to

$$\langle\bar{q}q\rangle = -12\int\frac{d^4k}{(2\pi)^4}\frac{i}{(1-a(k^2))^2}\frac{b(k^2)}{k^2-(\frac{b(k^2)}{1-a(k^2)})^2}. \tag{1.22}$$

This expression tells us the important logic as follows.

1. The spontaneous chiral symmetry breaking is equivalent to non-vanishing $b(k^2)$.
2. It can be concluded that there must exist *non-perturbative effects* in the quark self-energy if $b(k^2)$ does not vanish[§], because perturbative calculations cannot bring a finite value of $b(k^2)$ in the case of the massless limit. In other words, spontaneous chiral symmetry breaking is induced by non-perturbative effects.
3. When the chiral symmetry is spontaneously broken, the quark acquires effective mass by non-perturbative effects because of the non-vanishing $b(k)$ term.

Intuitively speaking, since the hadrons consist of quarks, one would think that the hadrons should also acquire the masses due to the effective quark mass associated with the spontaneous symmetry breaking. However, we have not clarified the mechanism yet, in which a pion can stay massless although the constituent particles are massive. The logic stated above is diagrammatically summarized in Fig.1.2.

[§]The opposite logic cannot be concluded, namely, $b(k^2)$ can become zero even when there exist non-perturbative effects.

1.4 From QCD to Hadron

Let us briefly overview the guideline to investigate hadron properties from QCD.

1.4.1 Correlation function

The main object for studying hadron spectroscopy from QCD is a hadronic two point function, correlation function, defined as

$$\Pi(q^2) = i \int d^4x \mathrm{e}^{iqx} \langle 0|TJ(x)J^\dagger(0)|0\rangle, \tag{1.23}$$

in the momentum space. $J(x)$ is called current operator, which annihilates a hadron state. It must be a composite operator unlike elementary particles since hadrons are composite particles consisting of quarks. We define the operator in such a way to identify the quantum numbers and flavors of quarks in hadrons. We usually use J^{PC} as the quantum number. J, P and C are the total angular momentum, parity and charge conjugate, respectively. In meson cases, $J(x)$ is typically given by a bilinear form. The typical examples are seen in Table. 1.2.

Type	Bilinear form	J^{PC}
Scalar	$\bar{q}q$	0^{++}
Pseudoscalar	$i\bar{q}\gamma_5 q$	0^{-+}
Vector	$\bar{q}\gamma_\mu q$	1^{--}
Axial vector	$\bar{q}\gamma^\mu\gamma_5 q$	1^{++}

Table 1.2: Typical bilinear form.

Furthermore we also consider the isospin as the quantum number though the isospin symmetry is not exact in the real world due to the difference between the quark current masses. To construct a current operator with definite isospin, we take an appropriate linear combination. The current operators of typical light hadrons are summarized in Table 1.3. In baryon cases, such an operator was studied by Ioffe [18] for the first time.

1.4.2 Spectral representation

Spectral representation makes the physical meaning of the hadronic correlation function clear. We derive the spectral representation of the hadronic correlation function in the coordinate space $\langle 0|TJ(x)J(0)^\dagger|0\rangle$. Suppose that J is a scalar current for simplicity.

Firstly, we assume the complete set as follows:

$$\sum_n \int d^4k \, |k,n\rangle \, \langle k,n| = 1, \tag{1.24}$$

where k is the four momentum and n represents all the other possible quantum numbers. Inserting this complete set between the two current operators, we obtain

$$\begin{aligned} \langle 0|TJ(x)J(0)^\dagger|0\rangle &= \sum_n \int d^4k \{ \, \theta(x^0) \, \langle 0| \, J(x) \, |k,n\rangle \, \langle k,n| \, J(0)^\dagger \, |0\rangle \\ &\quad + \theta(-x^0) \, \langle 0| \, J(0)^\dagger \, |k,n\rangle \, \langle k,n| \, J(x) \, |0\rangle \, \}. \end{aligned} \tag{1.25}$$

Hadron	current operator	I	J^{PC}
f_0	$\frac{\bar{u}u+\bar{d}d}{2}$	0	0^{++}
a_0	$\frac{\bar{u}u-\bar{d}d}{2}$	1	0^{++}
η	$\frac{\bar{u}i\gamma_5 u+\bar{d}i\gamma_5 d}{2}$	0	0^{-+}
π^0	$\frac{\bar{u}i\gamma_5 u-\bar{d}i\gamma_5 d}{2}$	1	0^{-+}
ω	$\frac{\bar{u}\gamma^\mu u+\bar{d}\gamma^\mu d}{2}$	0	1^{--}
ρ^0	$\frac{\bar{u}\gamma^\mu u-\bar{d}\gamma^\mu d}{2}$	1	1^{--}
f_1	$\frac{\bar{u}\gamma^\mu\gamma_5 u+\bar{d}\gamma^\mu\gamma_5 d}{2}$	0	1^{++}
a_1	$\frac{\bar{u}\gamma^\mu\gamma_5 u-\bar{d}\gamma^\mu\gamma_5 d}{2}$	1	1^{++}

Table 1.3: Current operators for the typical light mesons.

Using the relation $\hat{O}(x) = \mathrm{e}^{i\hat{P}x}\hat{O}(0)\mathrm{e}^{-i\hat{P}x}$ and the translation invariance of the vacuum, we obtain

$$\begin{aligned}\langle 0|TJ(x)J(0)^\dagger|0\rangle &= \sum_n \int d^4k\{\mathrm{e}^{-ikx}\theta(x^0)+\mathrm{e}^{ikx}\theta(-x^0)\}\ |\langle 0|J(0)|k,n\rangle|^2 \\ &= \sum_n \int_0^\infty dm^2 \int d^3\boldsymbol{k}\frac{\{\mathrm{e}^{-ikx}\theta(x^0)+\mathrm{e}^{ikx}\theta(-x^0)\}_{k^0=E_{m,\boldsymbol{k}}}}{2E_{m,\boldsymbol{k}}} \\ &\qquad \times|\langle 0|J(0)|k,n\rangle|^2_{k^0=E_{m,\boldsymbol{k}}}\ . \end{aligned} \tag{1.26}$$

At the second line, we have changed the coordinate system of the integrand by using m^2 instead of k^0, where $m^2=(k^0)^2-\boldsymbol{k}^2$. That is, after integrating it with respect to the three-momenta on a mass shell and we integrate it with respect to masss. $E_{m,\boldsymbol{k}}=\sqrt{m^2+\boldsymbol{k}^2}$ in the denominator comes from the Jacobian determinant for the variable translation. We implicitly utilize the assumption that an intrinsic value of four momentum lies on the forward light-cone, $k^0>0$ and $m^2>0$. It is one of the conditions called *spectral ansatz*, which is generally required to let the field theory to be physically meaningful. In fact, $|\langle 0|J(0)|k,n\rangle|^2_{k^0=E_{m,\boldsymbol{k}}}$ does not depend on three-momentum if it is on the same mass shell. To understand it, let us change the notation as $\langle 0|J(0)|k,n\rangle|_{k^0=E_{m,\boldsymbol{k}}} = \langle 0|J(0)|m^2,\boldsymbol{k},n\rangle$. In the Lorentz transformation, there definitely exists Λ satisfying

$$|m^2,\boldsymbol{k},n\rangle = U(\Lambda)\,|m^2,\boldsymbol{k'},n\rangle \tag{1.27}$$

for arbitrary $\boldsymbol{k}$ and $\boldsymbol{k'}$. Since the vacuum is Lorentz invariant and J is scalar, we obtain

$$\begin{aligned} \langle 0|J(0)|m^2,\boldsymbol{k},n\rangle &= \langle 0|U(\Lambda)U^\dagger(\Lambda)J(0)U(\Lambda)|m^2,\boldsymbol{k'},n\rangle & (1.28)\\ &= \langle 0|J(0)|m^2,\boldsymbol{k'},n\rangle\,. & (1.29)\end{aligned}$$

Because the amplitude does not depend on $\boldsymbol{k}$, Eq. (1.26) can be written as follows:

$$(2\pi)^3\sum_n\int dm^2|\,\langle 0|J(0)|m^2,n\rangle\,|^2\int\frac{d^3\boldsymbol{k}}{(2\pi)^3}\frac{\{\mathrm{e}^{-ikx}\theta(x^0)+\mathrm{e}^{ikx}\theta(-x^0)\}_{k^0=E_{m,\boldsymbol{k}}}}{2E_{m,\boldsymbol{k}}}.$$

The integrand is nothing but the definition of the Feynman propagator of the scalar field. Then finally we obtain

$$\langle 0|TJ(x)J(0)^\dagger|0\rangle=(2\pi)^3\sum_n\int dm^2|\,\langle 0|J(0)|m^2,n\rangle\,|^2\int\frac{d^4k}{(2\pi)^4}\frac{i\ \mathrm{e}^{-ikx}}{k^2-m^2+i\epsilon}. \quad (1.30)$$

So the correlation function in the momentum space is represented as follows:

$$\begin{aligned}\Pi(q^2) &= i\int d^4q\mathrm{e}^{iqx}\langle 0|TJ(x)J(0)^\dagger|0\rangle & (1.31)\\ &= (2\pi)^3\sum_n\int dm^2|\,\langle 0|J(0)|m^2,n\rangle\,|^2\frac{-1}{q^2-m^2+i\epsilon}. & (1.32)\end{aligned}$$

Further, we can obtain its imaginary part as follows:

$$\begin{aligned}\frac{1}{\pi}\mathrm{Im}\Pi(q^2) &= (2\pi)^3\sum_n\int dm^2|\,\langle 0|J(0)|m^2,n\rangle\,|^2\delta(q^2-m^2) & (1.33)\\ &\equiv \rho(q^2), & (1.34)\end{aligned}$$

where we used the identity $\mathrm{Im}[\frac{1}{x+i\epsilon}]=-\pi\delta(x)$. It is important that $|\,\langle 0|J(0)|m^2,n\rangle\,|^2$ is nonzero only when the state $|m^2,n\rangle$ has the same quantum numbers as J. Since we suppose that a hadron is a state in the complete set (or quantum superposition of them), the position of a peak appearing in $\rho(q^2)$ is nothing but the mass m^2 of the hadron which we are interested in. Furthermore if a continuum spectrum appears, we can regard it as two particle states whose total quantum numbers are same as J. So, the onset of continuum is the threshold where the two particles are created. By using the spectral representation, we can understand that the imaginary part of correlation function shows the property of the hadron. We usually call $\rho(q^2)$ *spectral function* and this is our main target.

1.5 Outline of this thesis

The thesis is organized as follows.

Chapter 1-3 are devoted to review. In Chapter 1, some basic topics in QCD are reviewed. In Chapter 2, the technique of QCD sum rule is briefly explained. In Chapter 3, operator product expansion in covariant gauge is explained.

Chapter 4-7 are the main parts of the studies in this thesis. In chapter 4, complex Borel sum rules (CBSR) is constructed and test analyses are given. In chapter 5, we apply CBSR to the charmonia at finite temperature. In Chapter 6, the technique for the partial infinite summation in the OPE is constructed and applied to the four typical light meson channels. In Chapter 7, the summary and conclusion of this thesis are given.

Chapter 2

Basics of QCD sum rules

2.1 Overview of QCD sum rules

QCD sum rules can be regarded as systems to obtain hadronic spectral functions from QCD [19, 20]. The systems consist of roughly two stages. The first one is the construction of integral rules for a hadronic spectral function from the first principle of QCD:

$$\mathcal{L}_{QCD} \quad \rightarrow \quad F(X) = \int_0^\infty \rho(s) K(s, X) ds, \tag{2.1}$$

where $F(X)$ is calculable but $\rho(s)$ is not. X represents the parameter of integral rules, e.g. the Borel mass. We sometimes refer to this equation itself as "sum rule". The second one is the determination of the spectral function from the obtained integral rules:

$$F(X) = \int_0^\infty \rho(s) K(s, X) ds \quad \rightarrow \quad \rho(s) = \cdots \tag{2.2}$$

This is a kind of the inverse problem. Therefore, in this stage, we can consider the problem separately from the details of the QCD calculation.

The construction of integral rules is, in principle, based on two important concepts: the *analyticity* and *factorization*. The analyticity of the correlation function gives the dispersion relation which is the relation between the integral value of the spectral function multiplied by an integral kernel and the correlation function. Thus we can construct the integral rule about a spectral function if an appropriate approximation for the correlation function in the hard region is given. Although a perturbative calculation in the hard region might work well because of the asymptotic freedom of QCD, it is known that a naive perturbation theory is insufficient to construct valid sum rules to determine a physical spectral function. It is understood that *non-perturbative* effects play important roles even when the momentum of the external line lies in the hard region. The momentum of the internal line in the loop integration generally runs over all the momentum region. When the internal momentum becomes soft, non-perturbative effects strongly contribute to correlation functions. Thus, the factorization strategy is employed to introduce such non-perturbative effects, resulting in the so-called operator product expansion (OPE). In this expansion, a correlation function can be expressed by the basic parameters of QCD (the quark masses and the coupling constant) and also additional parameters (the vacuum expectation values of composite operators). Actually the latter is an object reflecting the non-

perturbative effects, so that we can introduce non-perturbative effects by estimating their values from other theoretical approaches or phenomenology.

To determine the spectral function from the obtained integral rules, historically, a method called "one pole + continuum ansatz" has been used. In this method, the functional form of a spectral function is assumed to be one delta function and step function though a real spectral function must have more complicated structures. Nevertheless, such a simplified model is known to be successful to determine the mass of the ground state of the hadron. Recently, the application of the maximum entropy method (MEM) to QCD sum rules is suggested. In this method, we do not put any strong assumptions on the spectral function. We can, in principle, determine the mass of not only the ground state but also excited states by the MEM. However, it is known by some studies [21, 22] that only one peak is reproduced from the usual integral rule (Borel sum rules) with MEM. This problem is resolved by the generalization of Borel sum rules to the complex type, which is one of main topics in this thesis.

In early days, the technique of QCD sum rules was widely applied to various hadrons in vacuum [18–20, 23–48]. Later, they were also applied to hadrons at finite temperature [49–60] and density [61–88]. QCD sum rules are important tools even today especially for analyses at finite density. It is because the lattice QCD, another approach based on QCD, has the "sign problem" [89], which makes analyses at finite density by lattice QCD simulation almost impossible.

From the next section, we review the formalism of QCD sum rules and see the practical analyses.

2.2 Construction of sum rules

2.2.1 Dispersion relation

We implicitly assume the analyticity of a correlation function: The analytic continuation of the correlation function has no singularity on the complex plane except for the positive real axis where physical states lie. The residue theorem with this assumption leads to the equation

$$\Pi(q^2) = \oint_C \frac{1}{2\pi i} \frac{(q^2)^n \Pi(s)}{s^n (s - q^2)} ds, \tag{2.3}$$

where the contour C is shown in Fig. 2.1. n is a positive integer which is sufficiently large to eliminate the contribution from the circular path in the $R \to \infty$ limit.

Separating the contour into some parts and taking the limit ($R \to \infty$,$\epsilon \to +0$), we obtain the so-called dispersion relation:

$$\Pi(q^2) = \int_0^\infty \frac{\rho(s)}{s - q^2} ds + (\text{plynomial in } q^2), \tag{2.4}$$

where $\rho(s) \equiv \frac{1}{\pi}\text{Im}[\Pi(s)]$. This equation gives the relation between the integral value of the spectral function and the correlation function in the Euclidean region $q^2 < 0$. By calculating the left hand side in the asymptotic free region $1 \ll -q^2$, we can obtain the integral rules for the spectral function which contains the low energy region. The polynomial term in the right hand side can not be estimated by perturbative approaches since it contains the contribution from the low energy region. However, this troublesome extra term can be eliminated as will explained later. The detailed derivation of the dispersion relation is given in Appendix A.

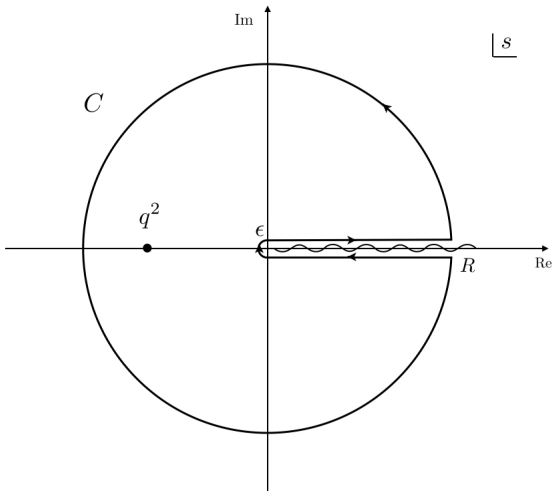

Figure 2.1: The contour integral C on the complex plane. The wavy line denotes the non-analytic cut (or poles) of $\Pi(q^2)$ on the positive side of the real axis.

2.2.2 Operator product expansion

By the asymptotic freedom in QCD, there is a chance that we can estimate the correlation function in the left hand side of Eq. (2.4) in the deep Euclidean region by the perturbation theory. Nevertheless, non-perturbative effects can participate even if the momentum of the external line is sufficiently large and are known to be negligible. Such effects come from the interval of the loop integration where the momentum is soft. The effects are related with the unphysical pole of the effective coupling constant in the lower energy region. In QCD sum rules, therefore, we do not employ the usual perturbation theory. To introduce non-perturbative effects, we separate the region of integration into the soft and hard parts and estimate each part by different approaches. For the hard region, we employ the perturbation supposing there are not large contributions from non-perturbative effects. For the soft energy region, we perform the power expansion with respect to a soft momentum, so that non-perturbative effects can be approximately introduced by vacuum expectation values of some operators. The above treatment, in fact, results in the so-called operator product expansion (OPE). In this section, we explain only the symbolical expression of the OPE. The more detailed discussion and calculation technique will be given in the next chapter, to understand that the significance of OPE is nothing but the scale factorization.

Symbolical expression of the OPE

The OPE is originally Wilson's assumption [90]. Let us consider two operators, $A(x)$ and $B(0)$. When the distance of the space-time coordinates become very close, their product can be expanded into the summation of local operators multiplied by coefficients as follows:

$$\mathrm{T}[A(x)B(0)] \xrightarrow{x\to 0} \sum_i C_i(x) O_i\Big(\frac{x}{2}\Big). \tag{2.5}$$

C_i is the C-number coefficient called Wilson coefficient. If this expansion is applied to $T[J(x)J^\dagger(0)]$ and the Fourier transformation is taken, the following expression is obtained for the correlation function.

$$\Pi(q^2) \xrightarrow{|q^2|\to\infty} \sum_i \tilde{C}_i(q^2)\langle 0|O_i|0\rangle \equiv \Pi^{\mathrm{OPE}}(q^2). \tag{2.6}$$

Here $\tilde{C}_i(q^2) = i\int d^4x \mathrm{e}^{iqx} C_i(x)$. The large $|q^2|$ limit corresponds to the short distance limit between the two points in the position space. This expansion is also regarded as an expansion by order of the dimension of local operators. Because each term should have the same mass dimension as the correlator, the dimension of the coefficient is determined by that of the operator. Supposing that the correlator has dimension D and the local operator has the dimension d, the coefficient C must have dimension $(D-d)$. Thus, the coefficient C behaves as the $(\frac{1}{q^2})^{(d-D)/2}$, so that higher dimensional terms are suppressed in the large q^2. O_0 is the identity operator in QCD and its Wilson coefficient is the perturbative series. The other operator O_i's consist of quark and gluon operators and their vacuum expectation values are generally called "vacuum condensate", e.g. quark condensate $\langle\bar{q}q\rangle$, gluon condensate $\langle G^2\rangle$ and so on. They are objects which reflect non-perturbative effects in the OPE. But some of them vanish, when they are sandwiched by the vacuum, due to the symmetries of QCD. Practically we calculate only the Wilson coefficients up to some dimension and treat condensates as additional parameters of QCD. Although we can,

in principle, obtain their values from QCD, we do not have any analytic approaches for them because they are non-perturbative objects. In QCD sum rules, the left hand side in Eq. (2.4) is symbolically obtained by the OPE as follows:

$$\Pi^{\mathrm{OPE}}(q^2; m, g, \langle\bar{q}q\rangle, \langle G^2\rangle, \cdots) = \int_0^\infty \frac{\rho(s)}{s - q^2} ds + (\text{ploynomial in } q^2), \tag{2.7}$$

where m is the quark mass and g is the coupling constant. In addition to such fundamental parameters of QCD, the left hand side explicitly depends on condensates which are not fundamental parameters. Since, for example, $\langle\bar{q}q\rangle$ is the order parameter of the spontaneous chiral symmetry breaking, this equation gives the relation between hadron properties and the spontaneous chiral symmetry breaking. Similar interpretations are possible for other condensates if they have such physical meanings. Given the value of condensate, this equation can be regarded as the integral rules for the hadronic spectral function. However, this integral rule must be improved to eliminate the polynomial terms.

2.2.3 Borel sum rules

We have already derived the sum rules Eq. (2.7) by using the dispersion relation and the OPE. However, it includes the unknown polynomial term which generally diverges. Even if we regularize it by a certain regularization technique, the remaining finite part depends on the regularization point and the scheme. To avoid such ambiguities, we generally must eliminate the polynomial terms by doing differentiation some times. For the meson case, only the one-time differentiation is enough. Then the simplest sum rule is

$$\frac{\partial \Pi(q^2)}{\partial q^2} = \int_0^\infty \frac{\rho(s)}{(s-q^2)^2} ds \ . \tag{2.8}$$

We can repeat differentiation and it leads to the so-called moment sum rules.

There are other types of improved sum rules: Borel sum rules, Gaussian sum rules and phase rotated sum rules. Since Borel transformed sum rules are conventionally used for some technical reasons, we here briefly explain its formalism. The Borel transformation can eliminate ambiguities coming from polynomial terms, regardless of the order of the power in polynomial terms. Furthermore, convergence of the OPE gets better by the Borel transformation. The Borel transformation for a real variable X is defined by the operator as

$$\hat{B}_{[X]} = \lim_{\substack{X,n\to\infty \\ X/n=M^2}} \frac{X^n}{(n-1)!}\Big(-\frac{\partial}{\partial X}\Big)^n. \tag{2.9}$$

Setting $X = -q^2$ and applying this transformation to Eq. (2.7), the polynomial terms are eliminated by the infinite order differential. By assuming that the Borel transformation is commutative to the integration, we obtain the Borel sum rules:

$$G^{\rm OPE}(M^2; m, g, \langle q\bar{q}\rangle, \langle GG\rangle, \cdots) = \frac{1}{M^2}\int_0^\infty \mathrm{e}^{-s/M^2}\rho(s) ds, \tag{2.10}$$

where $G^{\rm OPE}(M^2) \equiv \hat{B}_{[-q^2]}\Pi^{\rm OPE}(q^2)$ and we used the formula:

$$\hat{B}_{[-q^2]}\frac{1}{s-q^2} = \frac{1}{M^2}\mathrm{e}^{-s/M^2}. \tag{2.11}$$

Note that the original parameter q^2 in the dispersion relation is transformed into M^2 which is called Borel mass. By the formula

$$\hat{B}_{[-q^2]}\frac{1}{(q^2)^n} = \frac{(-1)^n}{n!}\frac{1}{(M^2)^n}, \tag{2.12}$$

we find that the convergence of the OPE is actually improved by the Borel transformation. Namely higher dimensional terms in the original OPE are suppressed by the factorial coefficients. To calculate the Borel transformation of a function there are two ways. One is naively using its definition Eq. (2.9). In the other way, we employ the dispersion relation again. For functions which have the same analyticity as the correlation function, we have

$$f(q^2) = \int_0^\infty \frac{1}{\pi}\frac{\mathrm{Im} f(s+i\epsilon)}{s-q^2} ds + (\text{polynomial term}) \ . \tag{2.13}$$

By performing the Borel transformation to each side and, we have the general formula:

$$\hat{B}_{[-q^2]}f(q^2) = \int_0^\infty \frac{1}{\pi}\mathrm{Im}f(s+i\epsilon)\frac{1}{M^2}\mathrm{e}^{-s/M^2}ds, \tag{2.14}$$

where we used Eq. (2.11). The polynomial term of the right hand side vanishes by the Borel transformation.

2.2.4 Condensate

Finally, to get the integral rules, we have to know the values of condensates. We summarize the value of typical condensates.

The quark condensate $\langle\bar{q}q\rangle$ is the lowest dimensional condensate among gauge invariant ones in QCD. The most famous way to determine its value is using the Gell-Mann-Oakes-Rennet (GMOR) relation [91] as follows:

$$m_\pi^2 f_\pi^2 = -2(m_u + m_d)\langle\bar{q}q\rangle \quad (q = u, d), \tag{2.15}$$

where m_π, f_π, m_u and m_d are the pion mass, pion decay constant, up and down quark masses, respectively. Using this relation and the phenomenological values of the other parameters, we obtain

$$\langle\bar{q}q\rangle = -(240 \pm 10\mathrm{MeV})^3, \tag{2.16}$$

where we supposed the flavor SU(2) symmetry. Note that this is the value normalized at 1GeV. Recently, the lattice QCD simulations, e.g. [92,93], also estimate the value of $\langle q\bar{q}\rangle$ with a smaller error. Since $\langle\bar{q}q\rangle$ is an order parameter of the spontaneous chiral symmetry breaking, non-vanishing $\langle\bar{q}q\rangle$ is believed to be the origin of the much larger hadron mass generation than the light quark masses. On the other hand, it must vanish when the chiral symmetry is completely restored. Actually, the investigation using the chiral effective theory [94] and the lattice QCD simulation [95] elucidated the chiral symmetry restoration at finite temperature.

When we analyze hadrons including the strange quarks, the value of the strange quark condensate is also necessary. The various values are reported as the ratio to the quark condensate in QCD sum rules analyses [96–103]. Among them, the standard value is estimated in analyses of strange baryons [96], resulting in

$$\frac{\langle\bar{s}s\rangle}{\langle\bar{q}q\rangle} = 0.8 \pm 0.2\ . \tag{2.17}$$

The next higher dimensional condensate is $\langle\frac{\alpha_s}{\pi}G^2\rangle \equiv \langle\frac{\alpha_s}{\pi}G^{a\mu\nu}G^a_{\mu\nu}\rangle$ whose dimension equals four. The value of this condensate is estimated by QCD sum rules analyses of charmonium [19]. Because the charmonium condensate $\langle\bar{c}c\rangle$ can be transformed into $\langle\frac{\alpha_s}{\pi}G^2\rangle$ by the heavy quark expansion [19], $\langle\frac{\alpha_s}{\pi}G^2\rangle$ only appears as the condensate in the OPE. Thus, we determined its value so that the experimental value of the charmonium mass is well reproduced by the QCD sum rules, resulting in

$$\langle\frac{\alpha_s}{\pi}G^2\rangle = 0.012 \pm 0.004\mathrm{GeV}^4\ . \tag{2.18}$$

The theoretical value of the gluon condensate has an ambiguity as other values are reported in Ref. [104, 105]

2.3 Determination of spectral function from sum rules

Since sum rules are just integral rules for the spectral function, we need a method to determine the spectral function from obtained sum rules. Let us review the conventional method called "one pole + continuum ansatz" and novel one called "maximum entropy method (MEM)".

2.3.1 One pole + continuum ansatz

The characteristic of this model is that we assume the functional form of the spectral function to be only one sharp peak plus continuum state with a threshold as follows:

$$\rho(s) = \lambda\delta(s - m_h^2) + \theta(s - s_0)\frac{1}{\pi}\mathrm{Im}\Pi^{pert.}(s). \tag{2.19}$$

where $\Pi^{pert.}(s)$ is the perturbative term in the OPE. The three free parameters of the hadron mass m^2, residue λ and threshold parameter s_0 are determined so that obtained sum rules are well satisfied in the following manner. Substituting Eq. (2.19) into the Borel sum rules Eq. (2.10), we obtain

$$\lambda\,\mathrm{e}^{-m^2/M^2} = G(M^2) - \frac{1}{\pi}\int_{s_0}^{\infty}\mathrm{e}^{-s/M^2}\mathrm{Im}\Pi^{pert.}(s)ds. \tag{2.20}$$

Differentiating this equation with respect to $1/M^2$, we get

$$m^2\,\lambda\,\mathrm{e}^{-m^2/M^2} = -\frac{\partial G(M^2)}{\partial(1/M^2)} - \frac{1}{\pi}\int_{s_0}^{\infty} s\,\mathrm{e}^{-s/M^2}\mathrm{Im}\Pi^{pert.}(s)ds. \tag{2.21}$$

Finally, Eq. (2.21) divided by Eq. (2.20) results in the hadron mass as the function with the variable of the Borel mass as follows:

$$m^2 = \frac{-\frac{\partial G(M^2)}{\partial(1/M^2)} - \frac{1}{\pi}\int_{s_0}^{\infty} s\,\mathrm{e}^{-s/M^2}\mathrm{Im}\Pi^{pert.}(s)ds}{G(M^2) - \frac{1}{\pi}\int_{s_0}^{\infty}\mathrm{e}^{-s/M^2}\mathrm{Im}\Pi^{pert.}(s)ds} \equiv \tilde{m}^2(M^2). \tag{2.22}$$

Since m^2 is constant, the right hand side of Eq. (2.22) also should be so. However, it clearly depends on the Borel mass M and s_0, so that we usually pick up a finite region of the Borel mass and a certain s_0 where the function $\tilde{m}^2(M^2)$ approximately behaves as a constant and employ the value of constant as the physical hadron mass. For example, when the OPE in the ρ meson channel is calculated as follows:

$$\Pi^{OPE}(q^2) = -\frac{1}{4\pi^2}\log(-q^2) + \frac{1}{12(q^2)^2}\langle\frac{\alpha_s}{\pi}G^2\rangle + \frac{32\pi\alpha_s}{9(q^2)^3}\langle q\bar{q}\rangle^2, \tag{2.23}$$

$\tilde{m}^2(M^2)$ behaves as shown in Fig. 2.2. At $s_0 = 1.5\mathrm{GeV}^2$, the curve seems to be almost flat in the plotted region, so that the value of about 0.65 GeV^2 is regarded as m^2. This is consistent with the experimental value of $m_\rho^2 = 0.59\mathrm{GeV}^2$.

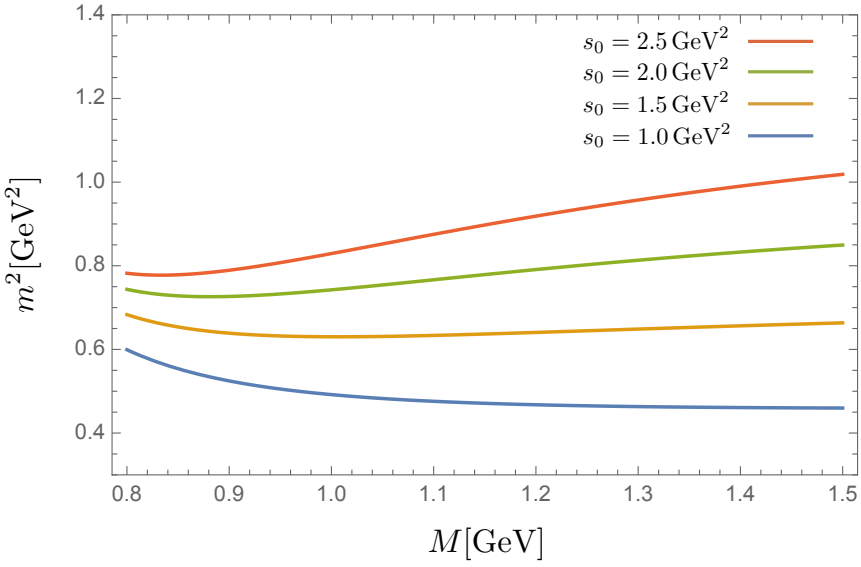

Figure 2.2: Borel curve at the various threshold parameters.

2.3.2 Maximum entropy method

The maximum entropy method enables us to determine the spectral function without reducing its parameter space to specific functional forms such as "pole + continuum" ansatz, by the help of the Bayesian probability theory. In MEM, a function which maximizes Q, defined below, is determined as the spectral function.

$$Q[\rho] = \alpha S[\rho] - L[\rho]. \tag{2.24}$$

The detailed derivation is given in Ref. [106]. Let us here mention that in actual analyses we do not investigate $\rho(s)$ but the corresponding spectral function whose argument is ω ($= \sqrt{s}$). Hence, we will use $\rho(\omega)$ from now on. $S[\rho]$ stands for the Shannon-Jaynes entropy. This term insures the positive definiteness of the spectral function because of the logarithm in its definition:

$$S[\rho] = \int_0^\infty d\omega[\rho(\omega) - m(\omega) - \rho(\omega)\log\frac{\rho(\omega)}{m(\omega)}]. \tag{2.25}$$

Here, $m(s)$ is some positive definite function called default model, which is an input of the MEM framework. $S[\rho]$ takes its maximum value when $\rho(\omega) = m(\omega)$. In this method, thus, the spectral functions is determined as $m(\omega)$ if there is not $L(\rho)$. In this sense, we usually choose $m(\omega)$ as some function which approximates the asymptotic form of the spectral function in the higher energy region. The dependence of the determined spectral function on its choice should be usually examined in the analyses.

$L[\rho]$ is called likelihood function. This term contains all the information provided by the sum rules. In the case of the Borel sum rules, it is expressed as

$$L[\rho] = \frac{1}{2N}\sum_i \frac{|G^{OPE}(M_i^2) - \int_0^\infty d\omega\, 2\omega \frac{1}{M_i^2}\mathrm{e}^{-\omega^2/M_i^2}\rho(\omega)|^2}{\sigma_i^2}, \tag{2.26}$$

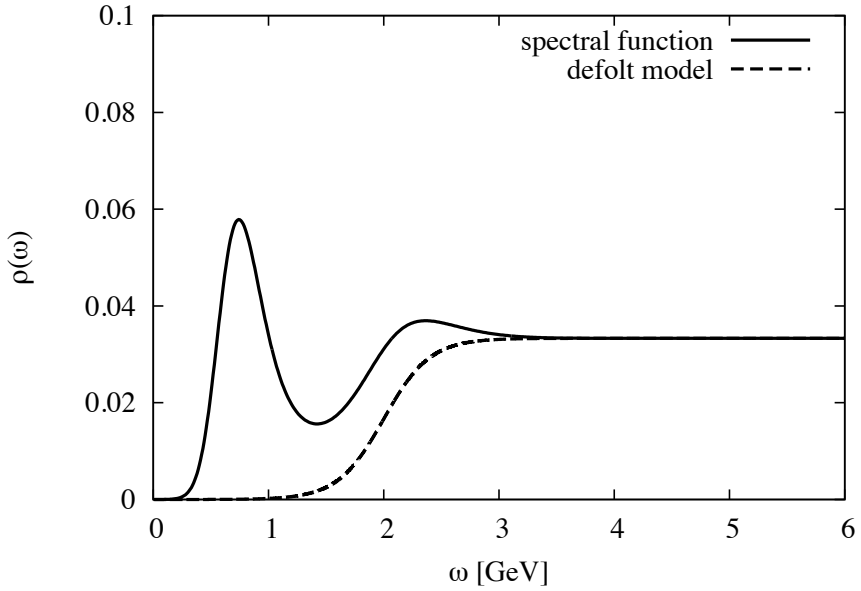

Figure 2.3: ρ meson spectral function determined by MEM.

where the subscript i specifies the discretized Borel mass. The lower limit of the Borel mass is systematically determined by considering the convergence of the OPE. On the other hand, there are no such ways for the upper limit, so that we usually choose the typical one and check that the spectral function does not strongly depend on the choice. σ_i is the error of the OPE data $G^{\mathrm{OPE}}(M_i^2)$, which is determined by the uncertainties of the vacuum condensates and other input parameters, e.g. the quark masses and the coupling constant. N is the number of discretized Borel masses. Note that the MEM is consistent with the chi-square fitting if the entropy term S is ignored.

Considering both the two terms, it can be understood that in the MEM we do an analysis like a chi-square fitting with the constraint of positive definiteness on a spectral function. α is a positive real number and in principle a free parameter, on which the spectral function maximizing $Q[\rho]$ depends. However, it is possible to systematically determine its range and to calculate a weighted average of the obtained spectral functions over α, which gives the final solution. For the details of this procedure, we refer to [21, 106].

For example, the ρ meson spectral function determined by MEM is shown in Fig. 2.3, where we used the Borel sum rule with the same OPE as Eq. (2.23). The region of the Borel mass is chosen to be $0.8\,\mathrm{GeV} < M < 1.3\,\mathrm{GeV}$. Looking at this figure, we observe a peak in the lower energy region. Its position is about $0.74\,\mathrm{GeV}$, which agrees well with the ρ-meson mass $0.77\,\mathrm{GeV}$.

Chapter 4

Development of complex Borel sum rules

Borel transformed QCD sum rules conventionally use a real valued parameter (the Borel mass) for specifying the exponential weight over which hadronic spectral functions are averaged. In this chapter, it is shown that the Borel mass can be generalized to have complex values and that new classes of sum rules can be derived from the resulting averages over the spectral functions. The real and imaginary parts of these novel sum rules turn out to have damped oscillating kernels and potentially contain a larger amount of information on the hadronic spectrum than the real valued QCD sum rules. As a first practical test, we have formulated the complex Borel sum rules for the ϕ meson channel and have analyzed them using the maximum entropy method, by which we can extract the most probable spectral function from the sum rules without strong assumptions on its functional form. As a result, it is demonstrated that, compared to earlier studies, the complex valued sum rules allow us to extract the spectral function with a significantly improved resolution and thus to study more detailed structures of the hadronic spectrum than previously possible.

4.1 Introduction

The spectral function of hadrons is one of the main targets in studies of low energy QCD. At low energy, non-perturbative approaches are inevitable as the coupling constant is large and the QCD vacuum has non-trivial quark and gluon condensates. In order to take into account effects of these vacuum condensates, QCD sum rules [19, 20, 96] have been extensively used to explore hadron spectra.

QCD sum rules utilize the operator product expansion (OPE) for evaluating correlation functions, which is valid in the deep Euclidean four-momentum region. A dispersion relation based on analyticity of the correlation function on the other hand yields a relation between an integral over the spectral function and the vacuum condensates. Inverting the integral relation and extracting the spectral function thus is the central issue of QCD sum rule analyses. In conventional approaches, the spectral function is most often parametrized using a "pole + continuum" functional form, whose parameters are determined to satisfy the sum rule. This technique is, however, not always applicable because in reality the spectral functions are not restricted to a particular shape.

Recently, a new method was proposed that directly provides the spectral function without assuming a functional shape [21]. It utilizes the maximum entropy method (MEM), which generally helps to determine the most probable spectral function from an integral relation [106].

Thus, the obtained spectral function is chosen from infinitely many functional forms, while the conventional approach only gives the best fitted "pole + continuum" type function. So far, this novel method has been applied to the ρ-meson [21] and nucleon [22,117] channels in vacuum and to charmonium [59] and bottomonium [60] channels at finite temperature. It has, however, not yet shown its full strength, giving only the ground state peak structure, while usually neither reproducing excitation nor continuum spectra. We believe that this is not a consequence of the limitation of MEM, but rather due to the limited information provided by the conventional QCD sum rules.

In this chapter, we propose to extend the QCD sum rules to the complex plane of the squared-momentum, $z = q^2$, by which we are able to extract more information on the spectral function.* As the sum rules are based on the analytic continuation of the correlation function on the q^2 plane, they can be naturally generalized to the complex plane. As a result, it is found that after using the Borel transform to enhance the convergence of the OPE, the Borel sum rule is valid also for the complex Borel parameter.

Applying the MEM to the newly constructed sum rules, we study the spectral function of the vector meson composed of the strange quark ($s\bar{s}$), i.e. the spectral function in the ϕ meson channel. Our results show that the new sum rule improves the reproducibility of the spectral function compared to the conventional Borel sum rules, in particular in the large momentum region.

This chapter is organized as follows. In Section 4.2, we explain the central idea of our novel complex Borel plane sum rules, demonstrate in detail how the sum rules are constructed and discuss their properties. After all, it will be shown that our formulation can be considered to be just a simple generalization of conventional Borel sum rules to complex Borel mass values. Next, we briefly introduce MEM and define the likelihood function for the complex Borel plane sum rules to apply MEM to them in Section 4.3. In Section 4.4 the results of the analyses are outlined. Here, we will not only show the results of the complex Borel plane sum rules but also the ones of the original Borel sum rules for comparison. Summary and conclusions are given in Section 4.6.

4.2 Complex Borel sum rules

In this section, we formulate the complex Borel sum rules (CBSR). The general procedure is the same as that used for deriving the conventional QCD sum rules with real variables (RBSR).

4.2.1 Dispersion relation on the complex plane

The basic idea of the CBSR is to consider the squared four-momentum q^2 as a complex parameter when deriving the sum rules. The validity of this generalization is guaranteed by the dispersion relation.

The elementary ingredients of the derivation, Cauchy's residue theorem and the analyticity of the correlator, do not restrict q^2 to real numbers but rather allow it to have any value on the complex plane except the region around the positive real axis (see Fig. 4.1). In other words, for the correlator $\Pi(q^2)$, Cauchy's residue theorem and analyticity guarantee

$$\Pi(z) = \frac{1}{2\pi i} \oint_C \frac{z^n \Pi(s)}{s^n (s - z)} ds, \tag{4.1}$$

*Extension of QCD to the complex q^2 plane has been proposed earlier by Ioffe and Zyablyuk [118].

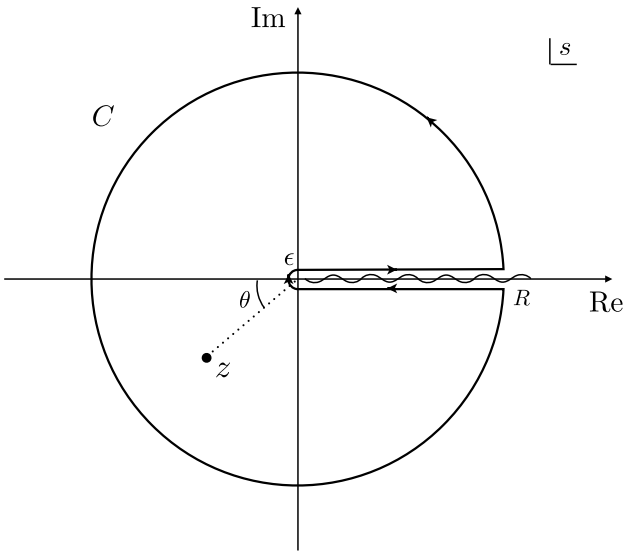

Figure 4.1: The contour integral C on the complex plane of the variable s, used in Eq.(4.1). For the actual calculations, the radius of the outer circle of C is taken to infinity. The wavy line denotes the non-analytic cut (or poles) of $\Pi(s)$ on the positive side of the real axis.

for any complex $z = q^2$. Here, n is a positive integer, chosen to be large enough for the integral to converge. The detailed definition of the $\Pi(q^2)$ depends on the specific channel. In the case of the vector channel, which will be studied in this chapter, $\Pi(q^2)$ can be defined as shown in Eq.(21). Following the same steps used when deriving the conventional sum rules, we obtain the following dispersion relation (see Appendix A for details):

$$\Pi(z) = \int_0^\infty \frac{\rho(s)}{s - z} ds + (\text{polynomial in } z), \tag{4.2}$$

where $\rho(s) = \frac{1}{\pi}\text{Im}\,\Pi(s + i\epsilon)$ (for a real s and an infinitesimal ϵ (> 0)) is the spectral function. Although this looks just like the conventional diversion relation, it potentially contains novel kinds of sum rules for the spectral function, extracted from both its real and imaginary parts. Our strategy is employing Eq.(4.2) as a starting point for deriving the actual sum rules.

4.2.2 Analytic continuation of the OPE

In QCD sum rules, it is common to replace the left hand side of Eq.(4.2) by its respective OPE, which is valid in the deep Euclidean region, i.e. large real $(-q^2)$. Extending this to the complex plane, we consider the OPE for the complex variable $z = q^2$. In practice, the OPE must be truncated at a certain operator dimension and one can only hope that it converges at sufficiently large $(-q^2)$. In the region where the OPE is convergent, the left hand side of Eq.(4.2) can be extended to the complex argument z as $\Pi^{\text{OPE}}(z)$, which is the analytically continued function of $\Pi^{\text{OPE}}(q^2)$. It is important to note that $\Pi^{\text{OPE}}(q^2)$ depends on q^2 only through the Wilson coefficients and therefore has the same vacuum expectation values of the local operators. After all, we obtain the complex sum rules as,

$$\Pi^{\text{OPE}}(z) = \int_0^\infty \frac{\rho(s)}{s - z} ds + (\text{polynomial in } z). \tag{4.3}$$

4.2.3 Borel transformation

The unknown polynomial in Eq.(4.3) can be removed by the Borel transform, defined by

$$\hat{B}_{[X]} = \lim_{\substack{X,n\to\infty \\ X/n=M^2}} \frac{X^n}{(n-1)!}\Big(-\frac{\partial}{\partial X}\Big)^n, \tag{4.4}$$

where X is a real variable.

By substituting $z = |z|\mathrm{e}^{i(\theta-\pi)}$, where θ is defined as shown in Fig. 4.1, Eq.(4.3) can be considered as a relation depending on $|z|$ and θ. As polynomials in z are linear combinations of $|z|^k\mathrm{e}^{ik(\theta-\pi)}$, differentiating Eq.(4.3) infinite times by $|z|$ eliminates them. It is hence understood that $\hat{B}_{[|z|]}$ is suitable for our present purposes. On the right hand side of Eq.(4.3), the integral term is transformed as

$$\begin{aligned}
\hat{B}_{[|z|]}\int_0^\infty \frac{\rho(s)}{s-z}ds &= \lim_{\substack{|z|,n\to\infty \\ |z|/n=M^2}} \frac{|z|^n}{(n-1)!}\Big(-\frac{\partial}{\partial|z|}\Big)^n \int_0^\infty \frac{\rho(s)}{s-z}ds \\
&= \lim_{\substack{|z|,n\to\infty \\ |z|/n=M^2}} \frac{|z|^n}{(n-1)!}\int_0^\infty \frac{n!\mathrm{e}^{in\theta}}{(s+|z|\mathrm{e}^{i\theta})^{n+1}}\rho(s)ds \\
&= \lim_{\substack{|z|,n\to\infty \\ |z|/n=M^2}} \frac{n}{|z|\mathrm{e}^{i\theta}}\int_0^\infty \Big(\frac{|z|\mathrm{e}^{i\theta}}{s+|z|\mathrm{e}^{i\theta}}\Big)^{n+1}\rho(s)ds \\
&= \lim_{n\to\infty} \frac{1}{M^2\mathrm{e}^{i\theta}}\int_0^\infty \Big(1+\frac{1}{n}\frac{s}{M^2\mathrm{e}^{i\theta}}\Big)^{-(n+1)}\rho(s)ds.
\end{aligned} \tag{4.5}$$

The integral kernel is transformed into an exponential function *if* the limit $n\to\infty$ can be interchanged with the integral over s. At first sight, this seems to be a trivially allowed manipulation, but a careful inspection, in fact, shows that it is not necessarily correct. Relying on a theorem (which is similar to Lebesgue's "dominated convergence theorem"), it is possible to show that the two operations indeed can be interchanged for $\cos\theta > 0$. An explicit proof of this statement is given in Appendix B. On the other hand, for $\cos\theta < 0$, one sees that the $n\to\infty$ limit and the integral over s are not interchangeable. This is so because if one could interchange the limit with the integral, the ensuing integrand would diverge exponentially at large $s\to\infty$, which is apparently inconsistent with the left hand side, which remains finite for $\cos\theta < 0$, as we will see in the discussion given below. We thus conclude that only for $\cos\theta > 0$, the Borel transform leads to the following result:

$$\hat{B}_{[|z|]}\int_0^\infty \frac{\rho(s)}{s-z}ds = \frac{1}{M^2\mathrm{e}^{i\theta}}\int_0^\infty \mathrm{e}^{-s/(M^2\mathrm{e}^{i\theta})}\rho(s)ds. \tag{4.6}$$

Note that this region includes $\cos\theta = 1$ ($\theta = 0$), which gives the RBSR.

Next, let us discuss the Borel transformation of the left hand side of Eq.(4.3). As above, we substitute $z = |z|\mathrm{e}^{i(\theta-\pi)}$ into the given analytically continued OPE expression and then apply

$\hat{B}_{[|z|]}$. Doing this, we obtain

$$\begin{aligned}
\hat{B}_{[|z|]}\, z^k &= 0, \\
\hat{B}_{[|z|]} \left(\frac{1}{z}\right)^k &= \frac{(-1)^k}{(k-1)!}\Big(\frac{1}{M^2 \mathrm{e}^{i\theta}}\Big)^k, \\
\hat{B}_{[|z|]}\, z^k \ln\left(-\frac{z}{\mu^2}\right) &= -k!(M^2\mathrm{e}^{i\theta})^k, \\
\hat{B}_{[|z|]} \left(\frac{1}{s-z}\right)^k &= \frac{1}{(k-1)!}\frac{1}{(M^2\mathrm{e}^{i\theta})^k}\mathrm{e}^{-s/(M^2\mathrm{e}^{i\theta})},
\end{aligned} \tag{4.7}$$

for which detailed derivations are given in Appendix C. Here let us compare these results with the following pre-existing formulae for the corresponding real functions:

$$\begin{aligned}
\hat{B}_{[-q^2]}\, (q^2)^k &= 0, \\
\hat{B}_{[-q^2]} \left(\frac{1}{q^2}\right)^k &= \frac{(-1)^k}{(k-1)!}\Big(\frac{1}{M^2}\Big)^k, \\
\hat{B}_{[-q^2]}\, (q^2)^k \ln\left(-\frac{q^2}{\mu^2}\right) &= -k!(M^2)^k, \\
\hat{B}_{[-q^2]} \left(\frac{1}{s-q^2}\right)^k &= \frac{1}{(k-1)!}\frac{1}{(M^2)^k}\mathrm{e}^{-s/(M^2)}.
\end{aligned} \tag{4.8}$$

These all suggest that the Borel transformation of the analytically continued of OPE equals that of the original OPE with a complex valued Borel mass. We can thus set

$$\hat{B}_{[|z|]}\Pi(z) = G^{\mathrm{OPE}}(M^2\mathrm{e}^{i\theta}), \tag{4.9}$$

where $G^{\mathrm{OPE}}(M^2)$ is defined as $G^{\mathrm{OPE}}(M^2) \equiv \hat{B}_{[-q^2]}\Pi^{\mathrm{OPE}}(q^2)$.

Finally, we obtain

$$G^{\mathrm{OPE}}(\mathcal{M}^2) = \frac{1}{\mathcal{M}^2}\int_0^\infty \mathrm{e}^{-s/\mathcal{M}^2}\rho(s)ds \qquad (\mathrm{Re}[\mathcal{M}^2] > 0) \tag{4.10}$$

where $\mathcal{M}^2 \equiv M^2\mathrm{e}^{i\theta}$. This form of the complex plane QCD sum rule is nothing but the well known real valued Borel sum rule, in which the real Borel mass is replaced by its complex analogue, $\mathcal{M}^2$. Therefore, the complex Borel plane sum rules is found to be a simple generalization of the ordinary Borel sum rules to the complex Borel mass plane and of course includes the latter at $\theta = 0$.

4.2.4 Properties of the CBSR

Although the CBSR of Eq.(4.10) looks similar to its real counterpart, its content is quite different. Since Eq.(4.10) is complex valued, it simultaneously gives two sum rules which can be obtained from its real and imaginary part. Specifically, we have

$$\begin{cases}
\mathrm{Re}[G^{\mathrm{OPE}}(\mathcal{M}^2)] &= \displaystyle\int_0^\infty K^{\mathrm{R}}(\mathcal{M}^2; s)\rho(s)ds, \\
\mathrm{Im}[G^{\mathrm{OPE}}(\mathcal{M}^2)] &= \displaystyle\int_0^\infty K^{\mathrm{I}}(\mathcal{M}^2; s)\rho(s)ds,
\end{cases} \tag{4.11}$$

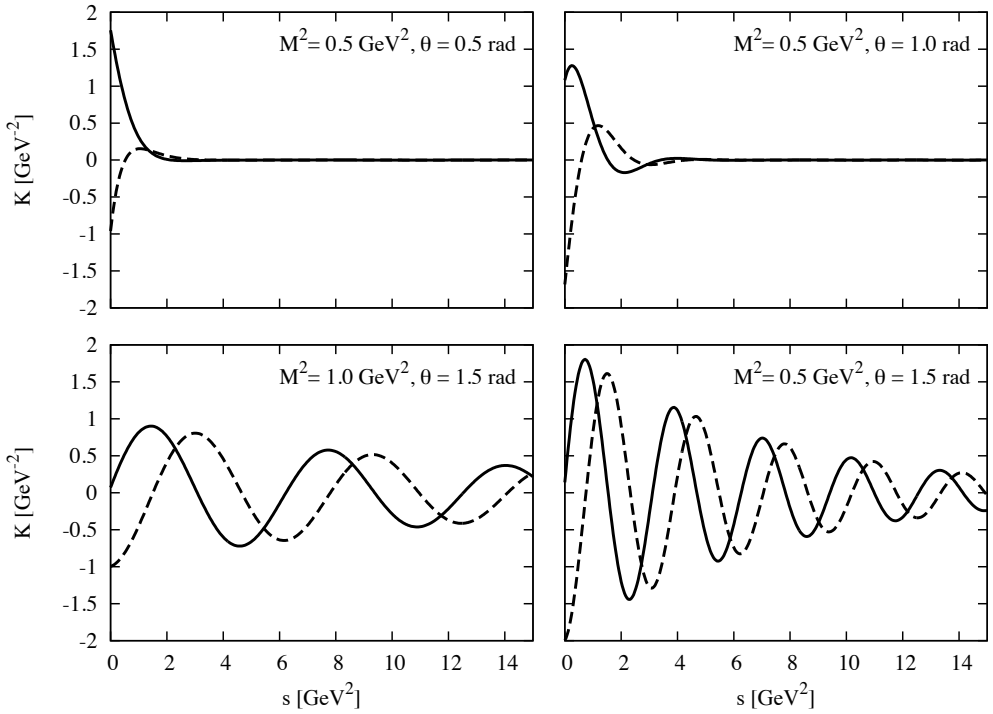

Figure 4.2: The kernels $K^{\mathrm{R}}(\mathcal{M}^2;s)$ (solid lines) and $K^{\mathrm{I}}(\mathcal{M}^2;s)$ (dashed lines), shown as a function of s, for various values of θ and M^2.

where $K^{\mathrm{R}}(\mathcal{M}^2;s)$ and $K^{\mathrm{I}}(\mathcal{M}^2;s)$ are defined as

$$\begin{aligned} K^{\mathrm{R}}(\mathcal{M}^2;s) &\equiv \mathrm{Re}\Big[\,\frac{1}{\mathcal{M}^2}\,\mathrm{e}^{-s/\mathcal{M}^2}\,\Big] \\ &= \frac{1}{M^2}\mathrm{e}^{-(\cos\theta/M^2)s}\cos\big[\,(\sin\theta/M^2)s-\theta\,\big], \end{aligned} \tag{4.12}$$

$$\begin{aligned} K^{\mathrm{I}}(\mathcal{M}^2;s) &\equiv \mathrm{Im}\Big[\,\frac{1}{\mathcal{M}^2}\,\mathrm{e}^{-s/\mathcal{M}^2}\,\Big] \\ &= \frac{1}{M^2}\mathrm{e}^{-(\cos\theta/M^2)s}\sin\big[\,(\sin\theta/M^2)s-\theta\,\big]. \end{aligned} \tag{4.13}$$

Both K^{R} and K^{I} are damped oscillating functions of s, as shown in Fig. 4.2 for several combinations of M^2 and θ. As can be observed in these plots, the oscillations have various frequencies, phases and damping factors depending on the values of M^2 and θ. We can hence expect that, compared with the RBSR, the sum rules with these kernels have the potential to resolve finer structures of the spectral function.

As a further point, let us note here that the sum rules with complex Borel masses and their complex conjugates are not independent. Looking at the explicit form of the kernels, it is clear that the right hand sides of the sum rules with complex conjugated Borel masses satisfy

$$\begin{cases} \displaystyle\int_0^\infty K^{\mathrm{R}}(\overline{\mathcal{M}^2};s)\rho(s)ds &= \displaystyle\int_0^\infty K^{\mathrm{R}}(\mathcal{M}^2;s)\rho(s)ds, \\ \displaystyle\int_0^\infty K^{\mathrm{I}}(\overline{\mathcal{M}^2};s)\rho(s)ds &= -\displaystyle\int_0^\infty K^{\mathrm{I}}(\mathcal{M}^2;s)\rho(s)ds. \end{cases} \tag{4.14}$$

In turn, the left hand side satisfies, according to the Schwarz reflection principle,

$$G^{\mathrm{OPE}}(\overline{\mathcal{M}^2}) = \overline{G^{\mathrm{OPE}}(\mathcal{M}^2)}. \tag{4.15}$$

Therefore the complex Borel sum rules are in essence identical to their complex conjugated counterparts.

4.2.5 Effective domain in complex Borel space

It is important to specify the region on the complex Borel plane, in which the CBSR of Eq.(4.10) (or Eq.(4.11)) can be effectively used for the analysis of the spectral function. Firstly, the CBSR does not work for $\mathrm{Re}[\mathcal{M}^2] \leq 0$, as we have explained in section 4.2.3. Secondly, the region with $\mathrm{Im}[\mathcal{M}^2] < 0$ gives sum rules with the same content as those with positive imaginary part of $\mathcal{M}^2$. Thirdly, we have to make sure to exclude the region, where the OPE might not be a valid approximation. To this end, we use the condition employed in standard QCD sum rule analyses, namely, we demand that the highest order OPE term is smaller than a critical ratio r_c of the whole OPE expression. We thus impose

$$\frac{|d^{\max}(\mathcal{M}^2)|}{|G^{\mathrm{OPE}}(\mathcal{M}^2)|} < r_c, \tag{4.16}$$

which is used in the RBSR analyses with a typical value of $r_c = 0.1$. For the present work, we will employ the same value. The only difference to the RBSR is that we here take ratios of moduli of complex valued functions instead of real ones. Eq.(4.16) produces a closed curve in the complex Borel mass plane in whose inner region the sum rules cannot be used.

With all these restrictions, the effective domain for the sum rule lies in the first quadrant of the $\mathcal{M}^2$ imaginary plane with an excluded small $|\mathcal{M}^2|$ region, as shown schematically in Fig. 3.

4.3 The maximum entropy method

Advantages of the CBSR can be most efficiently exploited with the help of the maximum entropy method (MEM). This method enables us to determine the spectral function from the sum rules without assuming a specific functional form such as the popular "pole + continuum" ansatz. Therefore, the more detailed the available information from the OPE is, the more realistic and accurate the spectral function obtained by MEM will be. Conversely, without enough physical information, the extracted spectral function will depend strongly on the "default model", which is an input of the MEM analysis, as will be explained below. In this sense, the CBSR is very useful for the MEM analysis as it provides more physical information thanks to the rich structure of its kernels. In the next few paragraphs, we shall briefly explain the essence of MEM and point out some issues specific to the analysis presented in this chapter.

MEM will lead us to the spectral function ρ that maximizes

$$Q[\rho] = \alpha S[\rho] - L[\rho], \tag{4.17}$$

where $S[\rho]$ stands for the Shannon-Jaynes entropy, defined by

$$S[\rho] = \int_0^\infty d\omega [\rho(\omega) - m(\omega) - \rho(\omega) \log \frac{\rho(\omega)}{m(\omega)}]. \tag{4.18}$$

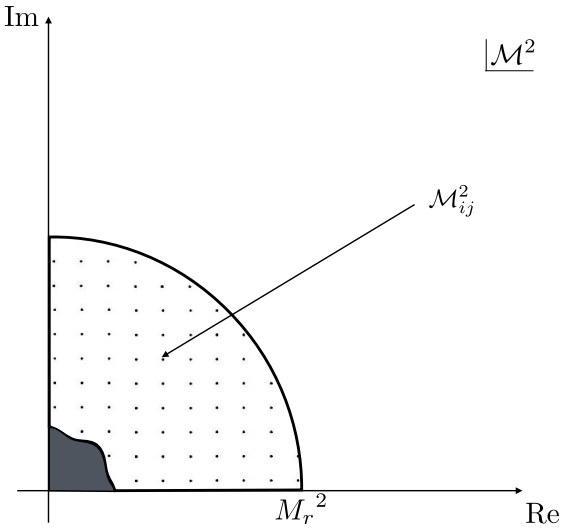

Figure 4.3: A schematic illustration of the data points to be used in the MEM analysis and their respective distribution on the complex plane of the squared Borel mass $\mathcal{M}^2$.

Here, $m(\omega)$ is some positive definite function called default model. (Note that we change the variable from s to $\omega = \sqrt{s}$ in the following.) $S[\rho]$ ensures the positive definiteness of the spectral function and takes the maximum value at $\rho(\omega) = m(\omega)$.

$L[\rho]$ is the likelihood function, which incorporates physical information provided by the sum rule. In the case of the real valued Borel sum rules, it is expressed as

$$L[\rho] = \frac{1}{2N} \sum_i \frac{1}{\sigma_i^2} \left| G^{OPE}(M_i^2) - \int_0^\infty d\omega \, \frac{2\omega}{M_i^2} \mathrm{e}^{-\omega^2/M_i^2} \rho(\omega) \right|^2 , \tag{4.19}$$

where the subscript i $(= 1, \ldots N)$ specifies the discretized Borel mass and σ_i is the error of the OPE data $G^{\mathrm{OPE}}(M_i^2)$. The error is determined from the uncertainty of the vacuum condensates. The factor 2ω, appearing in the integrand of Eq.(4.19) is a result of the variable change from s to ω.

The parameter α is a positive real number on which the spectral function maximizing $Q[\rho]$ depends. The range of this parameter is determined by MEM and we take a weighted average of the obtained spectral functions over α to get the final solution. For the details of this procedure, we refer the interested reader to [21].

In the application of MEM to the complex Borel plane sum rules, some modification in the likelihood function is necessary. As one complex Borel mass gives two sum rules, the real and imaginary parts, the likelihood function can be expressed as the sum of them as

$$\begin{aligned} L[\rho] = \frac{1}{2N} \sum_{(i,j)} \Bigg[& \frac{1}{\sigma_{ij}^{R\,2}} \left| \mathrm{Re}[G^{\mathrm{OPE}}(\mathcal{M}_{ij}^2)] - \int_0^\infty d\omega \, 2\omega K^R(\mathcal{M}_{ij}^2; \omega^2) \rho(\omega) \right|^2 \\ & + \frac{1}{\sigma_{ij}^{I\,2}} \left| \mathrm{Im}[G^{\mathrm{OPE}}(\mathcal{M}_{ij}^2)] - \int_0^\infty d\omega \, 2\omega K^I(\mathcal{M}_{ij}^2; \omega^2) \rho(\omega) \right|^2 \Bigg] . \end{aligned} \tag{4.20}$$

The subscripts ij here specify the discretized complex Borel mass $\mathcal{M}_{ij}^2$ in the (2-dimensional) complex plane, and N is the total number of the chosen Borel masses. The variances σ_{ij}^{R} and

$\sigma^{\rm I}_{ij}$ are the ambiguities of the real and imaginary parts of $G^{\rm OPE}(\mathcal{M}^2_{ij})$.

The discretized Borel masses are chosen in the first quadrant, according to the previous discussion and as shown in Fig. 4.3. We here can make use of the full allowed range of the argument of $\mathcal{M}^2 = M^2 e^{i\theta}$, which is $0 \leq \theta < \frac{\pi}{2}$. It is expected that choosing Borel masses which cover this whole range will provide the most complete amount of information on the spectral function provided by the CBSR. We will hence in the following use Borel masses $\mathcal{M}^2_{ij}$ which are evenly distributed in $0 \leq \theta < \frac{\pi}{2}$. The lower boundary of $|\mathcal{M}^2|$ is determined to satisfy Eq.(4.16). For the upper boundary, $|M^2_r|$, we do not have a definite restriction and in principle may choose it freely. We will illustrate the dependences of the results on different choices of M^2_r in the specific example given in the next section.

4.4 Analyses of OPE data

In this section, the CBSR is applied to the analysis of the spectral function for the ϕ meson channel as a first test of the validity of our method. We compare the results with those of the RBSR.

4.4.1 The CBSR for the ϕ meson

We consider the sum rule for the vector meson composed of s and $\bar{s}$, where s is the strange quark. The interpolating field operator is $J^\mu(x) = \bar{s}(x)\gamma^\mu s(x)$, which is supposed to create the ϕ (1020) meson from the vacuum.

The correlation function

$$\begin{aligned}\Pi^{\mu\nu}(q^2) &= i\int d^4x\, e^{iq\cdot x}\langle 0|T(J^\mu(x)J^\nu(0)|0\rangle \\ &= (q^\mu q^\nu - g^{\mu\nu}q^2)\Pi(q^2)\end{aligned} \tag{4.21}$$

describes the spectrum of the ϕ meson and its excited states.

The OPE of the function $\Pi(q^2)$ has been obtained [20] as follows:

$$\begin{aligned}\Pi^{\rm OPE}(q^2) =& -\frac{1}{4\pi^2}(1+\frac{\alpha_s}{\pi})\ln(-\frac{q^2}{\mu^2}) + \frac{3m_s^2}{2\pi^2}\frac{1}{q^2} + 2m_s\langle\bar{s}s\rangle\frac{1}{q^4} \\ &+ \frac{\langle\frac{\alpha_s}{\pi}G^2\rangle}{12}\frac{1}{q^4} + \frac{224\pi\alpha_s}{81}\kappa\langle\bar{s}s\rangle^2\frac{1}{q^6}.\end{aligned} \tag{4.22}$$

Note that in writing down the above result, we have assumed the vacuum saturation approximation for the dimension 6 four-quark condensate term and have parametrized the possible violation of this approximation by the parameter κ. Replacing q^2 with $z = |z|e^{i(\pi-\theta)}$ in Eq.(4.22) and performing the Borel transformation, we can easily derive the OPE for the CBSR:

$$\begin{aligned}G^{\rm OPE}(\mathcal{M}^2) =& \frac{1}{4\pi^2}(1+\frac{\alpha_s}{\pi}) - \frac{3m_s^2}{2\pi^2}\frac{1}{\mathcal{M}^2} + 2m_s\langle\bar{s}s\rangle\frac{1}{\mathcal{M}^4} \\ &+ \frac{\langle\frac{\alpha_s}{\pi}G^2\rangle}{12}\frac{1}{\mathcal{M}^4} - \frac{112\pi\alpha_s}{81}\kappa\langle\bar{s}s\rangle^2\frac{1}{\mathcal{M}^6},\end{aligned} \tag{4.23}$$

where $\mathcal{M}^2 = M^2 e^{i\theta}$. As we mentioned, this form is equal to that of the real valued Borel sum rule, the Borel mass being simply replaced by the complex Borel mass. When we use the polar

form for $\mathcal{M}^2$, the respective real and imaginary parts can be explicitly given as follows:

$$\begin{cases} \frac{1}{4\pi^2}(1+\frac{\alpha_s}{\pi}) - \frac{3m_s^2}{2\pi^2}\frac{\cos\theta}{M^2} + 2m_s\langle\bar{s}s\rangle\frac{\cos 2\theta}{M^4} + \frac{\langle\frac{\alpha_s}{\pi}G^2\rangle}{12}\frac{\cos 2\theta}{M^4} - \frac{112\pi\alpha_s}{81}\kappa\langle\bar{s}s\rangle^2\frac{\cos 3\theta}{M^6} \\ \qquad = \frac{1}{M^2}\int_0^\infty \mathrm{e}^{-(\cos\theta/M^2)s}\cos\big[(\sin\theta/M^2)s-\theta\big]\rho(s)ds, \\ \frac{3m_s^2}{2\pi^2}\frac{\sin\theta}{M^2} - 2m_s\langle\bar{s}s\rangle\frac{\sin 2\theta}{M^4} - \frac{\langle\frac{\alpha_s}{\pi}G^2\rangle}{12}\frac{\sin 2\theta}{M^4} + \frac{112\pi\alpha_s}{81}\kappa\langle\bar{s}s\rangle^2\frac{\sin 3\theta}{M^6} \\ \qquad = \frac{1}{M^2}\int_0^\infty \mathrm{e}^{-(\cos\theta/M^2)s}\sin\big[(\sin\theta/M^2)s-\theta\big]\rho(s)ds. \end{cases} \tag{4.24}$$

The values and uncertainties of the quark mass, strong coupling constant and and vacuum condensates appearing in the OPE used in our analysis are given in Table 5.1.

We choose $r_c = 0.1$ in the condition (4.16) for the domain of valid complex Borel mass. It is then restricted outside the region specified in Fig. 4.4.

$\langle\bar{q}q\rangle$	$-(0.2723 \pm 0.0018)^3$ GeV^3 [92]
$\langle\frac{\alpha_s}{\pi}G^2\rangle$	0.012 ± 0.0036 GeV^4 [119]
$\langle\bar{s}s\rangle$	$(0.8 \pm 0.1)\langle\bar{q}q\rangle$ [96]
m_s	95 ± 5 MeV [120]
κ	2 ± 1 [121]
$\alpha_s(\mu = 1\text{GeV})$	0.505 ± 0.0167 [122]

Table 4.1: Values and respective uncertainties of the condensates and other parameters used for evaluating the OPE of Eq.(4.24).

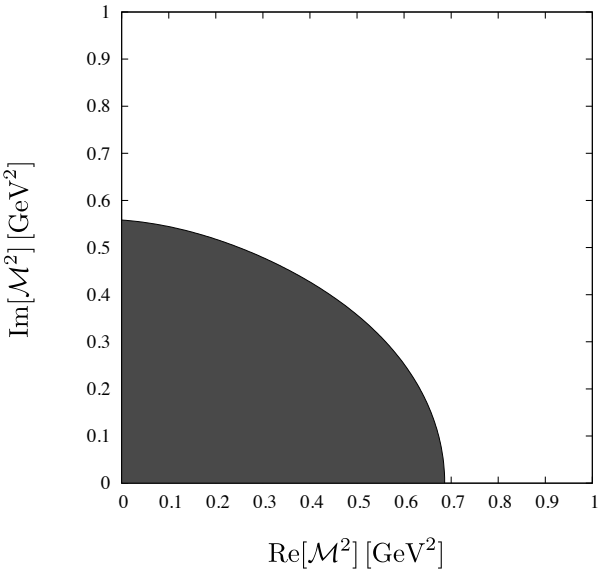

Figure 4.4: The allowed (prohibited) regions of the complex OPE are shown as white (black) areas in the complex $\mathcal{M}^2$ plane. The convergence criterion, determining the two areas and their boundary, is given in Eq.(4.16).

4.4.2 Analysis results with a single default model and M_r^2 value

In our MEM analysis, we have some freedom to choose the default model $m(\omega)$ and the outer circle radius M_r^2. A reasonable choice for $m(\omega)$ should reflect our prior knowledge on the spectral function, because it gives its most probable form when no constraints from the sum rules are available. A suitable choice for its form is thus, as has been already discussed in [21], a function which tends to zero at low energy and approaches the perturbative high energy limit for large ω. A parametrization which has these properties and smoothly interpolates between the low and high energy limit, is given as

$$m_{\mathrm{step}}(\omega) = \frac{1}{4\pi^2}(1+\frac{\alpha_s}{\pi})\ \frac{1}{1+\mathrm{e}^{\frac{\omega_0-\omega}{\delta}}}. \tag{4.25}$$

Note that $\rho(s)$ in Eq.(4.24) is dimensionless in this case and is supposed to go to the asymptotic value, $\frac{1}{4\pi^2}(1+\frac{\alpha_s}{\pi})$ at high energy. For a first trial, we will use $\omega_0 = 4$ GeV and $\delta = 0.2$ GeV in the analysis of this subsection and later examine the effects of other default models. As for M_r^2, it should generally not be too large because for large M_r^2, the damping factor of the kernels becomes weak, which means that the integrals over the spectral function in Eq.(4.24) will have large contributions from the continuum. M_r^2 should on the other hand not be taken too small to allow a sufficiently large interval above the prohibited region shown in Fig. 4.4. As a parameter satisfying these conditions, we choose $M_r^2 = 1\,\mathrm{GeV}^2$ and will later investigate the effects of different choices for this value. For comparison, we have also analyzed the RBSR of the ϕ meson channel with MEM, as it was done for the ρ meson in [21]. The Borel mass for this analysis was taken as $0.69\ \mathrm{GeV}^2 \leq M^2 \leq 1\ \mathrm{GeV}^2$, which corresponds to the real axis of the area shown in Fig. 4.4.

The obtained results are shown in Fig. 4.5. Three peaks are generated in the analysis of the CBSR. The estimated errors on the MEM results are shown by the three horizontal limes at each peak. Among the three peaks, the first and second peak are statistically significant and can therefore presumably be considered to represent physical resonances. Further discussions on this point will follow in the next subsections. The third peak is on the other hand not statistically significant and hence no conclusions on its physical existence can be drawn. The positions of the first two peaks are given in Table 4.2, where it is observed that the peak positions agree quite well with the respective experimental values. Comparing this with the result of the RBSR on the right plot of Fig. 4.5, it is seen that for the latter case, only one relatively broad peak is extracted, which can be considered to be a smeared version of the first two peaks obtained from the CBSR. This is a reasonable result, as the CBSR contains more detailed information on the spectral function and thus allow for a better resolution of its MEM extraction.

	CBSR	RBSR	Experiment
1st peak [GeV]	0.94	1.15	1.02
2nd peak [GeV]	1.74		1.68

Table 4.2: Position of the peaks, extracted from the MEM analysis results shown in Fig. 4.5. The first two columns list the values obtained from the complex and real Borel sum rules, while the corresponding experimental values are given in the third column.

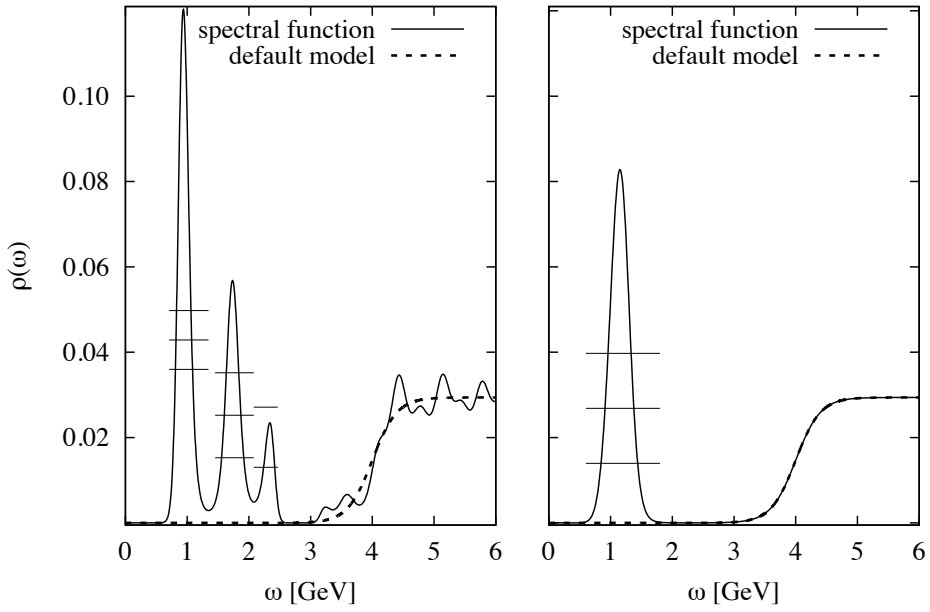

Figure 4.5: The analysis results of the CBSR (left plot) and RBSR (right plot). The solid lines show the spectral function extracted from the MEM analysis. The dashed lines show the default model defined in Eq.(4.25).

4.4.3 Analysis results with various choices of the default model and M_r^2

To get an idea on the systematic uncertainties of our results, it is important to study the dependence of the generated spectral functions on the default model and the used value of M_r^2. We will for this purpose not only use default models of the form given in Eq.(4.25), but also another version which contains no information on the asymptotic behavior of the spectrum at high energy. The most simple form of such a default model would be just a constant, however, much smaller than the asymptotic value, $\frac{1}{4\pi^2}(1+\frac{\alpha_s}{\pi}) \sim 0.03$. For this reason, the following function is chosen as an alternative default model:

$$m_0(\omega) \ = \ 10^{-6}. \tag{4.26}$$

For M_r^2, we take 1, 2, 5, 20 and 60 (all in units of [GeV^2]) to investigate the effect of a larger choice for this parameter. We have totally carried out ten different analyses for both the CBSR and RBSR, using two types of default models ($m_{\rm step}$ or m_0) and the above-mentioned five values of M_r^2. The corresponding results are shown in Fig.4.6 and Fig.4.7, respectively. The positions of the peaks are given in Tables 4.3 and 4.4.

Let us firstly examine the high energy region of the obtained spectral functions. Looking at the results with $m_0(\omega)$ on the right side of Fig. 4.6, it is clear that for larger M_r^2, the spectral functions approach the perturbative high energy limit at large ω values. This shows that the continuum can be reproduced by the CBSR irrespective of the chosen default model. In contrast, it is found that the reproduction of the continuum is much worse for the RBSR. As

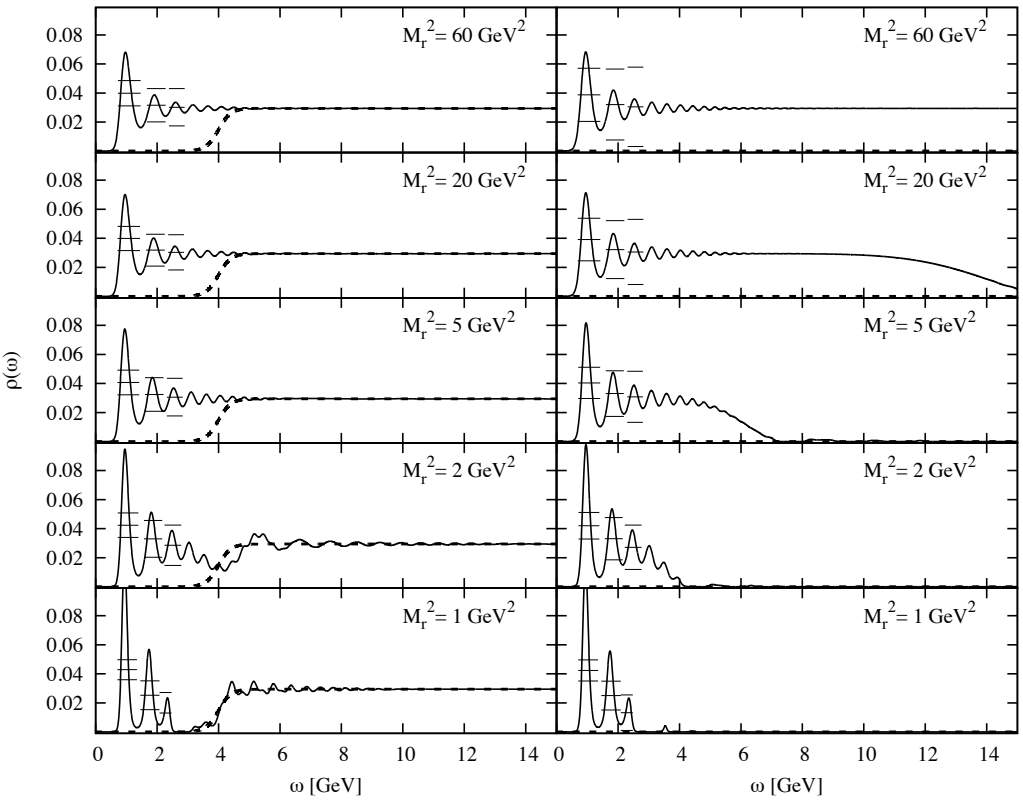

Figure 4.6: The analysis results of the CBSR using two default models (m_{step} on the left side and m_0 on the right side) and five values of M_r^2. The solid lines give the spectral function determined from the MEM analysis, while the dashed lines show the employed default model.

can be observed on the right side of Fig.4.7, MEM tries to reproduce some sort of continuum, but can only generate a strongly oscillating function with a large artificial peak somewhat above $\omega = M_r$. Although the continuum is reproduced for the results with $m_{\text{step}}(\omega)$ on the left side of Fig. 4.7, this behavior is simply a consequence of the default model used in this specific case.

Next, we focus on the low energy parts of the spectrum. For the lowest peak, which corresponds to the ϕ meson ground state, the obtained positions do not depend much on the choice of $m(\omega)$ or on the value of M_r^2, which means that the CBSR are sensitive to this state and that the MEM can extract it with only small systematic uncertainties. Specifically, it can be observed in Table 4.3 that the position of the lowest peak only moves as much as 30 MeV when $m(\omega)$ or M_r^2 are varied. The situation is again less clear for the RBSR results. The position of the 1st peak has a much stronger dependence on the choice of $m(\omega)$ and M_r^2 (see Table 4.4). Moreover, even the statistical significance remains only for $M_r^2 = 1$ and $2\,\text{GeV}^2$.

In the CBSR spectra of Fig. 4.6, it is furthermore seen that a statistically significant second peak is found for M_r^2 values up to $2\,\text{GeV}^2$. As can however be read off from Table 4.3, compared to the ground state, the position of this second peak depends significantly on $m(\omega)$ and M_r^2. It moreover loses its statistical significance for $M_r^2 \geq 5\,\text{GeV}^2$ and seems to be a part of the small oscillations that appear at the edge of the continuum for the largest few values of M_r^2. The properties of the second peak, therefore, depend on the MEM input parameters to some degree and it is not completely clear whether this peak is of physical origin or merely an artifact of the MEM analysis. We will further discuss this question in the the mock data analysis of the next

M_r^2 [GeV]^2	$m_{\rm step}$		m_0	
	1st peak [GeV]	2nd peak [GeV]	1st peak [GeV]	2nd peak [GeV]
60	0.97	1.91	0.95	1.85
20	0.96	1.89	0.95	1.85
5	0.95	1.85	0.96	1.84
2	0.95	1.81	0.95	1.80
1	0.94	1.74	0.94	1.74

Table 4.3: Position of the peaks, extracted from the MEM analysis results shown in Fig. 4.6.

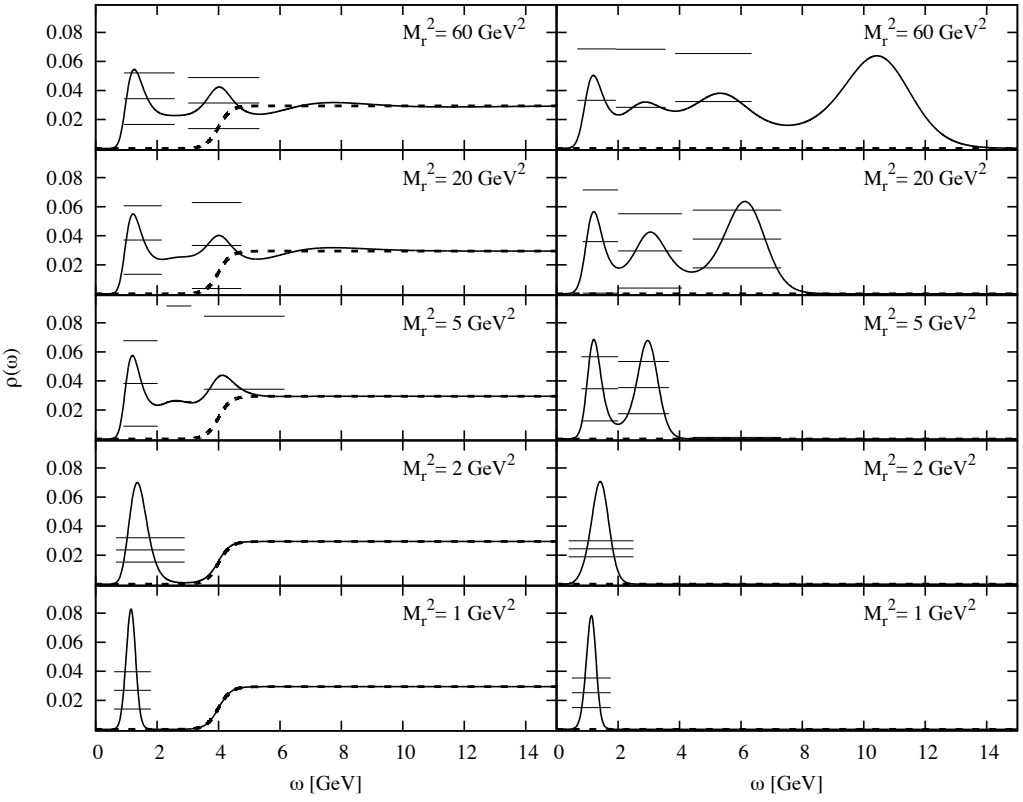

Figure 4.7: Same as for Fig. 4.6, but using the RBSR as input for the MEM analysis.

subsection.

4.5 Test analyses by using the mock spectral function

For better understanding what parts of the spectral function can be reliably studied with our method and what sort of artificial structures might appear in the MEM results, we have carried out a test analysis using the mock data generated from some specific input spectral function. Based on the results of this analysis, we will investigate whether the second peak found Figs. 4.5 and 4.6 is physical or just an MEM artifact and will further discuss the different reproducibilities of the CBSR and RBSR analyses. For the input mock spectral function of the ϕ-meson channel, we employ a relativistic Breit-Wigner peak and a smooth function describing the transition to

M_r^2 [GeV]^2	$m_{\rm step}$	m_0
	1st peak [GeV]	1st peak [GeV]
60	1.26	1.20
20	1.22	1.21
5	1.20	1.21
2	1.36	1.42
1	1.15	1.13

Table 4.4: Position of the peaks, extracted from the MEM analysis results shown in Fig. 4.7.

the asymptotic value at high energies [123],

$$\rho^{\rm mock}(\omega) = \frac{3}{4\pi^2}\frac{52.4}{1+\frac{4(\omega-m)^2}{\Gamma^2}} + \frac{1}{4\pi^2}(1+\frac{\alpha_s}{\pi})\,\frac{1}{1+{\rm e}^{\frac{\omega_0-\omega}{\delta}}}, \tag{4.27}$$

which has been renormalized so that the asymptotic behavior of the spectral function at high energy is consistent with Eq.(4.22), the OPE used in this chapter. For the parameters appearing in Eq.(4.27), we use the following values:

$$\begin{aligned} &m = 1.02\ {\rm GeV}\,, \quad \Gamma = 4.26\ {\rm MeV} \\ &\omega_0 = 1.5\ {\rm GeV}\,, \quad \delta = 0.4\ {\rm GeV}\,, \quad \alpha_s = 0.505 \end{aligned} \tag{4.28}$$

The mock data are then numerically generated as shown below for the CBSR case:

$$G^{\rm mock}(\mathcal{M}_{ij}^2) \equiv \frac{1}{\mathcal{M}_{ij}^2}\int_0^\infty {\rm e}^{-\omega^2/\mathcal{M}_{ij}^2}\rho^{\rm mock}(\omega)2\omega d\omega. \tag{4.29}$$

In the actual MEM analysis, we have treated $G^{\rm mock}(\mathcal{M}_{ij}^2)$ like OPE data, meaning that we use the the same errors and Borel mass ranges which were used in the OPE data analyses of the previous sections. Specifically, we have analyzed two cases. In the first case, we have taken $M_r^2 = 1\,{\rm GeV}^2$ and used $m_{\rm step}(\omega)$ of Eq.(4.25) for the default model. The respective results are shown in Fig. 4.8, which should be compared to Fig. 4.5, where the OPE data have been analyzed under exactly the same conditions. For the second case, we have used $M_r^2 = 60\,{\rm GeV}^2$ with the default model $m_0(\omega)$ of Eq.(4.26), the result being shown in Fig. 4.9. This case corresponds to the top right plots of Figs. 4.6 and 4.7 for the OPE data analyses.

Firstly, let us investigate the mock data analysis results of the first case with $M_r^2 = 1\,{\rm GeV}^2$. Looking at the left plot of Fig.4.8, it is found that for the CBSR an artificial second peak can be generated by the MEM analysis even if such a peak is not present in the original spectral function. This phenomenon can be thought of as a result of the MEM trying to reproduce the continuum, but not having enough information due to the small value of M_r^2. The extracted spectral function therefore eventually approaches the default model, leading to an artificial peak. In contrast to the OPE data analysis result of Fig. 4.5, this peak is however not statistically significant. Also the strengths of the peaks are different: while the second peak obtained from the OPE data clearly rises above the continuum, the respective mock data peak does not. These findings show, that while it is possible that small artificial bumps or peaks can be produced by the MEM analysis, these will not be as large as the second peak seen in Fig.4.5. We hence can conclude that this peak is likely to reflect the properties of a physical state, the first excited state of the ϕ meson. As a further point, comparing both plots of Fig. 4.8, it is observed that CBSR reproduces the

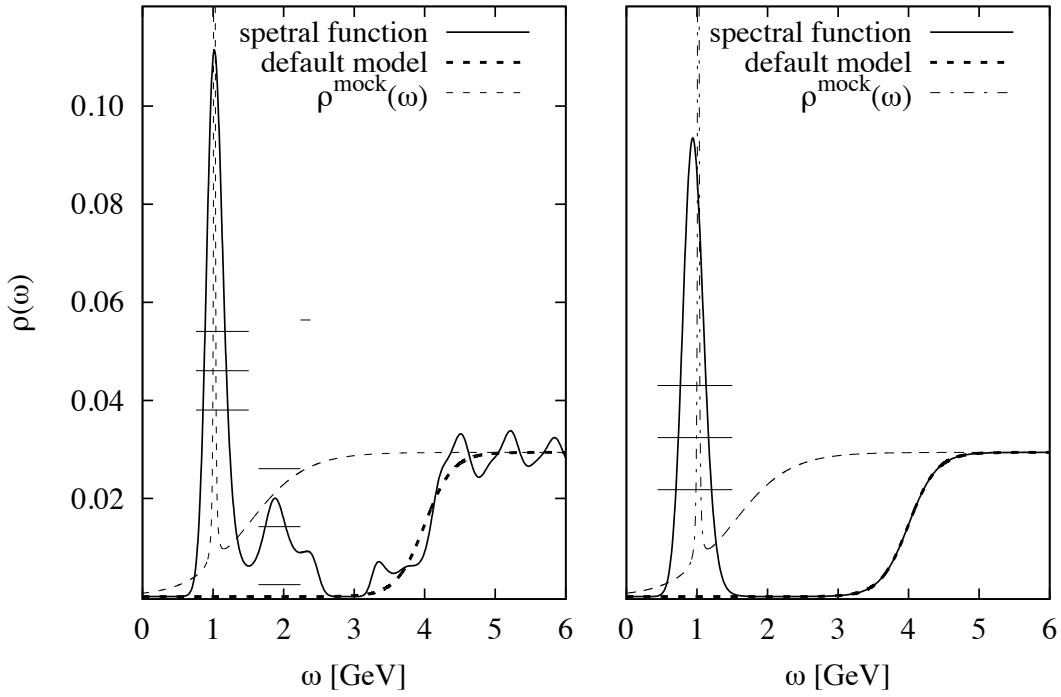

Figure 4.8: Test analysis results of the CBSR (left plot) and RBSR (right plot) using mock data. In analogy to Fig. 4.5, we have employed $M_r^2 = 1\,\mathrm{GeV}^2$ and m_{step} for obtaining these spectra. The solid lines show the spectral function extracted from the MEM analysis, the thick dashed lines depict the default model and the thin dashed lines gives the mock spectral function, ρ^{mock}.

position of the first peak with much better precision than the RBSR. Furthermore, considering the width of the lowest peak, it is seen that CBSR shows some improvement compared to the RBSR, but is nevertheless not able to reproduce the very narrow physical width of the ϕ meson.

Next, we examine the results for $M_r^2 = 60\,\mathrm{GeV}^2$. From Fig. 4.9, we can confirm that at large energy CBSR is able to reproduce the continuum without relying on the default model. This is not the case for the RBSR, which instead of a constant behavior produces large oscillations. On the other hand, we found that at the lower edge of the continuum, the CBSR generates artificial oscillations, which are damped out toward higher energies. It is hence understood that the periodic peaks found in the OPE data analysis above the ground state peak for large values of M_r^2 (see Fig. 4.6) are mainly MEM artifacts. Even though the spectral functions obtained from the OPE data show a somewhat stronger second peak, which can probably be explained by the existence of a physical state in that region, this difference is too small to allow any definitive conclusions. To recapitulate, for large values of M_r^2, the sum rules are dominated by the continuum (which is thus well reproduced) and contains relatively less information on the low energy part of the spectrum. For obtaining information on the possible existence of excited states, one therefore needs to choose small enough M_r^2 values.

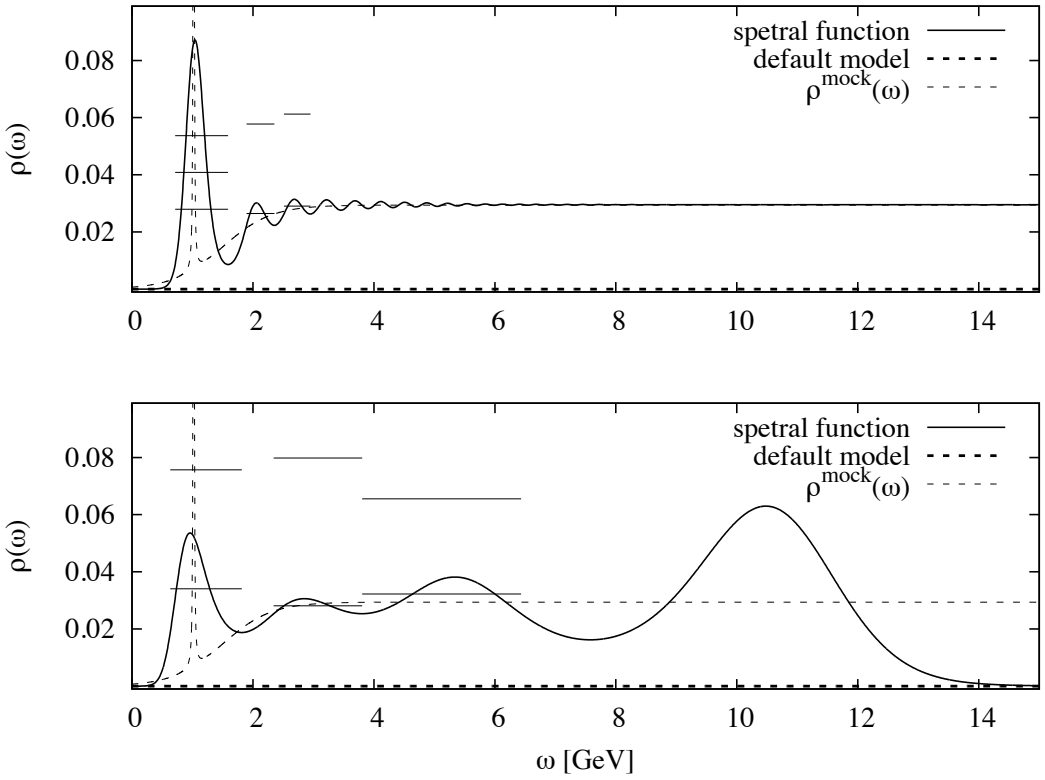

Figure 4.9: Same as in Fig. 4.8, but with $M_r^2 = 60\,\mathrm{GeV}^2$ and m_0. The upper plot gives the result for the CBSR, while the lower plot shows the spectrum extracted from the RBSR.

4.6 Summary and conclusion

We have in this study constructed the complex Borel plane QCD sum rules (CBSR) and have applied it to the ϕ meson channel as a first test of its validity and usefulness. We have explicitly demonstrated that the CBSR can be obtained by simply replacing the Borel mass M^2 of the real Borel QCD sum rules (RBSR) with a complex parameter $\mathcal{M}^2$. Since the Borel mass can thus take values on the complex plane and not only on the real axis, the CBSR allows us to extract more information on the spectral function than it was previously possible. To check whether the CBSR works in practice, to examine the quality of the information provided by the sum rules and to compare the ability of the CBSR with the RBSR, we have studied the ϕ meson channel with the help of MEM. The main results of this investigation are as follows:

- For both the CBSR and RBSR, the MEM analysis generates a lowest peak, which corresponds to the physical $\phi(1020)$ state. Comparing the results for this peak, the CBSR is clearly found to be superior to the RBSR. Firstly, the dependence of the peak position on arbitrary input parameters is much smaller for the CBSR (compare Tables 4.3 and 4.4). Secondly, the lowest peak generated by the CBSR is, in contrast to the RBSR, always statistically significant, irrespective of the MEM analysis details.

- Only for the CBSR, a second peak, which may correspond to the first excited state of the ϕ meson channel, also appears in the obtained spectral function. This peak is only statistically significant when OPE data close to the origin of the complex Borel mass plane

are analyzed (i.e. when a rather low M_r^2 value is used). Making M_r^2 larger, it is found to mix with artificially generated peaks which have no physical significance. Nevertheless, the fact that the peak is statistically significant at least for low M_r^2 together with the results of our mock data analysis indicates that this peak is not completely artificial, but a reflection of an actual physical state. Our calculations show that this state lies in the range of $1.74 \sim 1.85\,\mathrm{GeV}$, which is somewhat larger than the experimental value of $1.68\,\mathrm{GeV}$. Presently, we cannot make any more precise statements on the mass of this excited state since the MEM result depends significantly on the default model and the used value of M_r^2. In the present analyses, we have treated all the allowed complex angles, θ, with equal weights. Further analyses may be necessary to investigate possible correlation between θ and the position of the second peak.

- Besides the lowest two peaks, we have shown that the CBSR is capable of reproducing the continuum at high energy. Specifically, as long as M_r^2 is chosen to be sufficiently large, the MEM analysis generates the correct high energy limit of the spectral function even if the default model has a different limiting value.

The CBSR hence appears to be a useful tool for analyzing hadronic spectral functions, which is superior to the conventional RBSR. This finding is in essence a consequence of the higher resolution of the oscillating kernels of the CBSR and the additional amount of information provided by the independent sum rules corresponding to each point on the first quadrant of the complex Borel plane shown schematically in Fig. 4.3. It is important to note here that only by using MEM, we can exploit the full power of the CBSR, as MEM in principle allows the spectral function to have any specific (positive definite) form.

Chapter 7

Summary and conclusion

In this thesis, we have attempted to improve or to go beyond the QCD sum rule which is a non-perturbative approach to extract QCD spectral functions. To this end, we reconsidered the two important key words about the QCD sum rules, *analyticity* and *factorization*. So our studies led to the two novel concepts, the generalization of Borel sum rules to complex type and the infinite summation of the operator product expansion (OPE). We have achieved the applications of these ideas to practical analyses, to obtain the novel results in each work. The chapter 1∼3 are the review parts to understand the basics of QCD sum rules and OPE. Our main studies are given in Chapter 4∼6 and summarized below.

Complex Borel sum rules

The first work is the generalization of Borel sum rules to the complex type. By deeply considering the analyticity of correlation functions, we found that the parameter of the dispersion relation, which is conventionally considered to be a real value, can have also a complex value.

In Chapter 4, we formalized the complex Borel sum rules (CBSR) based on this simple discovery. In CBSR Borel masses are generalized to have complex values. We organize the analysis manner where we utilize the maximum entropy method (MEM) to extract spectral functions from CBSR. We performed the test for our analysis method in the ϕ meson channel. We found that our approach had the ability to reproduce the second peak in the spectral function. Namely, we can address the analysis of excited states, which have not done in the conventional QCD sum rule analyses.

In Chapter 5, this approach was also applied to charmonia (in the vector and pseudoscalar channels) in vacuum and at finite temperature. The two statistically significant peaks in both the channels are reproduced. Namely, physical states, J/ψ, ψ', η_c and η_c' were reproduced in our analyses. By introducing finite temperature effects, we observed that all the obtained peaks are deformed and gradually disappear as the temperature increases. It would be a signal that the ground and excited states simultaneously disappear in QGP.

Infinite summation of the operator product expansion

The second work is to take an infinite summation of partial series in the OPE. It is the OPE in the whole system of QCD sum rules that reflects the non-perturbative feature of QCD to hadronic spectral functions. Usually one truncates the expansion at a certain dimension of operators. However, it is theoretically interesting to study what kind of role such a truncated

infinite series plays. This work is motivated by the hope that we can directly calculate hadron properties without the analytic continuation which is indispensable in the usual QCD sum rules analyses. Although QCD sum rules work well by the help of the analytic continuation, it, at the same time, induces uncertainties of the prediction.

In Chapter 6, we proposed the new approach where one can systematically take an infinite summation of partial series of the OPE by using the Schwinger-Dyson equations. As a first test, we actually resummed the power series of $\langle\bar{q}q\rangle$ by this approach. The obtained correlation functions of the vector, axial vector and scalar channels show the finite pole shifts proportional to $|\langle\bar{q}q\rangle^{\frac{1}{3}}|$. It indicates that the hadrons acquire their masses by the spontaneous chiral symmetry breaking. In the pseudoscalar channel, there does not exist such a pole shift, so that its mass is still zero even when $\langle\bar{q}q\rangle \neq 0$. It may be regarded as a Nambu-Goldstone boson, pion in the chiral limit. On the contrary, some negative aspects are observed in the results, e.g. the gauge parameter does not disappear in the final results of the axial vector and scalar channels.

Summary of the whole study

In the first work we deeply focused on the analyticity (analytic continuation), which is one of the key words of QCD sum rules, and succeed to construct novel integral rules, CBSR. It is a kind of improvement of the QCD sum rules. However, we cannot avoid the inverse problem as long as we utilize the analytic continuation. The inverse problem inevitably brings us uncertainty of the prediction.

In fact, the second work was devoted to renounce the analyticity from our analyses. To this end, we thought deeply about the factorization (OPE), which is the other key word of QCD sum rules, and gained the idea of the infinite summation of the OPE. We actually achieved to sum up the infinite power series of the chiral condensate by utilizing the SDEs. As a result, we realized the finite pole shifts of the correlation functions without the analytic continuation. We regard this work as the first step for the novel analysis which goes beyond QCD sum rules because the inverse problem is no longer necessary. To resolve the remaining problem mentioned in Chapter 6, we should perform further analyses.

Acknowledgements

First, I would like to express the deepest appreciation to Professor Makoto Oka as my surpervisor for his continuous encouragement throughout the 6 years of my doctoral, master's and bachelor's degrees in Tokyo Institute of Technology. I appreciate him for generously allowing me to study just as I want and for giving me many inspiring discussions and countless comments. I am also grateful for his gentle guidance and advices about the matters in my laboratory life.

Furthermore, I gratefully appreciate the senior members of the nuclear theory group, Prof. Shigehiro Yasui, Dr. Kiyoshi Sasaki, Dr. Keisuke Ohtani, Dr. Kei Suzuki and Dr. Tomokazu Miyamoto for the fruitful advices and discussions. I especially thank Dr. Keisuke Ohtani and Dr. Kei Suzuki for collaborating with me and Dr. Kiyoshi Sasaki for helping me with numerical calculation and giving me fruitful advice for the revision of this thesis. I would like to offer my special thanks to Dr. Philip Gubler, who is the previous member of our laboratory, for warmly instructing me in basics of QCD sum rules when I was student in the master's course. I also appreciate all the previous members in our laboratory.

Moreover, I am indebted to all the students in our laboratory, Mr. Akira Yokota, Mr. Sergio Calle Jimenez, Ms. Saori Maeda, Mr. Tetsuya Yoshida, Mr. Can Cadir Utuk, Ms. Je Hee Lee, Mr. Yoya Irie, Mr. Takuya Higashi and Mr. Sachio Iwasaki, for my joyful and funny life in the laboratory.

I would also like to express my gratitude for the financial support by JSPS KAKENHI Grant Number JP15J11897.

Finally, I thank my family for everything they have done for me.

Appendix A

Derivation of dispersion relation

In this Appendix, we derive the the dispersion relation in detail, to reconfirm that complex q^2 is allowed to be the parameter. Using the analyticity except for the positive real q^2, we can apply the Cauchy's residue theorem for the correlation function and obtain the following equation:

$$\Pi(z) = \frac{1}{2\pi i}\int_C \frac{z^n \Pi(s)}{s^n(s-z)} ds, \tag{A.1}$$

where the contour is given in Fig.A.1 and z refers to complex q^2. Fistly, the contour C is divided as shown in Fig.A.1 to be $C_R + C_{\leftarrow} + C_{\epsilon} + C_{\rightarrow}$ and then n is supposed to be sufficiently large (but finite) so that the integral along C_R is convergent to be zero when taking the limit $R \to \infty$ and $\epsilon \to 0$, to give

$$\frac{1}{2\pi i}\int_{C_R} \frac{z^n \Pi(s)}{s^n(s-z)} ds \xrightarrow{\epsilon\to+0,\ R\to\infty} 0 \tag{A.2}$$

Next, the contributions of the other contours are considered. The integrals along $C_{\rightarrow}$ and $C_{\leftarrow}$ are calculated together.

$$\begin{aligned}
&\frac{1}{2\pi i}\int_{C_{\rightarrow}} \frac{z^n \Pi(s)}{s^n(s-z)} ds \quad + \quad \frac{1}{2\pi i}\int_{C_{\leftarrow}} \frac{z^n \Pi(s)}{s^n(s-z)} ds \\
=&\frac{1}{2\pi i}\int_0^R \frac{z^n \Pi(s+i\epsilon)}{(s+i\epsilon)^n(s+i\epsilon-z)} ds \quad + \quad \frac{1}{2\pi i}\int_R^0 \frac{z^n \Pi(s-i\epsilon)}{(s-i\epsilon)^n(s-i\epsilon-z)} ds \\
=&\frac{1}{2\pi i}\int_0^R \frac{z^n(s-i\epsilon)^n(s-i\epsilon-z)\Pi(s+i\epsilon) \ - \ z^n(s+i\epsilon)^n(s+i\epsilon-z)\Pi(s-i\epsilon)}{s^{2n}(s-z)^2} ds \\
=&\frac{1}{\pi}\int_0^R \frac{z^n \mathrm{Im}\Pi(s+i\epsilon)}{s^n(s-z)} ds \quad + \quad O(\epsilon) \\
&\xrightarrow{\epsilon\to+0,\ R\to\infty} \int_0^\infty \frac{z^n \rho(s)}{s^n(s-z)} ds = \int_0^\infty \frac{\rho(s)}{s-z} ds \quad + \quad \text{polynomial in z}
\end{aligned} \tag{A.3}$$

We used following equation on the last line.

$$\frac{z^n}{s^n(s-z)} = \frac{1}{s-z} - \sum_{k=0}^{n-1} \frac{z^k}{s^{k+1}} \tag{A.4}$$

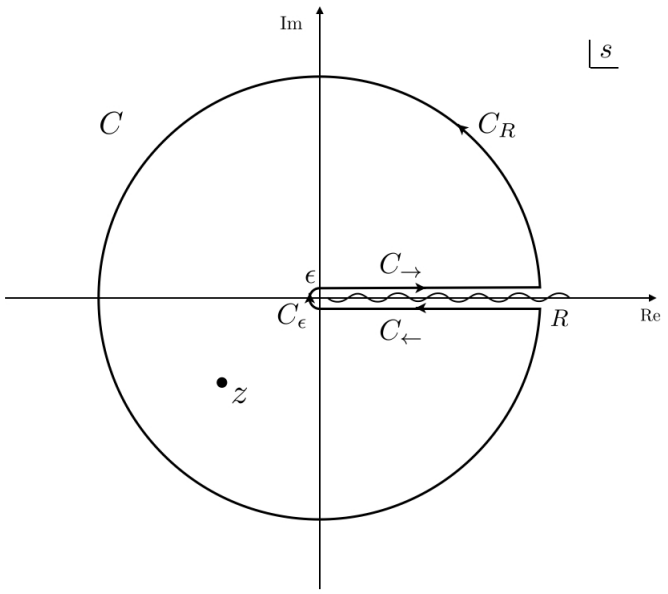

Figure A.1: The contour integral C on the complex plane of the variable q_0, used in Eq.(4.1).

As for the integral along the small half circle C_ϵ, we also use this equation to obtain

$$\begin{aligned}\frac{1}{2\pi i}\int_{C_\epsilon}\frac{z^n\Pi(s)}{s^n(s-z)}ds = \frac{\epsilon}{2\pi}\int_{\frac{3\pi}{2}}^{\frac{\pi}{2}}\frac{\Pi(\epsilon e^{i\theta})}{\epsilon e^{i\theta}-z}e^{i\theta}d\theta \quad + \quad \text{polynomial in z} \\ \xrightarrow{\epsilon\to+0,\ R\to\infty} \text{polynomial in z.}\end{aligned} \tag{A.5}$$

After all, we obtain

$$\Pi(z) = \int_0^\infty \frac{\rho(s)}{s-z}ds \quad + \quad \text{polynomial in z.} \tag{A.6}$$

The important point is that the above equation is derived without restricting z to real number. We would like to mention that although we chosed contour C which does not contain the origin, we can also choose one which contains it. In that case, $-\sum_{k=0}^{n-1}\frac{\Pi^{(n)}(0)}{k!}z^k$ are added in Eq.(A.1). However, the final result does not change its form since they are polynomial in z and is exactly consistent with Eq.(A.6).

Appendix B

Proof that the Borel transformation interchanges with the integral

In this section, we prove it is possible that Borel transformation interchange with the integral for $0 < \mathrm{Re}[\mathcal{M}^2]$ relying on following theorem [166].

Thorem B.0.1 The sequence of continuous function $\{f_n(x)\}$ which is defined in $I = (a, \infty)$ and function $g(x)$ satisfies the following conditions :

- for all $n \in \mathbb{N}$ and $x \in I |f_n(x)| \leq g(x)$
- $\int_a^\infty g(x) < \infty$
- there exists $f(x) := \lim_{n\to\infty} f_n(x)$ and $f(x)$ is continuous in I

Then the limit can be interchanged with the integral.

$$\lim_{n\to\infty} \int_a^\infty f_n(x)dx = \int_a^\infty \Big(\lim_{n\to\infty} f_n(x)\Big)dx = \int_a^\infty f(x)dx \tag{B.1}$$

Calucutating the Borel transformation of the right hand side of Eq.(4.3), finally we obtain

$$\hat{B}_{|z|} \int_0^\infty \frac{\rho(s)}{s-z}ds = \lim_{n\to\infty} \int_0^\infty F_n(s)ds, \tag{B.2}$$

where

$$F_n(s) = \frac{1}{M^2 \mathrm{e}^{i\theta}} \Big(1 + \frac{1}{n} \frac{s}{M^2 \mathrm{e}^{i\theta}}\Big)^{-(n+1)} \rho(s). \tag{B.3}$$

Therfore, being able to interchanging Borel transformation with integral means

$$\begin{aligned} \lim_{n\to\infty} \int_0^\infty \mathrm{Re}[F_n(s)]ds &= \int_0^\infty \lim_{n\to\infty} \mathrm{Re}[F_n(s)]ds, \\ \lim_{n\to\infty} \int_0^\infty \mathrm{Im}[F_n(s)]ds &= \int_0^\infty \lim_{n\to\infty} \mathrm{Im}[F_n(s)]ds. \end{aligned} \tag{B.4}$$

We shall prove both them for $0 < \cos\theta$ by the theorem. First, there exists $\lim_{n\to\infty} \mathrm{Re}[F_n(s)]$,

which is continuous. Next, the absolute value of the real part can be estimated as follows.

$$\begin{aligned} |\mathrm{Re}[F_n(s)]| &\leq |F_n(s)| \\ &= \frac{1}{M^2}\Big(1+\frac{2s\cos\theta}{nM^2}+\frac{s^2}{n^2M^4}\Big)^{-\frac{n+1}{2}}\rho(s) \\ &\leq \frac{1}{M^2}\Big(1+\frac{2s\cos\theta}{nM^2}\Big)^{-\frac{n}{2}}\rho(s) \end{aligned} \tag{B.5}$$

Because function $(1+a/x)^{-x}$ is monotone decreasing function with the variable x if $0<a$, we obtain

$$|\mathrm{Re}[F_n(s)]| \leq \frac{1}{M^2}\Big(1+\frac{2s\cos\theta}{NM^2}\Big)^{-N/2}\rho(s) \qquad \text{(for all n} \geq \text{N)}, \tag{B.6}$$

where N is a natural number. We can take finite N so that

$$\int_0^\infty \frac{1}{M^2}\frac{\rho(s)}{(1+\frac{2s\cos\theta}{NM^2})^{N/2}}ds \ < \infty \tag{B.7}$$

because the behavior of $\rho(s)$ in higher energy region is supposed to be polynomial. Redefining $\mathrm{Re}[F_n(s)]$ by taking $n=n+N$ (it does not matter since we are intereted in $n\to\infty$) , we obtain

$$|\mathrm{Re}[F_n(s)]| \leq \frac{1}{M^2}\frac{\rho(s)}{(1+\frac{2s\cos\theta}{NM^2})^{N/2}} \qquad \text{(for all n)} \tag{B.8}$$

Then by identifying $\frac{\rho(s)}{(1+\frac{2s\cos\theta}{NM^2})^{N/2}}$ with g in the theorem, the proof is finished. The proof for the imaginary part is just the same as above. After all, It is proved that we can interchange the Borel transformation with the integral for $0<\cos\theta$.

Appendix C

Borel transformation for complex OPE

In this appendix, we derive the Borel transformations of the complex functions given in section 4.2.3, i.e.

$$\hat{B}_{|z|}\, z^k = 0, \tag{C.1}$$

$$\hat{B}_{|z|}\left(\frac{1}{z}\right)^k = \frac{(-1)^k}{(k-1)!}\left(\frac{1}{M^2\mathrm{e}^{i\theta}}\right)^k, \tag{C.2}$$

$$\hat{B}_{|z|}\, z^k \ln\left(-\frac{z}{\mu^2}\right) = -k!(M^2\mathrm{e}^{i\theta})^k, \tag{C.3}$$

$$\hat{B}_{|z|}\left(\frac{1}{s-z}\right)^k = \frac{1}{(k-1)!}\frac{1}{(M^2\mathrm{e}^{i\theta})^k}\mathrm{e}^{-s/(M^2\mathrm{e}^{i\theta})}, \tag{C.4}$$

Although we can derive them following the definition of $\hat{B}_{|z|}$, we utilize the following formulas for the Borel transformation of real functions for simplicity.

$$\hat{B}_{|z|}\, |z|^k = 0 \tag{C.5}$$

$$\hat{B}_{|z|}\left(\frac{1}{|z|}\right)^k = \frac{1}{(k-1)!}\left(\frac{1}{M^2}\right)^k \tag{C.6}$$

$$\hat{B}_{|z|}\, |z|^k \ln\left(\frac{|z|}{\mu^2}\right) = -(-1)^k k!(M^2)^k \tag{C.7}$$

$$\hat{B}_{|z|}\left(\frac{1}{s+|z|}\right)^k = \frac{1}{(k-1)!}\frac{1}{(M^2)^k}\mathrm{e}^{-s/(M^2)} \tag{C.8}$$

which are respectively consistent with (4.8).

The strategy is drawing out the phase of z by substituting $z = |z|\mathrm{e}^{i(\theta-\pi)}$. Then the calculations are straight forward as follows:

$$\hat{B}z^k = (-\mathrm{e}^{ik\theta})^k \hat{B}_{|z|}|z|^k = 0 \tag{C.9}$$

$$\begin{aligned}\hat{B}_{|z|}\Big(\frac{1}{z}\Big)^k &= \frac{1}{(-\mathrm{e}^{i\theta})^k}\hat{B}_{|z|}\frac{1}{|z|^k}\\ &= \frac{1}{(-\mathrm{e}^{i\theta})^k}\frac{1}{(k-1)!}\frac{1}{(M^2)^k}\\ &= \frac{(-1)^k}{(k-1)!}\frac{1}{(M^2\mathrm{e}^{i\theta})^k}\end{aligned} \tag{C.10}$$

$$\begin{aligned}\hat{B}_{|z|}z^k\ln\Big(-\frac{z}{\mu^2}\Big) &= \hat{B}_{|z|}(-\mathrm{e}^{i\theta})^k|z|^k\ln\Big(\frac{|z|\mathrm{e}^{i\theta}}{\mu^2}\Big)\\ &= (-\mathrm{e}^{i\theta})^k\Big[\ \hat{B}_{|z|}|z|^k\ln\Big(\frac{|z|}{\mu^2}\Big)+i\theta\hat{B}_{|z|}|z|^k\ \Big]\\ &= (-\mathrm{e}^{i\theta})^k[-(-1)^k k!(M^2)^k]\\ &= -k!(M^2\mathrm{e}^{i\theta})^k\end{aligned} \tag{C.11}$$

Although, as for Eq.(C.4) we can also consider the corresponding formula Eq.(C.8) as above, it is not clear (actually right) that it is available since the phase cannot be isolated. Then we directly derive it.

$$\begin{aligned}\hat{B}_{|z|}\Big(\frac{1}{s-z}\Big)^k &= \lim_{\substack{|z|,n\to\infty\\ |z|/n=M^2}}\frac{|z|^n}{(n-1)!}\Big(-\frac{\partial}{\partial|z|}\Big)^n\Big(\frac{1}{s-z}\Big)^k\\ &= \lim_{\substack{|z|,n\to\infty\\ |z|/n=M^2}}\frac{|z|^n}{(n-1)!}\frac{(k+n-1)!}{(k-1)!}\mathrm{e}^{in\theta}\Big(\frac{1}{s+|z|\mathrm{e}^{i\theta}}\Big)^{k+n}\\ &= \lim_{n\to\infty}\frac{(nM^2)^n}{(n-1)!}\frac{(k+n-1)!}{(k-1)!}\mathrm{e}^{in\theta}\Big(\frac{1}{s+nM^2\mathrm{e}^{i\theta}}\Big)^{k+n}\\ &= \lim_{n\to\infty}\frac{(k+n-1)!}{(n-1)!(n^k)}\frac{1}{(k-1)!}\frac{1}{(M^2\mathrm{e}^{i\theta})^k}\Big(\frac{nM^2\mathrm{e}^{i\theta}}{s+nM^2\mathrm{e}^{i\theta}}\Big)^{k+n}\\ &= \frac{1}{(k-1)!}\frac{1}{(M^2\mathrm{e}^{i\theta})^k}\mathrm{e}^{-s/(M^2\mathrm{e}^{i\theta})}\end{aligned} \tag{C.12}$$

Appendix D

Verification of the replacement trick

In this Appendix, we confirm validity of the replacement trick $\partial \to D$ performed in Chapter 3. We will calculate the Wilson coefficient of $\langle \bar{q} \not{A} q \rangle_\nu$, denoted as $C_{\langle \bar{q} \not{A} q \rangle}$. Then we check if the relation $C_{\langle \bar{q} \not{A} q \rangle} = g C_{\langle \bar{q}(i\partial\!\!\!/ q) \rangle}$ is satisfied. This relation justifies the replacement trick in this case. The related diagram is shown in the right side of Fig.D.1. The amplitude is given by

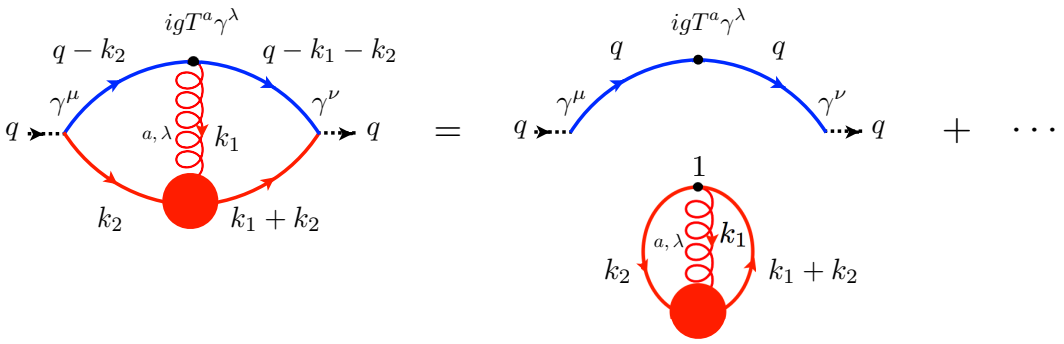

Figure D.1: Schematic picture of the term of $\langle \bar{q} \not{A} q \rangle_\nu$ in the OPE.

$$\Pi^{\mu\nu} = 2 \times (-i) \iint\limits_{k_1,k_2,k_1+k_2<\nu} \frac{d^D k_1}{(2\pi)^D} \frac{d^D k_2}{(2\pi)^D} \mathrm{Tr}\Big[\gamma^\mu S(q+k_1+k_2) i g T^a \gamma^\lambda S(q+k_2)\gamma^\nu \times [G_3(k_1,k_2,-k_1-k_2)]^a_\lambda \Big], \tag{D.1}$$

where the factor 2 comes from the symmetry factor of the diagram. $[G_3(k_1,k_2,k_3)]^a_\lambda$ is the quark-quark-gluon three-point Green function as diagrammatically defined in Fig. D.2. In the equations above, the integration with respect to k_3 was already carried out and both the indices of the spinor (α,β) and color (i,j) of the quarks were omitted.

By the power expansion at the zeroth order with respect to both the k_1 and k_2, we can estimate the diagram as follows:

$$\Pi^{\mu\nu} \approx 2 \times (-i) \mathrm{Tr}\Big[\gamma^\mu S(q) i g T^a \gamma^\lambda S(q) \gamma^\nu \iint\limits_{k_1,k_2,k_1+k_2<\nu} \frac{d^D k_1}{(2\pi)^D} \frac{d^D k_2}{(2\pi)^D} [G_3(k_1,k_2,-k_1-k_2)]^a_\lambda \Big], \tag{D.2}$$

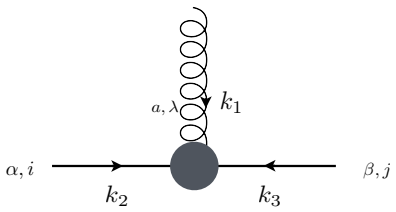

$$= [G_3(k_1,k_2,k_3)]^{a\,\alpha\beta}_{\lambda\,ij}(2\pi)^D\delta^D(k_1+k_2+k_3)$$

Figure D.2: Quark-quark-gluon three-point Green function.

where this expansion is diagrammatically shown in the right side of Fig. D.1. The tensor structure of the integration can be given by

$$\iint\limits_{k_1,k_2,k_1+k_2<\nu}\frac{d^Dk_1}{(2\pi)^D}\frac{d^Dk_2}{(2\pi)^D}[G_3(k_1,k_2,-k_1-k_2)]^{a\,\alpha\beta}_{\lambda\,ij}=[\gamma_\lambda]^{\alpha\beta}[T^a]_{ij}X_{\not{A}q\bar{q}} \tag{D.3}$$

in vacuum case. By using Eq. (D.3), the trace calculation in Eq. (D.2) can be performed as follows:

$$\Pi^{\mu\nu} \approx 2\frac{DN\left(\left(Dm^2-2m^2\right)g^{\mu\nu}+(4-D)q^2g^{\mu\nu}-4q^\mu q^\nu\right)}{\left(q^2-m^2\right)^2}\times g\,\mathrm{Tr}[T^aT^a]\;X_{\not{A}q\bar{q}} \tag{D.4}$$

$$= -D^2N\,C_{\langle\bar{q}(i\partial\!\!\!/q)\rangle}\times\;g\,C_F\;X_{\not{A}q\bar{q}}, \tag{D.5}$$

where we utilized the calculation result for the coefficient of $X_{i\partial\!\!\!/q\bar{q}}$ in Eq. (3.38) since the only difference between them is the factor of $g\mathrm{Tr}[T^aT^a]$.

Next, let us consider the definition of $X_{\not{A}q\bar{q}}$ in the coordinate space. We define

$$\langle TA^a_\lambda(x)q^\alpha_i(y)\bar{q}^\beta_j(z)\rangle_\nu \equiv \iiint\limits_{k_1,k_2,k_3<\nu}\frac{d^Dk_1}{(2\pi)^D}\frac{d^Dk_2}{(2\pi)^D}\frac{d^Dk_3}{(2\pi)^D}\mathrm{e}^{-i(k_1x+k_2y+k_3z)} \tag{D.6}$$

$$\times[G_3(k_1,k_2,k_3)]^{a\,\alpha\beta}_{\lambda\,ij}(2\pi)^D\delta^D(k_1+k_2+k_3). \tag{D.7}$$

Using Eq. (D.3) and Eq. (D.7), we obtain

$$-\langle\bar{q}\;\not{A}q\rangle_\nu = [\gamma^\lambda]^{\beta\alpha}[T^a]_{ji}\lim_{x,y,z\to0}\langle TA^a_\lambda(x)q^\alpha_i(y)\bar{q}^\beta_j(z)\rangle_\nu \tag{D.8}$$

$$= \mathrm{Tr}[\gamma^\lambda\gamma_\lambda T^aT^a]\,X_{\not{A}q\bar{q}} \tag{D.9}$$

$$= D^2C_FN\,X_{\not{A}q\bar{q}}, \tag{D.10}$$

where the negative sign appears since the quarks are anti-commutative fields. Thus $X_{\not{A}q\bar{q}}$ can be rewritten in the coordinate space as

$$X_{\not{A}q\bar{q}} = -\frac{\langle\bar{q}\;\not{A}q\rangle_\nu}{D^2C_FN}. \tag{D.11}$$

By substituting Eq. (D.11) for Eq. (D.5), we finally obtain

$$\Pi^{\mu\nu}\approx gC_{\langle(i\partial\!\!\!/q)\bar{q}\rangle}\langle\not{A}q\bar{q}\rangle_\nu. \tag{D.12}$$

The relation $C_{\langle\not{A}q\bar{q}\rangle} = gC_{\langle(i\partial\!\!\!/q)\bar{q}\rangle}$ has been proven.

Appendix E

Master formula for one loop integration with massless fermion

Generally, every one loop integration with massless fermion can be reduced to the linear combination of one loop scalar integration of the form below:

$$\int \frac{d^D p}{(2\pi)^D} \frac{1}{[p^2]^a [(p-q)^2]^b}, \tag{E.1}$$

where a and b are positive integers. Here we calculate the analytic result of this integration with the variable a,b and D.

Utilizing the Feynman parametrization, $\frac{1}{A^a B^b} = \frac{\Gamma(a+b)}{\Gamma(a)\Gamma(b)} \int_0^1 dx \frac{x^{a-1}(1-x)^{b-1}}{[Ax+B(1-x)]^{a+b}}$, Eq.(E.1) transforms into

$$\frac{\Gamma(a+b)}{\Gamma(a)\Gamma(b)} \int_0^1 dx\, x^{a-1}(1-x)^{b-1} \int \frac{d^D p}{(2\pi)^D} \frac{1}{[p^2 x + (p-q)^2(1-x)]^{a+b}}. \tag{E.2}$$

We know the integration formula

$$\int \frac{d^D p}{(2\pi)^D} \frac{1}{(k^2 - 2k\cdot P - M^2)^\alpha} = \frac{i(-1)^\alpha \Gamma(\alpha - D/2)}{(4\pi)^{D/2}\Gamma(\alpha)} \frac{1}{(P^2+M^2)^{\alpha - D/2}} \tag{E.3}$$

with the technique of the dimensional regularization. By identifying $k = p$, $P = q(1-x)$, $M^2 = -q^2(1-x)$ and $\alpha = a+b$, Eq.(E.2) reads

$$\frac{i\Gamma(a+b-D/2)}{(-4\pi)^{D/2}\Gamma(a)\Gamma(b)(q^2)^{a+b-D/2}} \int_0^1 dx\, x^{D/2-1-b}(1-x)^{D/2-1-a}. \tag{E.4}$$

After using the result $\int_0^1 x^\alpha (1-x)^\beta = \frac{\Gamma(\alpha+1)\Gamma(\beta+1)}{\Gamma(\alpha+\beta+2)}$, we finally obtain the master formula:

$$\int \frac{d^D p}{(2\pi)^D} \frac{1}{[p^2]^a [(p-q)^2]^b} = \frac{i\,\Gamma(D/2-a)\Gamma(D/2-b)\Gamma(a+b-D/2)}{(-4\pi)^D/2\Gamma(a)\Gamma(b)\Gamma(-a-b+D)} \left(\frac{1}{q^2}\right)^{a+b-D/2}. \tag{E.5}$$

Appendix F

The modification of the SDEs with the OPE by the massive quark propagator

In this Appendix, we list the explicit forms of $\tilde{f}'s$ and f' when we make the quark mass in the free propagator finite as

$$i\frac{\not{q}}{q^2} \to i\frac{\not{q}+m}{q^2-m^2}. \tag{F.1}$$

Note that the the spinor basis of three-point 1PI function for each channel (V, A, S and P) does not change by this replacement. We also keep the space-time dimension and the gauge parameter generic. All the the results are listed below:

F.1 Vector

$$\begin{aligned}
&\tilde{f}_1(f_1,f_2,f_3,f_4)\\
=\;& f_1(q)\;\frac{X_{q\bar{q}}^2 g^4 C_F^2 (D+\xi-3)}{\left(X_{q\bar{q}}^2 g^4 C_F^2 (D+\xi-1)^2+q^2\left(q^2\left(m^2-q^2\right)-2X_{q\bar{q}}g^2 m C_F(D+\xi-1)\right)\right)^2}\\
&\times(X_{q\bar{q}}^2 g^4 C_F^2 (D+\xi-3)(D+\xi-1)^2-2X_{q\bar{q}}g^2 m q^2 C_F(D+\xi-3)(D+\xi-1)\\
&+m^2 q^4(D+\xi-3)+q^6(-D+\xi+3))\\
&+f_2(q)\;\frac{2X_{q\bar{q}}^2 g^4 \xi q^4 C_F^2 (D+\xi-3)\left(X_{q\bar{q}}g^2 C_F(D+\xi-1)-mq^2\right)}{\left(X_{q\bar{q}}^2 g^4 C_F^2 (D+\xi-1)^2+q^2\left(q^2\left(m^2-q^2\right)-2X_{q\bar{q}}g^2 m C_F(D+\xi-1)\right)\right)^2}\\
&+\frac{2X_{q\bar{q}}^2 g^4 C_F^2 (D+\xi-2)(D+\xi-1)+q^2\left(X_{q\bar{q}}g^2 m C_F(-3D-3\xi+5)+q^2\left(m^2-q^2\right)\right)}{X_{q\bar{q}}^2 g^4 C_F^2 (D+\xi-1)^2+q^2\left(q^2\left(m^2-q^2\right)-2X_{q\bar{q}}g^2 m C_F(D+\xi-1)\right)}.
\end{aligned} \tag{F.2}$$

$$
\begin{aligned}
&\tilde{f}_2(f_1,f_2,f_3,f_4)\\
&= -f_1(q)\ \frac{2X_{q\bar{q}}^2 g^4 \xi q^2 C_F^2 (D-\xi-3)\left(X_{q\bar{q}} g^2 C_F (D+\xi-1)-mq^2\right)}{\left(X_{q\bar{q}}^2 g^4 C_F^2 (D+\xi-1)^2+q^2\left(q^2\left(m^2-q^2\right)-2X_{q\bar{q}} g^2 m C_F (D+\xi-1)\right)\right)^2}\\
&\quad +f_2(q)\ \frac{X_{q\bar{q}}^2 g^4 C_F^2 (D-\xi-3)}{\left(X_{q\bar{q}}^2 g^4 C_F^2 (D+\xi-1)^2+q^2\left(q^2\left(m^2-q^2\right)-2X_{q\bar{q}} g^2 m C_F (D+\xi-1)\right)\right)^2}\\
&\quad \times\Big[X_{q\bar{q}}^2 g^4 C_F^2 (D-\xi-3)(D+\xi-1)^2-2X_{q\bar{q}} g^2 m q^2 C_F (D-\xi-3)(D+\xi-1)\\
&\quad +m^2 q^4 (D-\xi-3)+q^6(-(D+\xi-3))\Big]\\
&\quad + \frac{X_{q\bar{q}} g^2 q^2 C_F (-D+\xi+3)}{X_{q\bar{q}}^2 g^4 C_F^2 (D+\xi-1)^2+q^2\left(q^2\left(m^2-q^2\right)-2X_{q\bar{q}} g^2 m C_F (D+\xi-1)\right)}. \qquad \text{(F.3)}
\end{aligned}
$$

$$
\begin{aligned}
&\tilde{f}_3(f_1,f_2,f_3,f_4)\\
&= -f_1(q)\ \frac{2X_{q\bar{q}}^2 g^4 q^2 C_F^2\left((D-2)D+(\xi+1)^2\right)\left(X_{q\bar{q}} g^2 C_F (D+\xi-1)-mq^2\right)}{\left(X_{q\bar{q}}^2 g^4 C_F^2 (D+\xi-1)^2+q^2\left(q^2\left(m^2-q^2\right)-2X_{q\bar{q}} g^2 m C_F (D+\xi-1)\right)\right)^2}\\
&\quad +f_2(q)\ \frac{1}{\left(X_{q\bar{q}}^2 g^4 C_F^2 (D+\xi-1)^2+q^2\left(q^2\left(m^2-q^2\right)-2X_{q\bar{q}} g^2 m C_F (D+\xi-1)\right)\right)^2}\\
&\quad \times\Big[2X_{q\bar{q}}^2 g^4 C_F^2 (2X_{q\bar{q}}^2 (D-2) g^4 (\xi+1) C_F^2 (D+\xi-1)^2-4X_{q\bar{q}} (D-2) g^2 m (\xi+1) q^2 C_F (D+\xi-1)\\
&\quad +2(D-2)m^2(\xi+1)q^4+q^6\left((D-4)D-\xi^2+5\right)\Big)\Big]\\
&\quad +f_3(q)\ \frac{X_{q\bar{q}}^2 g^4 C_F^2 (D+\xi-1)}{\left(X_{q\bar{q}}^2 g^4 C_F^2 (D+\xi-1)^2+q^2\left(q^2\left(m^2-q^2\right)-2X_{q\bar{q}} g^2 m C_F (D+\xi-1)\right)\right)^2}\\
&\quad \times\Big[X_{q\bar{q}}^2 g^4 C_F^2 (D+\xi-1)^3-2X_{q\bar{q}} g^2 m q^2 C_F (D+\xi-1)^2+m^2 q^4 (D+\xi-1)+q^6 (D-\xi-1)\Big]\\
&\quad -f_4(q)\ \frac{2X_{q\bar{q}}^2 (D-1) g^4 q^4 C_F^2 (D+\xi-1)\left(mq^2-X_{q\bar{q}} g^2 C_F (D+\xi-1)\right)}{\left(X_{q\bar{q}}^2 g^4 C_F^2 (D+\xi-1)^2+q^2\left(q^2\left(m^2-q^2\right)-2X_{q\bar{q}} g^2 m C_F (D+\xi-1)\right)\right)^2}\\
&\quad - \frac{2X_{q\bar{q}} g^2 (\xi+1) q^2 C_F}{X_{q\bar{q}}^2 g^4 C_F^2 (D+\xi-1)^2+q^2\left(q^2\left(m^2-q^2\right)-2X_{q\bar{q}} g^2 m C_F (D+\xi-1)\right)}. \qquad \text{(F.4)}
\end{aligned}
$$

$$
\begin{aligned}
&\tilde{f}_4(f_1,f_2,f_3,f_4)\\
=\;& -f_1(q)\;\frac{2X_{q\bar{q}}^2 g^4 C_F^2}{q^2\left(X_{q\bar{q}}^2 g^4 C_F^2(D+\xi-1)^2+q^2\left(q^2\left(m^2-q^2\right)-2X_{q\bar{q}}g^2 m C_F(D+\xi-1)\right)\right)^2}\\
&\times\Big[2X_{q\bar{q}}^2(D-2)g^4(\xi-1)C_F^2(D+\xi-1)^2-4X_{q\bar{q}}(D-2)g^2 m(\xi-1)q^2 C_F(D+\xi-1)\\
&+2(D-2)m^2(\xi-1)q^4+q^6\left(-(D-4)D+\xi^2-5\right)\Big]\\
&-f_2(q)\;\frac{2X_{q\bar{q}}^2 g^4 q^2 C_F^2\left((D-2)D+(\xi-1)^2\right)\left(X_{q\bar{q}}g^2 C_F(D+\xi-1)-mq^2\right)}{\left(X_{q\bar{q}}^2 g^4 C_F^2(D+\xi-1)^2+q^2\left(q^2\left(m^2-q^2\right)-2X_{q\bar{q}}g^2 m C_F(D+\xi-1)\right)\right)^2}\\
&-f_3(q)\;\frac{2X_{q\bar{q}}^2(D-1)g^4 q^2 C_F^2(D-\xi-1)\left(X_{q\bar{q}}g^2 C_F(D+\xi-1)-mq^2\right)}{\left(X_{q\bar{q}}^2 g^4 C_F^2(D+\xi-1)^2+q^2\left(q^2\left(m^2-q^2\right)-2X_{q\bar{q}}g^2 m C_F(D+\xi-1)\right)\right)^2}\\
&+f_4(q)\;\frac{X_{q\bar{q}}^2 g^4 C_F^2(D-\xi-1)}{\left(X_{q\bar{q}}^2 g^4 C_F^2(D+\xi-1)^2+q^2\left(q^2\left(m^2-q^2\right)-2X_{q\bar{q}}g^2 m C_F(D+\xi-1)\right)\right)^2}\\
&\times\Big[X_{q\bar{q}}^2 g^4 C_F^2(D-\xi-1)(D+\xi-1)^2+2X_{q\bar{q}}g^2 m q^2 C_F\left(\xi^2-(D-1)^2\right)\\
&+m^2q^4(D-\xi-1)+q^6(D+\xi-1)\Big]\\
&\quad+\;\frac{2X_{q\bar{q}}g^2(\xi-1)C_F\left(X_{q\bar{q}}g^2 C_F(D+\xi-1)-mq^2\right)}{q^2\left(X_{q\bar{q}}^2 g^4\left(-C_F^2\right)(D+\xi-1)^2+2X_{q\bar{q}}g^2 m q^2 C_F(D+\xi-1)-m^2q^4+q^6\right)}. \qquad \text{(F.5)}
\end{aligned}
$$

$$
f_1(q) = \frac{2X_{q\bar{q}}^2(D-2)g^4C_F^2(D+\xi-1)-X_{q\bar{q}}g^2mq^2C_F(3D+\xi-5)+m^2q^4-q^6}{4X_{q\bar{q}}^2(D-2)g^4C_F^2-2X_{q\bar{q}}(D-1)g^2mq^2C_F+m^2q^4-q^6} \qquad \text{(F.6)}
$$

$$
f_2(q) = \frac{X_{q\bar{q}}g^2q^2C_F(-D+\xi+3)}{4X_{q\bar{q}}^2(D-2)g^4C_F^2-2X_{q\bar{q}}(D-1)g^2mq^2C_F+m^2q^4-q^6} \qquad \text{(F.7)}
$$

$$
\begin{aligned}
f_3(q) =\;& \frac{2X_{q\bar{q}}g^2C_F}{\left(4X_{q\bar{q}}^2(D-2)g^4C_F^2-2X_{q\bar{q}}(D-1)g^2mq^2C_F+m^2q^4-q^6\right)\left(2X_{q\bar{q}}g^2m\xi C_F-m^2q^2+q^4\right)}\\
&\times\Big[2X_{q\bar{q}}^2(D-2)g^4C_F^2(D+\xi-1)-X_{q\bar{q}}g^2mq^2C_F\left(D^2-2D+(\xi+1)^2\right)\\
&+m^2(\xi+1)q^4-(\xi+1)q^6\Big] \qquad \text{(F.8)}
\end{aligned}
$$

$$
\begin{aligned}
f_4(q) =\;& \frac{2X_{q\bar{q}}g^2C_F}{q^2\left(-4X_{q\bar{q}}^2(D-2)g^4C_F^2+2X_{q\bar{q}}(D-1)g^2mq^2C_F-m^2q^4+q^6\right)\left(2X_{q\bar{q}}g^2m\xi C_F-m^2q^2+q^4\right)}\\
&\times\Big[2X_{q\bar{q}}^2(D-2)g^4m(\xi-1)C_F^2(D+\xi-1)+q^4\left(X_{q\bar{q}}(D-2)g^2C_F(D+\xi-3)+m^3(\xi-1)\right)\\
&-X_{q\bar{q}}g^2m^2(\xi-1)q^2C_F(3D+\xi-5)+q^6(m-m\xi)\Big] \qquad \text{(F.9)}
\end{aligned}
$$

F.2 Axial vector

$$
\begin{aligned}
&\tilde{f}_1(f_1,f_2,f_3,f_4)\\
= \quad & f_1(q)\ \frac{X_{q\bar{q}}^2 g^4 C_F^2 (D+\xi-1)}{\left(X_{q\bar{q}}^2 g^4 C_F^2 (D+\xi-1)^2 + q^2\left(q^2\left(m^2-q^2\right) - 2X_{q\bar{q}} g^2 m C_F (D+\xi-1)\right)\right)^2}\\
&\times\Big[X_{q\bar{q}}^2 g^4 C_F^2 (D+\xi-1)^3 - 2X_{q\bar{q}} g^2 m q^2 C_F (D+\xi-1)^2 + m^2 q^4 (D+\xi-1) + q^6(-D+\xi+1)\Big]\\
&+f_2(q)\ \frac{2X_{q\bar{q}}^2 g^4 \xi q^4 C_F^2 (D+\xi-1)\left(X_{q\bar{q}} g^2 C_F (D+\xi-1) - mq^2\right)}{\left(X_{q\bar{q}}^2 g^4 C_F^2 (D+\xi-1)^2 + q^2\left(q^2\left(m^2-q^2\right) - 2X_{q\bar{q}} g^2 m C_F (D+\xi-1)\right)\right)^2}\\
&+f_3(q)\ \frac{2X_{q\bar{q}}^2 g^4 q^2 C_F^2\left((D-3)^2+\xi^2+2\xi\right)\left(X_{q\bar{q}} g^2 C_F (D+\xi-1) - mq^2\right)}{\left(X_{q\bar{q}}^2 g^4 C_F^2 (D+\xi-1)^2 + q^2\left(q^2\left(m^2-q^2\right) - 2X_{q\bar{q}} g^2 m C_F (D+\xi-1)\right)\right)^2}\\
&+f_4(q)\ \frac{2X_{q\bar{q}}^2 g^4 C_F^2}{\left(X_{q\bar{q}}^2 g^4 C_F^2 (D+\xi-1)^2 + q^2\left(q^2\left(m^2-q^2\right) - 2X_{q\bar{q}} g^2 m C_F (D+\xi-1)\right)\right)^2}\\
&\times\Big[2X_{q\bar{q}}^2 (D-2) g^4 (\xi+1) C_F^2 (D+\xi-1)^2 - 4X_{q\bar{q}} (D-2) g^2 m (\xi+1) q^2 C_F (D+\xi-1)\\
&+2(D-2) m^2 (\xi+1) q^4 + q^6\left(-(D-4)D + \xi^2 - 5\right)\Big]\\
&+\ \frac{2X_{q\bar{q}} g^2 (\xi+1) q^2 C_F}{X_{q\bar{q}}^2 g^4 C_F^2 (D+\xi-1)^2 + q^2\left(q^2\left(m^2-q^2\right) - 2X_{q\bar{q}} g^2 m C_F (D+\xi-1)\right)}. \qquad \text{(F.10)}
\end{aligned}
$$

$$
\begin{aligned}
&\tilde{f}_2(f_1,f_2,f_3,f_4)\\
=\quad & -f_1(q)\ \frac{2X_{q\bar{q}}^2 g^4\xi q^2 C_F^2(D-\xi-1)\left(X_{q\bar{q}}g^2C_F(D+\xi-1)-mq^2\right)}{\left(X_{q\bar{q}}^2g^4C_F^2(D+\xi-1)^2+q^2\left(q^2\left(m^2-q^2\right)-2X_{q\bar{q}}g^2mC_F(D+\xi-1)\right)\right)^2}\\
& +f_2(q)\ \frac{X_{q\bar{q}}^2g^4C_F^2(D-\xi-1)}{\left(X_{q\bar{q}}^2g^4C_F^2(D+\xi-1)^2+q^2\left(q^2\left(m^2-q^2\right)-2X_{q\bar{q}}g^2mC_F(D+\xi-1)\right)\right)^2}\\
& \times\Big[X_{q\bar{q}}^2g^4C_F^2(D-\xi-1)(D+\xi-1)^2+2X_{q\bar{q}}g^2mq^2C_F\left(\xi^2-(D-1)^2\right)\\
& +m^2q^4(D-\xi-1)+q^6(-(D+\xi-1))\Big]\\
& -f_3(q)\ \frac{2X_{q\bar{q}}^2g^4C_F^2}{q^2\left(X_{q\bar{q}}^2g^4C_F^2(D+\xi-1)^2+q^2\left(q^2\left(m^2-q^2\right)-2X_{q\bar{q}}g^2mC_F(D+\xi-1)\right)\right)^2}\\
& \times\Big[2X_{q\bar{q}}^2(D-2)g^4(\xi-1)C_F^2(D+\xi-1)^2-4X_{q\bar{q}}(D-2)g^2m(\xi-1)q^2C_F(D+\xi-1)\\
& +2(D-2)m^2(\xi-1)q^4+q^6\left((D-4)D-\xi^2+5\right)\Big]\\
& +f_4(q)\ \frac{2X_{q\bar{q}}^2g^4q^2C_F^2\left((D-3)^2+\xi^2-2\xi\right)\left(X_{q\bar{q}}g^2C_F(D+\xi-1)-mq^2\right)}{\left(X_{q\bar{q}}^2g^4C_F^2(D+\xi-1)^2+q^2\left(q^2\left(m^2-q^2\right)-2X_{q\bar{q}}g^2mC_F(D+\xi-1)\right)\right)^2}\\
& -\ \frac{2X_{q\bar{q}}g^2(\xi-1)C_F\left(mq^2-X_{q\bar{q}}g^2C_F(D+\xi-1)\right)}{q^2\left(X_{q\bar{q}}^2g^4\left(-C_F^2\right)(D+\xi-1)^2+2X_{q\bar{q}}g^2mq^2C_F(D+\xi-1)-m^2q^4+q^6\right)}.
\end{aligned}
\tag{F.11}
$$

$$
\begin{aligned}
&\tilde{f}_3(f_1,f_2,f_3,f_4)\\
=\quad & f_3(q)\ \frac{X_{q\bar{q}}^2g^4C_F^2(D+\xi-3)}{\left(X_{q\bar{q}}^2g^4C_F^2(D+\xi-1)^2+q^2\left(q^2\left(m^2-q^2\right)-2X_{q\bar{q}}g^2mC_F(D+\xi-1)\right)\right)^2}\\
& \times\Big[X_{q\bar{q}}^2g^4C_F^2(D+\xi-3)(D+\xi-1)^2-2X_{q\bar{q}}g^2mq^2C_F(D+\xi-3)(D+\xi-1)\\
& +m^2q^4(D+\xi-3)+q^6(D-\xi-3)\Big]\\
& -f_4(q)\ \frac{2X_{q\bar{q}}^2(D-3)g^4q^4C_F^2(D+\xi-3)\left(X_{q\bar{q}}g^2C_F(D+\xi-1)-mq^2\right)}{\left(X_{q\bar{q}}^2g^4C_F^2(D+\xi-1)^2+q^2\left(q^2\left(m^2-q^2\right)-2X_{q\bar{q}}g^2mC_F(D+\xi-1)\right)\right)^2}\\
& +\ \frac{2X_{q\bar{q}}^2g^4C_F^2(D+\xi-1)+q^2\left(q^2\left(m^2-q^2\right)-X_{q\bar{q}}g^2mC_F(D+\xi+1)\right)}{X_{q\bar{q}}^2g^4C_F^2(D+\xi-1)^2+q^2\left(q^2\left(m^2-q^2\right)-2X_{q\bar{q}}g^2mC_F(D+\xi-1)\right)}.
\end{aligned}
\tag{F.12}
$$

$$
\begin{aligned}
&\tilde{f}_4(f_1,f_2,f_3,f_4)\\
=\;& -f_3(q)\;\frac{2X_{q\bar{q}}^2(D-3)g^4q^2C_F^2(D-\xi-3)\left(X_{q\bar{q}}g^2C_F(D+\xi-1)-mq^2\right)}{\left(X_{q\bar{q}}^2g^4C_F^2(D+\xi-1)^2+q^2\left(q^2\left(m^2-q^2\right)-2X_{q\bar{q}}g^2mC_F(D+\xi-1)\right)\right)^2}\\
&+f_4(q)\;\frac{X_{q\bar{q}}^2g^4C_F^2(D-\xi-3)}{\left(X_{q\bar{q}}^2g^4C_F^2(D+\xi-1)^2+q^2\left(q^2\left(m^2-q^2\right)-2X_{q\bar{q}}g^2mC_F(D+\xi-1)\right)\right)^2}\\
&\times\Big[X_{q\bar{q}}^2g^4C_F^2(D-\xi-3)(D+\xi-1)^2-2X_{q\bar{q}}g^2mq^2C_F(D-\xi-3)(D+\xi-1)\\
&+m^2q^4(D-\xi-3)+q^6(D+\xi-3)\Big]\\
&+\;\frac{X_{q\bar{q}}g^2q^2C_F(D-\xi-3)}{X_{q\bar{q}}^2g^4C_F^2(D+\xi-1)^2+q^2\left(q^2\left(m^2-q^2\right)-2X_{q\bar{q}}g^2mC_F(D+\xi-1)\right)}. \qquad \text{(F.13)}
\end{aligned}
$$

$$
\begin{aligned}
f_1(q) \;=\;& -\frac{2X_{q\bar{q}}g^2C_F}{2X_{q\bar{q}}(D-1)g^2mC_F-m^2q^2+q^4}\\
&\times\frac{1}{4X_{q\bar{q}}^2(D-2)g^4C_F^2(D+\xi-2)+q^2\left(q^2\left(m^2-q^2\right)-2X_{q\bar{q}}g^2mC_F(2D+\xi-4)\right)}\\
&\times\Big[2X_{q\bar{q}}^2(D-2)g^4C_F^2(D+\xi-2)(D+\xi-1)\\
&+q^2\left((\xi+1)q^2\left(m^2-q^2\right)-X_{q\bar{q}}g^2mC_F\left(D^2+D(4\xi-2)+(\xi-6)\xi+1\right)\right)\Big] \qquad \text{(F.14)}\\
f_2(q) \;=\;& -\frac{2X_{q\bar{q}}g^2C_F}{q^2\left(2X_{q\bar{q}}(D-1)g^2mC_F-m^2q^2+q^4\right)}\\
&\times\frac{1}{-4X_{q\bar{q}}^2(D-2)g^4C_F^2(D+\xi-2)+2X_{q\bar{q}}g^2mq^2C_F(2D+\xi-4)-m^2q^4+q^6}\\
&\times\Big[2X_{q\bar{q}}^2(D-2)g^4m(\xi-1)C_F^2(D+\xi-1)+q^2\big(q^2(X_{q\bar{q}}(D-2)g^2C_F(D+\xi-3)\\
&+m^3(\xi-1)+q^2(m-m\xi))-X_{q\bar{q}}g^2m^2(\xi-1)C_F(3D+\xi-5)\big)\Big] \qquad \text{(F.15)}\\
f_3(q) \;=\;& \frac{2X_{q\bar{q}}^2(D-2)g^4C_F^2(D+\xi-1)+q^2\left(q^2\left(m^2-q^2\right)-X_{q\bar{q}}g^2mC_F(3D+\xi-5)\right)}{4X_{q\bar{q}}^2(D-2)g^4C_F^2(D+\xi-2)+q^2\left(q^2\left(m^2-q^2\right)-2X_{q\bar{q}}g^2mC_F(2D+\xi-4)\right)} \qquad \text{(F.16)}\\
f_4(q) \;=\;& \frac{X_{q\bar{q}}g^2q^2C_F(D-\xi-3)}{4X_{q\bar{q}}^2(D-2)g^4C_F^2(D+\xi-2)+q^2\left(q^2\left(m^2-q^2\right)-2X_{q\bar{q}}g^2mC_F(2D+\xi-4)\right)} \qquad \text{(F.17)}
\end{aligned}
$$

F.3 Scalar

$$\tilde{f}_1(f_1,f_2)$$

$$\begin{aligned}
= \quad & f_1(q)\ \frac{X_{q\bar{q}}^2 g^4 C_F^2 (D+\xi-1)}{\left(X_{q\bar{q}}^2 g^4 C_F^2 (D+\xi-1)^2 + q^2\left(q^2\left(m^2-q^2\right) - 2X_{q\bar{q}} g^2 m C_F (D+\xi-1)\right)\right)^2} \\
& \times\Big[X_{q\bar{q}}^2 g^4 C_F^2 (D+\xi-1)^3 - 2X_{q\bar{q}} g^2 m q^2 C_F (D+\xi-1)^2 + m^2 q^4 (D+\xi-1) + q^6 (D-\xi-1)\Big] \\
& -f_2(q)\ \frac{2X_{q\bar{q}}^2 (D-1) g^4 q^4 C_F^2 (D+\xi-1)\left(mq^2 - X_{q\bar{q}} g^2 C_F (D+\xi-1)\right)}{\left(X_{q\bar{q}}^2 g^4 C_F^2 (D+\xi-1)^2 + q^2\left(q^2\left(m^2-q^2\right) - 2X_{q\bar{q}} g^2 m C_F (D+\xi-1)\right)\right)^2} \\
& - \frac{q^2\left(X_{q\bar{q}} g^2 m C_F (D+\xi-1) - m^2 q^2 + q^4\right)}{X_{q\bar{q}}^2 g^4\left(-C_F^2\right)(D+\xi-1)^2 + 2X_{q\bar{q}} g^2 m q^2 C_F (D+\xi-1) - m^2 q^4 + q^6}. \qquad \text{(F.18)}
\end{aligned}$$

$$\tilde{f}_2(f_1,f_2)$$

$$\begin{aligned}
= \quad & -f_1(q)\ - \frac{2X_{q\bar{q}}^2 (D-1) g^4 q^2 C_F^2 (D-\xi-1)\left(X_{q\bar{q}} g^2 C_F (D+\xi-1) - mq^2\right)}{\left(X_{q\bar{q}}^2 g^4 C_F^2 (D+\xi-1)^2 + q^2\left(q^2\left(m^2-q^2\right) - 2X_{q\bar{q}} g^2 m C_F (D+\xi-1)\right)\right)^2} \\
& +f_2(q)\ \frac{X_{q\bar{q}}^2 g^4 C_F^2 (D-\xi-1)}{\left(X_{q\bar{q}}^2 g^4 C_F^2 (D+\xi-1)^2 + q^2\left(q^2\left(m^2-q^2\right) - 2X_{q\bar{q}} g^2 m C_F (D+\xi-1)\right)\right)^2} \\
& \times\Big[X_{q\bar{q}}^2 g^4 C_F^2 (D-\xi-1)(D+\xi-1)^2 + 2X_{q\bar{q}} g^2 m q^2 C_F\left(\xi^2 - (D-1)^2\right) \\
& +m^2 q^4 (D-\xi-1) + q^6 (D+\xi-1)\Big] \\
& + \frac{X_{q\bar{q}} g^2 q^2 C_F (D-\xi-1)}{X_{q\bar{q}}^2 g^4 C_F^2 (D+\xi-1)^2 + q^2\left(q^2\left(m^2-q^2\right) - 2X_{q\bar{q}} g^2 m C_F (D+\xi-1)\right)}. \qquad \text{(F.19)}
\end{aligned}$$

$$f_1(q) = \frac{2X_{q\bar{q}}^2 (D-1) g^4 C_F^2 (D+\xi-1) + q^2\left(q^2\left(m^2-q^2\right) - X_{q\bar{q}} g^2 m C_F (3D+\xi-3)\right)}{4X_{q\bar{q}}^2 (D-1) g^4 C_F^2 (D+\xi-1) + q^2\left(q^2\left(m^2-q^2\right) - 2X_{q\bar{q}} g^2 m C_F (2D+\xi-2)\right)} \qquad \text{(F.20)}$$

$$f_2(q) = \frac{X_{q\bar{q}} g^2 q^2 C_F (D-\xi-1)}{4X_{q\bar{q}}^2 (D-1) g^4 C_F^2 (D+\xi-1) + q^2\left(q^2\left(m^2-q^2\right) - 2X_{q\bar{q}} g^2 m C_F (2D+\xi-2)\right)} \qquad \text{(F.21)}$$

F.4 Pseudoscalar

$$
\begin{aligned}
&\tilde{f}_1(f_1,f_2)\\
= \quad & f_1(q)\ \frac{X_{q\bar{q}}^2 g^4 C_F^2 (D+\xi-1)}{\left(X_{q\bar{q}}^2 g^4 C_F^2 (D+\xi-1)^2 + q^2\left(q^2\left(m^2-q^2\right)-2X_{q\bar{q}} g^2 m C_F (D+\xi-1)\right)\right)^2}\\
&\times\Big[X_{q\bar{q}}^2 g^4 C_F^2 (D+\xi-1)^3 - 2X_{q\bar{q}} g^2 m q^2 C_F (D+\xi-1)^2 + m^2 q^4 (D+\xi-1) + q^6(-D+\xi+1)\Big]\\
&+f_2(q)\ \frac{2X_{q\bar{q}}^2 g^4 \xi q^4 C_F^2 (D+\xi-1)\left(X_{q\bar{q}} g^2 C_F (D+\xi-1) - m q^2\right)}{\left(X_{q\bar{q}}^2 g^4 C_F^2 (D+\xi-1)^2 + q^2\left(q^2\left(m^2-q^2\right)-2X_{q\bar{q}} g^2 m C_F (D+\xi-1)\right)\right)^2}\\
&\quad + \frac{i\left(2X_{q\bar{q}}^2 g^4 C_F^2 (D+\xi-1)^2 + q^2\left(q^2\left(m^2-q^2\right)-3X_{q\bar{q}} g^2 m C_F (D+\xi-1)\right)\right)}{X_{q\bar{q}}^2 g^4 C_F^2 (D+\xi-1)^2 + q^2\left(q^2\left(m^2-q^2\right)-2X_{q\bar{q}} g^2 m C_F (D+\xi-1)\right)}.
\end{aligned}
\tag{F.22}
$$

$$
\begin{aligned}
&\tilde{f}_2(f_1,f_2)\\
= \quad & -f_1(q)\frac{2X_{q\bar{q}}^2 g^4 \xi q^2 C_F^2 (D-\xi-1)\left(X_{q\bar{q}} g^2 C_F (D+\xi-1) - m q^2\right)}{\left(X_{q\bar{q}}^2 g^4 C_F^2 (D+\xi-1)^2 + q^2\left(q^2\left(m^2-q^2\right)-2X_{q\bar{q}} g^2 m C_F (D+\xi-1)\right)\right)^2}\\
&+f_2(q)\frac{X_{q\bar{q}}^2 g^4 C_F^2 (D-\xi-1)}{\left(X_{q\bar{q}}^2 g^4 C_F^2 (D+\xi-1)^2 + q^2\left(q^2\left(m^2-q^2\right)-2X_{q\bar{q}} g^2 m C_F (D+\xi-1)\right)\right)^2}\\
&\times\Big[X_{q\bar{q}}^2 g^4 C_F^2 (D-\xi-1)(D+\xi-1)^2 + 2X_{q\bar{q}} g^2 m q^2 C_F\left(\xi^2-(D-1)^2\right)\\
&+m^2 q^4 (D-\xi-1) + q^6(-(D+\xi-1))\Big]\\
&\quad - \frac{i X_{q\bar{q}} g^2 q^2 C_F (D-\xi-1)}{X_{q\bar{q}}^2 g^4 C_F^2 (D+\xi-1)^2 + q^2\left(q^2\left(m^2-q^2\right)-2X_{q\bar{q}} g^2 m C_F (D+\xi-1)\right)}.
\end{aligned}
\tag{F.23}
$$

$$
f_1(q) = \frac{i\left(-2X_{q\bar{q}}^2 (D-1) g^4 C_F^2 (D+\xi-1) + X_{q\bar{q}} g^2 m q^2 C_F (3D+\xi-3) - m^2 q^4 + q^6\right)}{q^2\left(2X_{q\bar{q}} (D-1) g^2 m C_F - m^2 q^2 + q^4\right)} \tag{F.24}
$$

$$
f_2(q) = \frac{i X_{q\bar{q}} g^2 C_F (D-\xi-1)}{2X_{q\bar{q}} (D-1) g^2 m C_F - m^2 q^2 + q^4} \tag{F.25}
$$

Bibliography

[1] M. Gell-Mann, "A Schematic Model of Baryons and Mesons," *Phys. Lett.* **8** (1964) 214–215.

[2] G. Zweig, "An SU(3) model for strong interaction symmetry and its breaking. Version 1,".

[3] G. Zweig, "An SU(3) model for strong interaction symmetry and its breaking. Version 2," in *Developments in the quark theory of hadrons. Vol. 1. 1964 - 1978*, D. Lichtenberg and S. P. Rosen, eds.

[4] C.-N. Yang and R. L. Mills, "Conservation of Isotopic Spin and Isotopic Gauge Invariance," *Phys. Rev.* **96** (1954) 191–195.

[5] **Particle Data Group** Collaboration, C. Patrignani *et al.*, "Review of Particle Physics," *Chin. Phys.* **C40** no. 10, (2016) 100001.

[6] D. J. Gross and F. Wilczek, "Ultraviolet Behavior of Nonabelian Gauge Theories," *Phys. Rev. Lett.* **30** (1973) 1343–1346.

[7] H. D. Politzer, "Reliable Perturbative Results for Strong Interactions?," *Phys. Rev. Lett.* **30** (1973) 1346–1349.

[8] M. Gell-Mann and F. E. Low, "Quantum electrodynamics at small distances," *Phys. Rev.* **95** (1954) 1300–1312.

[9] K. Symanzik, "Small distance behavior in field theory and power counting," *Commun. Math. Phys.* **18** (1970) 227–246.

[10] C. G. Callan, Jr., "Broken scale invariance in scalar field theory," *Phys. Rev.* **D2** (1970) 1541–1547.

[11] W. E. Caswell, "Asymptotic Behavior of Nonabelian Gauge Theories to Two Loop Order," *Phys. Rev. Lett.* **33** (1974) 244.

[12] D. R. T. Jones, "Two Loop Diagrams in Yang-Mills Theory," *Nucl. Phys.* **B75** (1974) 531.

[13] E. Egorian and O. V. Tarasov, "Two Loop Renormalization of the QCD in an Arbitrary Gauge," *Teor. Mat. Fiz.* **41** (1979) 26–32. [Theor. Math. Phys.41,863(1979)].

[14] O. V. Tarasov, A. A. Vladimirov, and A. Yu. Zharkov, "The Gell-Mann-Low Function of QCD in the Three Loop Approximation," *Phys. Lett.* **B93** (1980) 429–432.

[15] S. A. Larin and J. A. M. Vermaseren, "The Three loop QCD Beta function and anomalous dimensions," *Phys. Lett.* **B303** (1993) 334–336, `arXiv:hep-ph/9302208 [hep-ph]`.

[16] Y. Nambu and G. Jona-Lasinio, "Dynamical Model of Elementary Particles Based on an Analogy with Superconductivity. 1.," *Phys. Rev.* **122** (1961) 345–358.

[17] M. E. Peskin and D. V. Schroeder, *An Introduction to quantum field theory*.

[18] B. Ioffe, "Calculation of Baryon Masses in Quantum Chromodynamics," *Nucl.Phys.* **B188** (1981) 317–341.

[19] M. A. Shifman, A. Vainshtein, and V. I. Zakharov, "QCD and Resonance Physics. Sum Rules," *Nucl.Phys.* **B147** (1979) 385–447.

[20] M. A. Shifman, A. Vainshtein, and V. I. Zakharov, "QCD and Resonance Physics: Applications," *Nucl.Phys.* **B147** (1979) 448–518.

[21] P. Gubler and M. Oka, "A Bayesian approach to QCD sum rules," *Prog.Theor.Phys.* **124** (2010) 995–1018, `arXiv:1005.2459 [hep-ph]`.

[22] K. Ohtani, P. Gubler, and M. Oka, "A Bayesian analysis of the nucleon QCD sum rules," *Eur. Phys. J.* **A47** (2011) 114.

[23] V. Novikov, L. Okun, M. A. Shifman, A. Vainshtein, M. Voloshin, and V. I. Zakharov, "Sum Rules for Charmonium and Charmed Mesons Decay Rates in Quantum Chromodynamics," *Phys.Rev.Lett.* **38** (1977) 626.

[24] V. Novikov, L. Okun, M. A. Shifman, A. Vainshtein, M. Voloshin, *et al.*, "Sum Rules for the Decays of the C Even Charmonium States," *Phys.Lett.* **B67** (1977) 409.

[25] V. Novikov, L. Okun, M. A. Shifman, A. Vainshtein, M. Voloshin, *et al.*, "Charmonium and Gluons: Basic Experimental Facts and Theoretical Introduction," *Phys.Rept.* **41** (1978) 1–133.

[26] A. Vainshtein, V. I. Zakharov, and M. A. Shifman, "Gluon condensate and lepton decays of vector mesons. (in Russian)," *JETP Lett.* **27** (1978) 55–58.

[27] M. A. Shifman, A. Vainshtein, M. Voloshin, and V. I. Zakharov, "eta(c) Puzzle in Quantum Chromodynamics," *Phys.Lett.* **B77** (1978) 80–83.

[28] V. Novikov, M. A. Shifman, A. Vainshtein, and V. I. Zakharov, "eta-prime Meson as Pseudoscalar Gluonium," *Phys.Lett.* **B86** (1979) 347.

[29] V. Novikov, M. A. Shifman, A. Vainshtein, and V. I. Zakharov, "In a Search for Scalar Gluonium," *Nucl.Phys.* **B165** (1980) 67.

[30] L. Reinders, H. Rubinstein, and S. Yazaki, "QCD contributions to vacuum polarization," *Phys.Lett.* **B94** (1980) 203.

[31] L. Reinders, H. Rubinstein, and S. Yazaki, "Masses of Lowest Lying Heavy Mesons in QCD," *Phys.Lett.* **B95** (1980) 103.

[32] L. Reinders, H. Rubinstein, and S. Yazaki, "QCD Contribution to Vacuum Polarization 2. The Pseudoscalar Unequal Mass Case," *Phys.Lett.* **B97** (1980) 257.

[33] L. Reinders, H. Rubinstein, and S. Yazaki, "QCD Sum Rules for Heavy Quark Systems," *Nucl.Phys.* **B186** (1981) 109.

[34] T. Aliev and M. A. Shifman, "Old Tensor Mesons in QCD Sum Rules," *Phys.Lett.* **B112** (1982) 401.

[35] Y. Chung, H. G. Dosch, M. Kremer, and D. Schall, "QCD Sum Rules for 'Baryonic Currents'," *Phys.Lett.* **B102** (1981) 175.

[36] L. Reinders, S. Yazaki, and H. Rubinstein, "Two Point Functions for Flavor Changing Currents in QCD," *Phys.Lett.* **B103** (1981) 63.

[37] L. Reinders, S. Yazaki, and H. Rubinstein, "Masses and Couplings of Open Beauty States in QCD," *Phys.Lett.* **B104** (1981) 305.

[38] Y. Chung, H. G. Dosch, M. Kremer, and D. Schall, "Baryon Sum Rules and Chiral Symmetry Breaking," *Nucl.Phys.* **B197** (1982) 55.

[39] L. Reinders, S. Yazaki, and H. Rubinstein, "L = 1 Light Quark Mesons in QCD," *Nucl.Phys.* **B196** (1982) 125.

[40] E. V. Shuryak, "Hadrons Containing a Heavy Quark and QCD Sum Rules," *Nucl.Phys.* **B198** (1982) 83.

[41] V. Nesterenko and A. Radyushkin, "Pion Form-factor and QCD Sum Rules," *JETP Lett.* **35** (1982) 488.

[42] V. Belyaev and B. Ioffe, "Determination of baryon and baryonic masses from QCD sum rules. Strange baryons," *Sov.Phys.JETP* **57** (1983) 716–721.

[43] B. Ioffe and A. V. Smilga, "Pion Form-Factor at Intermediate Momentum Transfer in QCD," *Phys.Lett.* **B114** (1982) 353.

[44] V. Nesterenko and A. Radyushkin, "Sum Rules and Pion Form-Factor in QCD," *Phys.Lett.* **B115** (1982) 410.

[45] B. Ioffe and A. V. Smilga, "Meson Widths and Form-Factors at Intermediate Momentum Transfer in Nonperturbative QCD," *Nucl.Phys.* **B216** (1983) 373.

[46] T. Aliev and V. Eletsky, "On Leptonic Decay Constants of Pseudoscalar D and B Mesons," *Sov.J.Nucl.Phys.* **38** (1983) 936.

[47] B. Ioffe and A. V. Smilga, "Proton and Neutron Magnetic Moments in QCD," *JETP Lett.* **37** (1983) 298.

[48] B. Ioffe and A. V. Smilga, "Nucleon Magnetic Moments and Magnetic Properties of Vacuum in QCD," *Nucl.Phys.* **B232** (1984) 109.

[49] T. Hatsuda, Y. Koike, and S.-H. Lee, "Finite temperature QCD sum rules reexamined: rho, omega and A1 mesons," *Nucl. Phys.* **B394** (1993) 221–266.

[50] T. Hatsuda, Y. Koike, and S.-H. Lee, "Pattern of chiral restoration at low temperature from QCD sum rules," *Phys. Rev.* **D47** (1993) 1225–1230.

[51] C. Adami, T. Hatsuda, and I. Zahed, "QCD SUM RULES AT LOW TEMPERATURE," *Phys. Rev.* **D43** (1991) 921–932.

[52] R. J. Furnstahl, T. Hatsuda, and S. H. Lee, "Applications of QCD Sum Rules at Finite Temperature," *Phys. Rev.* **D42** (1990) 1744–1756.

[53] Y. Kwon, C. Sasaki, and W. Weise, "Vector mesons at finite temperature and QCD sum rules," *Phys. Rev.* **C81** (2010) 065203, arXiv:1004.1059 [nucl-th].

[54] J. I. Kapusta and E. V. Shuryak, "Weinberg type sum rules at zero and finite temperature," *Phys. Rev.* **D49** (1994) 4694–4704, arXiv:hep-ph/9312245 [hep-ph].

[55] K. Morita and S. H. Lee, "Mass shift and width broadening of J/psi in QGP from QCD sum rule," *Phys. Rev. Lett.* **100** (2008) 022301, arXiv:0704.2021 [nucl-th].

[56] K. Morita and S. H. Lee, "Critical behavior of charmonia across the phase transition: A QCD sum rule approach," *Phys. Rev.* **C77** (2008) 064904, arXiv:0711.3998 [hep-ph].

[57] Y.-H. Song, S. H. Lee, and K. Morita, "In-medium modification of P-wave charmonia from QCD sum rules," *Phys. Rev.* **C79** (2009) 014907, arXiv:0808.1153 [hep-ph].

[58] K. Morita and S. H. Lee, "Heavy quarkonium correlators at finite temperature: QCD sum rule approach," *Phys.Rev.* **D82** (2010) 054008, arXiv:0908.2856 [hep-ph].

[59] P. Gubler, K. Morita, and M. Oka, "Charmonium spectra at finite temperature from QCD sum rules with the maximum entropy method," *Phys. Rev. Lett.* **107** (2011) 092003, arXiv:1104.4436 [hep-ph].

[60] K. Suzuki, P. Gubler, K. Morita, and M. Oka, "Thermal modification of bottomonium spectra from QCD sum rules with the maximum entropy method," *Nucl. Phys.* **A897** (2013) 28–41, arXiv:1204.1173 [hep-ph].

[61] H.-c. Kim and M. Oka, "Update on pion weak decay constants in nuclear matter," *Nucl.Phys.* **A720** (2003) 368–381, arXiv:hep-ph/0301227 [hep-ph].

[62] M. Asakawa and C. Ko, "Medium effects on the rho meson," *Phys.Rev.* **C48** (1993) 526–529.

[63] M. Asakawa and C. Ko, "QCD sum rules for a rho meson in dense matter," *Nucl.Phys.* **A560** (1993) 399–410.

[64] T. Hatsuda, S. H. Lee, and H. Shiomi, "QCD sum rules, scattering length and the vector mesons in nuclear medium," *Phys.Rev.* **C52** (1995) 3364–3372, arXiv:nucl-th/9505005 [nucl-th].

[65] X.-m. Jin and D. B. Leinweber, "Valid QCD sum rules for vector mesons in nuclear matter," *Phys.Rev.* **C52** (1995) 3344–3352, arXiv:nucl-th/9510064 [nucl-th].

[66] Y. Koike and A. Hayashigaki, "QCD sum rules for rho, omega, phi meson - nucleon scattering lengths and the mass shifts in nuclear medium," *Prog.Theor.Phys.* **98** (1997) 631–652, arXiv:nucl-th/9609001 [nucl-th].

[67] F. Klingl, N. Kaiser, and W. Weise, "Current correlation functions, QCD sum rules and vector mesons in baryonic matter," *Nucl.Phys.* **A624** (1997) 527–563, arXiv:hep-ph/9704398 [hep-ph].

[68] S. H. Lee, "Vector mesons in-medium with finite three momentum," *Phys.Rev.* **C57** (1998) 927–930, arXiv:nucl-th/9705048 [nucl-th].

[69] S. Leupold, W. Peters, and U. Mosel, "What QCD sum rules tell about the rho meson," *Nucl.Phys.* **A628** (1998) 311–324, arXiv:nucl-th/9708016 [nucl-th].

[70] S. Leupold and U. Mosel, "On QCD sum rules for vector mesons in nuclear medium," *Phys.Rev.* **C58** (1998) 2939–2957, arXiv:nucl-th/9805024 [nucl-th].

[71] S. Leupold, "QCD sum rule analysis for light vector and axial - vector mesons in vacuum and nuclear matter," *Phys.Rev.* **C64** (2001) 015202, arXiv:nucl-th/0101013 [nucl-th].

[72] S. Zschocke, O. Pavlenko, and B. Kampfer, "Evaluation of QCD sum rules for light vector mesons at finite density and temperature," *Eur.Phys.J.* **A15** (2002) 529–537, arXiv:nucl-th/0205057 [nucl-th].

[73] B. Kampfer and S. Zschocke, "Finite width QCD sum rules for rho and omega mesons," *Prog.Part.Nucl.Phys.* **53** (2004) 317–327, arXiv:nucl-th/0311042 [nucl-th].

[74] S. Zschocke and B. Kampfer, "rho - omega splitting and mixing in nuclear matter," *Phys.Rev.* **C70** (2004) 035207, arXiv:hep-ph/0404176 [hep-ph].

[75] J. Ruppert, T. Renk, and B. Muller, "Mass and width of the rho meson in a nuclear medium from Brown-Rho scaling and QCD sum rules," *Phys.Rev.* **C73** (2006) 034907, arXiv:hep-ph/0509134 [hep-ph].

[76] Y. Kwon, M. Procura, and W. Weise, "QCD sum rules for rho mesons in vacuum and in-medium, re-examined," *Phys.Rev.* **C78** (2008) 055203, arXiv:0803.3262 [nucl-th].

[77] T. Hilger, R. Thomas, B. Kampfer, and S. Leupold, "The impact of chirally odd condensates on the rho meson," *Phys.Lett.* **B709** (2012) 200–206, arXiv:1005.4876 [nucl-th].

[78] T. Hatsuda and S. H. Lee, "QCD sum rules for vector mesons in nuclear medium," *Phys.Rev.* **C46** (1992) 34–38.

[79] S. Zschocke, O. Pavlenko, and B. Kampfer, "In-medium spectral change of omega mesons as a probe of QCD four quark condensate," *Phys.Lett.* **B562** (2003) 57–62, arXiv:hep-ph/0212201 [hep-ph].

[80] R. Thomas, S. Zschocke, and B. Kampfer, "Evidence for in-medium changes of four-quark condensates," *Phys.Rev.Lett.* **95** (2005) 232301, arXiv:hep-ph/0510156 [hep-ph].

[81] B. Steinmueller and S. Leupold, "Weighted finite energy sum rules for the omega meson in nuclear matter," *Nucl.Phys.* **A778** (2006) 195–216, arXiv:hep-ph/0604054 [hep-ph].

[82] M. Asakawa and C. Ko, "Phi meson mass in hot and dense matter," *Nucl.Phys.* **A572** (1994) 732–748.

[83] B. Kampfer, O. Pavlenko, and S. Zschocke, "Probing the strange quark condensate by dielectrons from phi meson decays in heavy ion collisions at SIS energies," *Eur.Phys.J.* **A17** (2003) 83–87, arXiv:nucl-th/0211067 [nucl-th].

[84] F. Klingl, S.-s. Kim, S. H. Lee, P. Morath, and W. Weise, "J / psi and eta(c) in the nuclear medium: QCD sum rule approach," *Phys.Rev.Lett.* **82** (1999) 3396–3399, arXiv:nucl-th/9811070 [nucl-th].

[85] A. Hayashigaki, "J / psi nucleon scattering length and in-medium mass shift of J / psi in QCD sum rule analysis," *Prog.Theor.Phys.* **101** (1999) 923–935, arXiv:nucl-th/9811092 [nucl-th].

[86] S.-s. Kim and S. H. Lee, "QCD sum rules for J / psi in the nuclear medium: Contributions from dimension-six operators," *Nucl.Phys.* **A679** (2001) 517–548, arXiv:nucl-th/0002002 [nucl-th].

[87] K. Ohtani, P. Gubler, and M. Oka, "Negative-parity nucleon excited state in nuclear matter," *Phys. Rev.* **C94** no. 4, (2016) 045203, arXiv:1606.09434 [hep-ph].

[88] P. Gubler and K. Ohtani, "Constraining the strangeness content of the nucleon by measuring the ϕ meson mass shift in nuclear matter," arXiv:1404.7701 [hep-ph].

[89] D. E. Miller and K. Redlich, "Exact Implementation of Baryon Number Conservation in Lattice Gauge Theory," *Phys. Rev.* **D35** (1987) 2524.

[90] K. G. Wilson, "Nonlagrangian models of current algebra," *Phys.Rev.* **179** (1969) 1499–1512.

[91] M. Gell-Mann, R. J. Oakes, and B. Renner, "Behavior of current divergences under SU(3) x SU(3)," *Phys. Rev.* **175** (1968) 2195–2199.

[92] S. Borsanyi, S. Durr, Z. Fodor, S. Krieg, A. Schafer, E. E. Scholz, and K. K. Szabo, "SU(2) chiral perturbation theory low-energy constants from 2+1 flavor staggered lattice simulations," *Phys. Rev.* **D88** (2013) 014513, arXiv:1205.0788 [hep-lat].

[93] **TWQCD, JLQCD** Collaboration, H. Fukaya, S. Aoki, T. W. Chiu, S. Hashimoto, T. Kaneko, J. Noaki, T. Onogi, and N. Yamada, "Determination of the chiral condensate from QCD Dirac spectrum on the lattice," *Phys. Rev.* **D83** (2011) 074501, arXiv:1012.4052 [hep-lat].

[94] P. Gerber and H. Leutwyler, "Hadrons Below the Chiral Phase Transition," *Nucl. Phys.* **B321** (1989) 387–429.

[95] P. Chen *et al.*, "The Finite temperature QCD phase transition with domain wall fermions," *Phys. Rev.* **D64** (2001) 014503, arXiv:hep-lat/0006010 [hep-lat].

[96] L. Reinders, H. Rubinstein, and S. Yazaki, "Hadron Properties from QCD Sum Rules," *Phys.Rept.* **127** (1985) 1.

[97] N. Paver, Riazuddin, and M. D. Scadron, "Flavor Symmetry Breaking in Quark Vacuum Condensates," *Phys. Lett.* **B197** (1987) 430–436.

[98] G. Amoros, J. Bijnens, and P. Talavera, "QCD isospin breaking in meson masses, decay constants and quark mass ratios," *Nucl.Phys.* **B602** (2001) 87–108, arXiv:hep-ph/0101127 [hep-ph].

[99] C. McNeile, A. Bazavov, C. Davies, R. Dowdall, K. Hornbostel, *et al.*, "Direct determination of the strange and light quark condensates from full lattice QCD," *Phys.Rev.* **D87** (2013) 034503, arXiv:1211.6577 [hep-lat].

[100] H. G. Dosch, M. Jamin, and S. Narison, "Baryon Masses and Flavor Symmetry Breaking of Chiral Condensates," *Phys. Lett.* **B220** (1989) 251–257.

[101] C. A. Dominguez, A. Ramlakan, and K. Schilcher, "Ratio of strange to nonstrange quark condensates in QCD," *Phys. Lett.* **B511** (2001) 59–65, arXiv:hep-ph/0104262 [hep-ph].

[102] M. Jamin, "Flavor symmetry breaking of the quark condensate and chiral corrections to the Gell-Mann-Oakes-Renner relation," *Phys.Lett.* **B538** (2002) 71–76, arXiv:hep-ph/0201174 [hep-ph].

[103] S. Narison, "Light and heavy quark masses, flavor breaking of chiral condensates, meson weak leptonic decay constants in QCD," arXiv:hep-ph/0202200 [hep-ph].

[104] S. Narison, "QCD as a theory of hadrons from partons to confinement," *Camb.Monogr.Part.Phys.Nucl.Phys.Cosmol.* **17** (2002) 1, arXiv:hep-ph/0205006 [hep-ph].

[105] B. Ioffe, "QCD at low energies," *Prog.Part.Nucl.Phys.* **56** (2006) 232–277, arXiv:hep-ph/0502148 [hep-ph].

[106] M. Asakawa, T. Hatsuda, and Y. Nakahara, "Maximum entropy analysis of the spectral functions in lattice QCD," *Prog. Part. Nucl. Phys.* **46** (2001) 459–508, arXiv:hep-lat/0011040 [hep-lat].

[107] V. Fock, "Proper time in classical and quantum mechanics," *Phys. Z. Sowjetunion* **12** (1937) 404–425.

[108] J. S. Schwinger, "On gauge invariance and vacuum polarization," *Phys. Rev.* **82** (1951) 664–679.

[109] A. V. Smilga, "Calculation of the degree corrections in fixed point gauge. (in Russian)," *Sov. J. Nucl. Phys.* **35** (1982) 271–277. [Yad. Fiz.35,473(1982)].

[110] B. L. Ioffe, V. S. Fadin, and L. N. Lipatov, *Quantum chromodynamics: Perturbative and nonperturbative aspects*. Cambridge Univ. Press, 2010.

[111] M. J. Lavelle and M. Schaden, "Propagators and Condensates in QCD," *Phys. Lett.* **B208** (1988) 297–302.

[112] M. A. Shifman, "Snapshots of hadrons or the story of how the vacuum medium determines the properties of the classical mesons which are produced, live and die in the QCD vacuum," *Prog.Theor.Phys.Suppl.* **131** (1998) 1–71, arXiv:hep-ph/9802214 [hep-ph].

[113] M. Neubert, "Scale setting in QCD and the momentum flow in Feynman diagrams," *Phys. Rev.* **D51** (1995) 5924–5941, arXiv:hep-ph/9412265 [hep-ph].

[114] P. Ball, M. Beneke, and V. M. Braun, "Resummation of (beta0 alpha-s)**n corrections in QCD: Techniques and applications to the tau hadronic width and the heavy quark pole mass," *Nucl. Phys.* **B452** (1995) 563–625, arXiv:hep-ph/9502300 [hep-ph].

[115] T. G. Steele, "Quark Condensate Contributions to the Gluon Selfenergy and the ρ Meson Sum Rule," *Z. Phys.* **C42** (1989) 499–503.

[116] M. Lavelle, "Gauge invariant effective gluon mass from the operator product expansion," *Phys. Rev.* **D44** (1991) 26–28.

[117] K. Ohtani, P. Gubler, and M. Oka, "Parity projection of QCD sum rules for the nucleon," *Phys. Rev.* **D87** no. 3, (2013) 034027, arXiv:1209.1463 [hep-ph].

[118] B. L. Ioffe and K. N. Zyablyuk, "The V - A sum rules and the operator product expansion in complex q**2 - plane from tau decay data," *Nucl. Phys.* **A687** (2001) 437–453, arXiv:hep-ph/0010089 [hep-ph].

[119] P. Colangelo and A. Khodjamirian, "QCD sum rules, a modern perspective," arXiv:hep-ph/0010175 [hep-ph].

[120] **Particle Data Group** Collaboration, J. Beringer *et al.*, "Review of Particle Physics (RPP)," *Phys.Rev.* **D86** (2012) 010001.

[121] D. B. Leinweber, "QCD sum rules for skeptics," *Annals Phys.* **254** (1997) 328–396, arXiv:nucl-th/9510051 [nucl-th].

[122] S. Bethke, "World Summary of α_s (2012)," arXiv:1210.0325 [hep-ex]. [Nucl. Phys. Proc. Suppl.234,229(2013)].

[123] E. V. Shuryak, "Correlation functions in the QCD vacuum," *Rev. Mod. Phys.* **65** (1993) 1–46.

[124] T. Matsui and H. Satz, "J/ψ Suppression by Quark-Gluon Plasma Formation," *Phys. Lett.* **B178** (1986) 416–422.

[125] F. Karsch, M. T. Mehr, and H. Satz, "Color Screening and Deconfinement for Bound States of Heavy Quarks," *Z. Phys.* **C37** (1988) 617.

[126] F. Karsch and H. Satz, "The Spectral analysis of strongly interacting matter," *Z. Phys.* **C51** (1991) 209–224.

[127] S. Digal, P. Petreczky, and H. Satz, "String breaking and quarkonium dissociation at finite temperatures," *Phys. Lett.* **B514** (2001) 57–62, arXiv:hep-ph/0105234 [hep-ph].

[128] C.-Y. Wong, "Heavy quarkonia in quark-gluon plasma," *Phys. Rev.* **C72** (2005) 034906, arXiv:hep-ph/0408020 [hep-ph].

[129] W. M. Alberico, A. Beraudo, A. De Pace, and A. Molinari, "Heavy quark bound states above T(c)," *Phys. Rev.* **D72** (2005) 114011, arXiv:hep-ph/0507084 [hep-ph].

[130] H. Satz, "Colour deconfinement and quarkonium binding," *J. Phys.* **G32** (2006) R25, arXiv:hep-ph/0512217 [hep-ph].

[131] A. Mocsy and P. Petreczky, "Can quarkonia survive deconfinement?," *Phys. Rev.* **D77** (2008) 014501, arXiv:0705.2559 [hep-ph].

[132] A. Mocsy and P. Petreczky, "Color screening melts quarkonium," *Phys. Rev. Lett.* **99** (2007) 211602, arXiv:0706.2183 [hep-ph].

[133] M. Laine, O. Philipsen, P. Romatschke, and M. Tassler, "Real-time static potential in hot QCD," *JHEP* **03** (2007) 054, arXiv:hep-ph/0611300 [hep-ph].

[134] A. Rothkopf, T. Hatsuda, and S. Sasaki, "Complex Heavy-Quark Potential at Finite Temperature from Lattice QCD," *Phys. Rev. Lett.* **108** (2012) 162001, arXiv:1108.1579 [hep-lat].

[135] M. Asakawa and T. Hatsuda, "J / psi and eta(c) in the deconfined plasma from lattice QCD," *Phys. Rev. Lett.* **92** (2004) 012001, arXiv:hep-lat/0308034 [hep-lat].

[136] T. Umeda, K. Nomura, and H. Matsufuru, "Charmonium at finite temperature in quenched lattice QCD," *Eur. Phys. J.* **C39S1** (2005) 9–26, arXiv:hep-lat/0211003 [hep-lat].

[137] S. Datta, F. Karsch, P. Petreczky, and I. Wetzorke, "Behavior of charmonium systems after deconfinement," *Phys. Rev.* **D69** (2004) 094507, arXiv:hep-lat/0312037 [hep-lat].

[138] H. Iida, T. Doi, N. Ishii, H. Suganuma, and K. Tsumura, "Charmonium properties in deconfinement phase in anisotropic lattice QCD," *Phys. Rev.* **D74** (2006) 074502, arXiv:hep-lat/0602008 [hep-lat].

[139] A. Jakovac, P. Petreczky, K. Petrov, and A. Velytsky, "Quarkonium correlators and spectral functions at zero and finite temperature," *Phys. Rev.* **D75** (2007) 014506, arXiv:hep-lat/0611017 [hep-lat].

[140] H. T. Ding, A. Francis, O. Kaczmarek, F. Karsch, H. Satz, and W. Soeldner, "Charmonium properties in hot quenched lattice QCD," *Phys. Rev.* **D86** (2012) 014509, arXiv:1204.4945 [hep-lat].

[141] S. Borsanyi *et al.*, "Charmonium spectral functions from 2+1 flavour lattice QCD," *JHEP* **04** (2014) 132, arXiv:1401.5940 [hep-lat].

[142] A. Ikeda, M. Asakawa, and M. Kitazawa, "In-medium dispersion relations of charmonia studied by maximum entropy method," arXiv:1610.07787 [hep-lat].

[143] H. Kim, K. Morita, and S. H. Lee, "Temperature dependence of dimension 6 gluon operators and their effects on Charmonium," *Phys. Rev.* **D93** no. 1, (2016) 016001, arXiv:1510.03563 [hep-ph].

[144] **CMS** Collaboration, V. Khachatryan *et al.*, "Measurement of Prompt $\psi(2S) \to J/\psi$ Yield Ratios in Pb-Pb and $p-p$ Collisions at $\sqrt{s_{NN}} = 2.76$ TeV," *Phys. Rev. Lett.* **113** no. 26, (2014) 262301, arXiv:1410.1804 [nucl-ex].

[145] **CMS** Collaboration, A. M. Sirunyan *et al.*, "Relative modification of prompt ψ(2S) and J/ψ yields from pp to PbPb collisions at $\sqrt{s_{\rm NN}} = 5.02$ TeV," *Submitted to: Phys. Rev. Lett.* (2016) , arXiv:1611.01438 [nucl-ex].

[146] **ALICE** Collaboration, J. Adam *et al.*, "Differential studies of inclusive J/ψ and ψ(2S) production at forward rapidity in Pb-Pb collisions at $\sqrt{s_{\rm NN}} = 2.76$ TeV," *JHEP* **05** (2016) 179, arXiv:1506.08804 [nucl-ex].

[147] **ALICE** Collaboration, J. Adam *et al.*, "Centrality dependence of ψ(2S) suppression in p-Pb collisions at $\sqrt{s_{\rm NN}} = 5.02$ TeV," *JHEP* **06** (2016) 050, arXiv:1603.02816 [nucl-ex].

[148] **PHENIX** Collaboration, A. Adare *et al.*, "Measurement of the relative yields of $\psi(2S)$ to $\psi(1S)$ mesons produced at forward and backward rapidity in p+p, p+Al, p+Au, and ^{3}He+Au collisions at $\sqrt{s_{_{NN}}} = 200$ GeV," arXiv:1609.06550 [nucl-ex].

[149] **LHCb** Collaboration, R. Aaij *et al.*, "Study of $\psi(2S)$ production and cold nuclear matter effects in pPb collisions at $\sqrt{s_{NN}} = 5$ TeV," *JHEP* **03** (2016) 133, arXiv:1601.07878 [nucl-ex].

[150] K. Suzuki, P. Gubler, and M. Oka, "D meson mass increase by restoration of chiral symmetry in nuclear matter," *Phys. Rev.* **C93** no. 4, (2016) 045209, arXiv:1511.04513 [hep-ph].

[151] K.-J. Araki, K. Ohtani, P. Gubler, and M. Oka, "QCD sum rules on the complex Borel plane," *PTEP* **2014** (2014) 073B03, arXiv:1403.6299 [hep-ph].

[152] G. Boyd, J. Engels, F. Karsch, E. Laermann, C. Legeland, M. Lutgemeier, and B. Petersson, "Thermodynamics of SU(3) lattice gauge theory," *Nucl. Phys.* **B469** (1996) 419–444, arXiv:hep-lat/9602007 [hep-lat].

[153] O. Kaczmarek, F. Karsch, F. Zantow, and P. Petreczky, "Static quark anti-quark free energy and the running coupling at finite temperature," *Phys. Rev.* **D70** (2004) 074505, arXiv:hep-lat/0406036 [hep-lat]. [Erratum: Phys. Rev.D72,059903(2005)].

[154] **Wuppertal-Budapest** Collaboration, S. Borsanyi, Z. Fodor, C. Hoelbling, S. D. Katz, S. Krieg, C. Ratti, and K. K. Szabo, "Is there still any Tc mystery in lattice QCD? Results with physical masses in the continuum limit III," *JHEP* **09** (2010) 073, arXiv:1005.3508 [hep-lat].

[155] A. Bazavov *et al.*, "The chiral and deconfinement aspects of the QCD transition," *Phys. Rev.* **D85** (2012) 054503, arXiv:1111.1710 [hep-lat].

[156] C. McNeile, C. T. H. Davies, E. Follana, K. Hornbostel, and G. P. Lepage, "High-Precision c and b Masses, and QCD Coupling from Current-Current Correlators in Lattice and Continuum QCD," *Phys. Rev.* **D82** (2010) 034512, arXiv:1004.4285 [hep-lat].

[157] F. J. Dyson, "The S matrix in quantum electrodynamics," *Phys. Rev.* **75** (1949) 1736–1755.

[158] J. S. Schwinger, "On the Green's functions of quantized fields. 1.," *Proc. Nat. Acad. Sci.* **37** (1951) 452–455.

[159] J. S. Schwinger, "On the Green's functions of quantized fields. 2.," *Proc. Nat. Acad. Sci.* **37** (1951) 455–459.

[160] J. Goldstone, A. Salam, and S. Weinberg, "Broken Symmetries," *Phys. Rev.* **127** (1962) 965–970.

[161] J. Goldstone, "Field Theories with Superconductor Solutions," *Nuovo Cim.* **19** (1961) 154–164.

[162] K. Higashijima, "Dynamical Chiral Symmetry Breaking," *Phys. Rev.* **D29** (1984) 1228.

[163] M. Harada and Y. Yoshida, "QCD S parameter from inhomogeneous Bethe-Salpeter equation," *Phys. Rev.* **D50** (1994) 6902–6910, `arXiv:hep-ph/9406402 [hep-ph]`.

[164] C. D. Roberts and A. G. Williams, "Dyson-Schwinger equations and their application to hadronic physics," *Prog. Part. Nucl. Phys.* **33** (1994) 477–575, `arXiv:hep-ph/9403224 [hep-ph]`.

[165] A. Bender, C. D. Roberts, and L. Von Smekal, "Goldstone theorem and diquark confinement beyond rainbow ladder approximation," *Phys. Lett.* **B380** (1996) 7–12, `arXiv:nucl-th/9602012 [nucl-th]`.

[166] K. Kodaira, *An Introduction to Calculus (Kaiseki Nyumon I)*. Iwanami-Shoten, 2003.